THE PROCEEDINGS OF THE PHYSICAL SOCIETY

VOL. 60, PART 5 — 1 May 1948 — No. 341

CONTENTS

Price to non-members 8*s.* 4*d.* net; 8*s.* 10*d.* inclusive of postage
Annual subscription 63*s.* inclusive of postage, payable in advance

Published by
THE PHYSICAL SOCIETY
1 Lowther Gardens, Prince Consort Road, London S.W.7

Printed by
TAYLOR AND FRANCIS, LTD.,
Red Lion Court, Fleet Street, London E.C.4

PROCEEDINGS OF THE PHYSICAL SOCIETY

Beginning in January 1948 (Volume 60), the *Proceedings* is now published monthly under the guidance of an Advisory Board.

ADVISORY BOARD

Chairman: The President of the Physical Society (G. I. FINCH, M.B.E., D.Sc., F.R.S.).

E. N. da C. ANDRADE, Ph.D., D.Sc., F.R.S.
Sir EDWARD APPLETON, G.B.E., K.C.B., D.Sc., F.R.S.
L. F. BATES, Ph.D., D.Sc.
P. M. S. BLACKETT, M.A., F.R.S.
Sir LAWRENCE BRAGG, O.B.E., M.A., Sc.D., D.Sc., F.R.S.
Sir JAMES CHADWICK, D.Sc., Ph.D., F.R.S.
Lord CHERWELL OF OXFORD, M.A., Ph.D., F.R.S.
Sir John COCKCROFT, C.B.E., M.A., Ph.D., F.R.S.
Sir CHARLES DARWIN, K.B.E., M.C., M.A., Sc.D., F.R.S.
N. FEATHER, Ph.D., F.R.S.
D. R. HARTREE, M.A., Ph.D., F.R.S.
N. F. MOTT, M.A., F.R.S.
M. L. OLIPHANT, Ph.D., D.Sc., F.R.S.
F. E. SIMON, C.B.E., M.A., D.Phil., F.R.S.
T. SMITH, M.A., F.R.S.
Sir GEORGE THOMSON, M.A., D.Sc., F.R.S.

Papers for publication in the *Proceedings* should be addressed to the Secretary-Editor, Miss A. C. STICKLAND, Ph.D., at the Office of the Physical Society, 1 Lowther Gardens, Prince Consort Road, London S.W.7. Telephone: KENsington 0048, 0049.

Detailed Instructions to Authors were included in the February issue of the *Proceedings*; separate copies can be obtained from the Secretary-Editor.

Report on

COLOUR TERMINOLOGY

by a Committee of

THE PHYSICAL SOCIETY
COLOUR GROUP

56 pp. 7*s. post free.*

Also still available

Report on

DEFECTIVE COLOUR VISION IN INDUSTRY

52 pp. 3*s.* 6*d. post free.*

Orders, with remittance, to

THE PHYSICAL SOCIETY
1 Lowther Gardens, Prince Consort Road, London S.W.7

CATALOGUES
OF THE
PHYSICAL SOCIETY'S
EXHIBITIONS
OF
SCIENTIFIC INSTRUMENTS
AND APPARATUS

The three post-war Catalogues are widely acknowledged as very useful records and valuable books of reference.

30th (1946) CATALOGUE (reprinted):
288+lxxx pages; 176 illustrations.
1*s.*; *by post* 2*s.*

31st (1947) CATALOGUE:
298+lxxxvi pages; 106 illustrations.
2*s.* 6*d.*; *by post* 3*s.* 6*d.*

32nd (1948) CATALOGUE:
288+lxxxiv pages; 139 illustrations.
5*s.*; *by post* 6*s.*

Orders, with remittances, should be sent to

THE PHYSICAL SOCIETY
1 Lowther Gardens, Prince Consort Road, London S.W.7

THE UNITED IMPERIAL AND AMERICAN PATENT SERVICE
(Patents, Designs, Trade Mark)

H. E. J. Gheury de Bray, A.M.I.E.E., Registered Patent Agent (London), Chartered Electrical Engineer and Fellow of the Physical Society.
H. J. Wittal, LL.B., Patent Attorney and Counsellor at Law (New York).

Booklet free on application.
Preliminary interview free by appointment.
102 Bishopsgate, E.C.2.
Telephone : Clerkenwell 1131 — Chancery 8579
London Wall 2121.
Telegraphic Address } IMPERATRIX CENT LONDON.

PROCEEDINGS OF THE PHYSICAL SOCIETY

The following war-time issues have now been reprinted :

Vol. 53, Part 1 (January 1941) **7/-**, *post free* **7/6**
Vol. 54, Part 5 (September 1942) **8/4**, *post free* **8/10**
Vol. 55, Part 2 (March 1943) **8/4**, *post free* **8/10**
Vol. 56, Part 1 (January 1944) **8/4**, *post free* **8/10**
Vol. 57, Part 1 (January 1945) **8/4**, *post free* **8/10**

Orders, with remittances, to
THE PHYSICAL SOCIETY,
1 Lowther Gardens, Prince Consort Road, London S.W.7

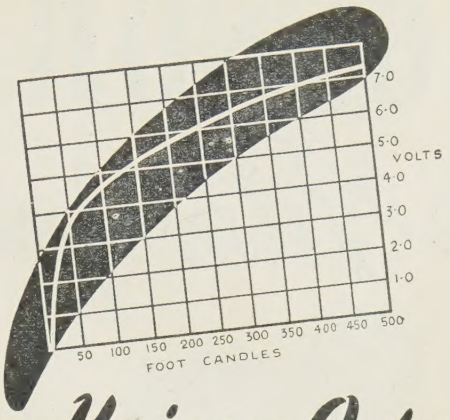

Unique Output

THE scientific worker will appreciate the possibilities offered by the unique self-generated voltage response of "EEL" TYPE M.I. Photo-Cells, particularly when it is realised that these cells have a special response approximating to that of the eye.

PHOTO-ELECTRIC TECHNIQUE attains a new importance with such remarkable output, and you are invited to apply for any further information you may require.

Readily available at **£4.10.0**

EEL
TYPE M.I SELENIUM PHOTO-CELLS

A product of
EVANS ELECTROSELENIUM LIMITED
Harlow, Essex

VACUUM LEAK DETECTION

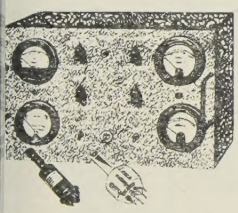

The B.A.R. Thermocouple-Ionisation Gauge Control. The newly developed Thermocouple-Ionisation Gauge Control, complete with Thermocouple and Ionisation Gauges, covers the pressure range from 2×10^{-7} mm. to 1 mm. Hg. Operation is dependable and simple. Full-scale meter deflection occurs at 1 mm. and 5, 1·0, 0·1 and 0·01 microns. The unit is removable from its cabinet for incorporation in a central panel.

The B.A.R. Alphatron is an ionisation-type vacuum gauge using the ionising power of alpha particles from a radium source to measure total pressure of any gas, vapour or mixed atmosphere from 1 micron to 10 mm. Hg with instantaneous linear response. The B.A.R. Alphatron is quickly available from batches now in production.

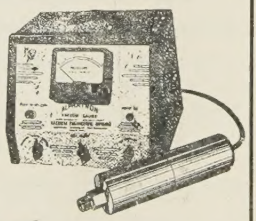

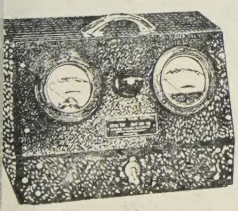

The B.A.R. Thermocouple Gauge Control is a light, portable instrument that may be carried to any part of a plant or system for vacuum testing. It is compact, rugged and built throughout to withstand hard industrial use.

Operating from any 115-volt, 50/60-cycle outlet, this unit gives pressure indications over a continuous range from 1 to 1000 microns Hg. These pressures are read directly on the microammeter, which is calibrated both in microns and microamperes. By means of increased filament current and special calibration, the unit will indicate pressures up to 2 mm. Hg. The gauge is undamaged by operation at atmospheric pressure.

BRITISH AMERICAN RESEARCH LTD

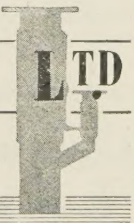

DESIGNERS AND MANUFACTURERS OF HIGH VACUUM GAUGES · VALVES · SEALS DIFFUSION PUMPS · STILLS · FURNACES · COATING EQUIPMENT AND DEHYDRATION PLANT
LOCK E2 · HILLINGTON NORTH · GLASGOW S.W.

COSSOR

Announce

THE NEW MODEL
1035
DOUBLE BEAM
OSCILLOGRAPH

The Model 1035 is a general purpose Oscillograph, consisting of a Double Beam Tube Unit, Time Base, Y Deflection Amplifiers and internal Power Supplies. The two traces are presented over the full area of a flat screen tube of 90 mm. internal diameter and operating at 2 kv. Signals are normally fed via the Amplifiers, with provision for input voltage calibration. The Time Base is designed for repetitive, triggered, or single stroke operation, and time measurement is provided by a directly calibrated Shift Control.

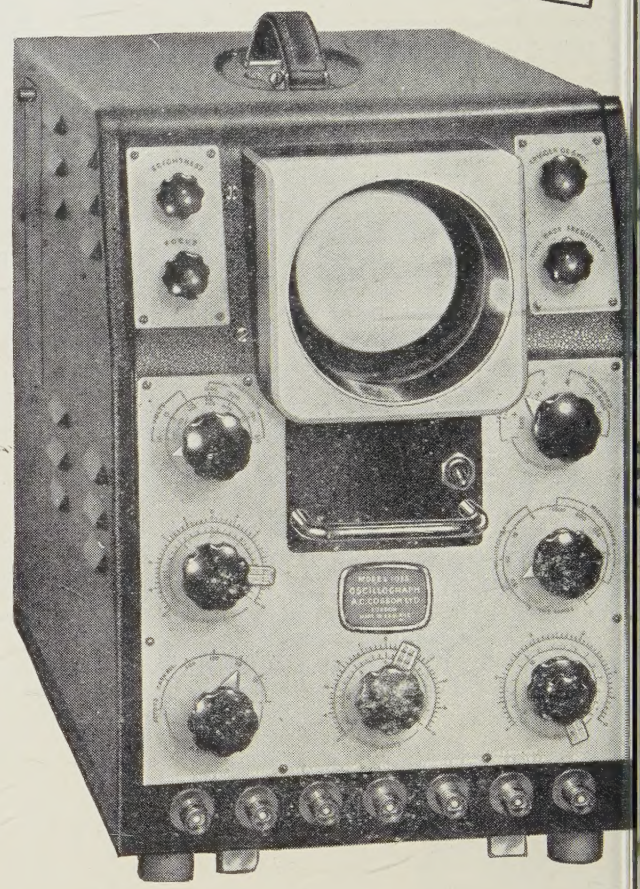

MODEL 1049
Industrial Oscillograph
is designed specifically for industrial use where the main interest is in the observation and measurement of low frequency phenomena. Its presentation is generally similar to that of Model 1035 illustrated and a comprehensive specification includes 4 kv tube operation for transient recording.

For photographic recording, both models have provision for the attachment of a Camera, Model 1428, which may be operated either manually or by motor drive. A similar camera, Model 427, is also available for use with Model 339 Oscillograph.

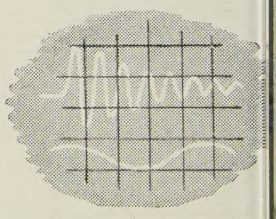

Further details on application to :—

A. C. COSSOR LTD., INSTRUMENT DEPT., HIGHBURY, LONDON, N

E.H.T.
DEVELOPMENTS

•

0kV DC

from two rectifiers, type 36EHT145*, in a 50 c.p.s. voltage-doubler circuit.

•

kV DC

from three rectifiers, type 36EHT35†, in a pulse voltage tripler circuit.

•

kV DC

from 350 volts A.C. using a Westeht EHT unit.

•

WESTINGHOUSE
WESTALITE
METAL RECTIFIERS

Write for literature to Dept. P.S. 5.

Interested manufacturers may obtain small supplies of samples.

* Each only $\frac{7}{16}'' \times 7\frac{1}{4}''$

† Each only $\frac{7}{16}'' \times 2\frac{1}{8}''$

Westinghouse Brake & Signal Co., Ltd.
2 York Way, King's Cross, London, N.1

DRAYTON
"Hydroflex"
Metal Bellows

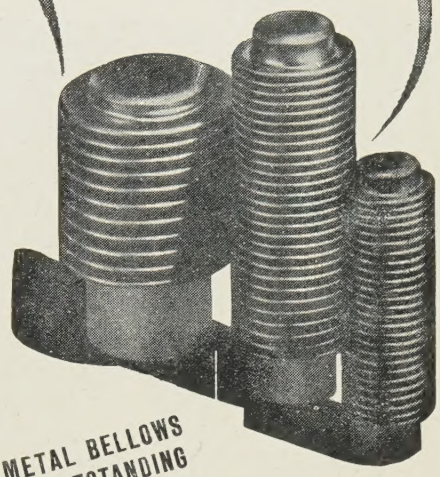

METAL BELLOWS WITH OUTSTANDING ADVANTAGES

(B.2)

These bellows are formed from the initial tube in one gradual continuous operation, resulting in a uniformity of wall-thickness unattainable by any other method. The tough resilient product is tested to many times the maximum rated working pressure during formation. Customers' end plates can be fitted prior to forming so that the soldered joint is also pressure tested.

For Gland Seals; Refrigeration Control; Thermostatic and Pressure Operated Devices, etc.

- **Every Gland uniform in life and performance.**
- **Pretested during forming.**
- **Absolutely reliable in operation.**
- **Provision of closed end eliminates one joint.**

Root Diam. 3/8" to 3" Outside Diam. 9/16" to 4½"

Write for the "Hydroflex" Brochure T

DRAYTON REGULATOR & INSTRUMENT CO. LTD.
WEST DRAYTON *West Drayton 2611.* **MIDDX.**

WESTON STANDARD CELL
TYPE D-402
Now available for immediate delivery

TYPE D-402-C (Unmounted)
Height 2¾ in. Width 2 1/16 in. Diameter of Tubes ⅝ in.

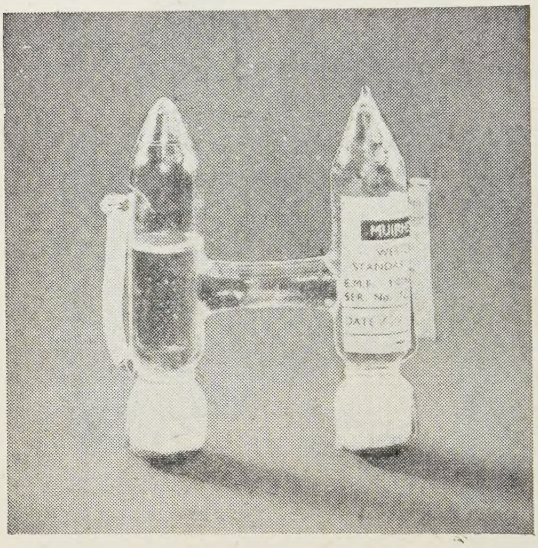

TYPE D-402-B
Height 4¾ in. Width 3 in. Depth 3⅜ in.

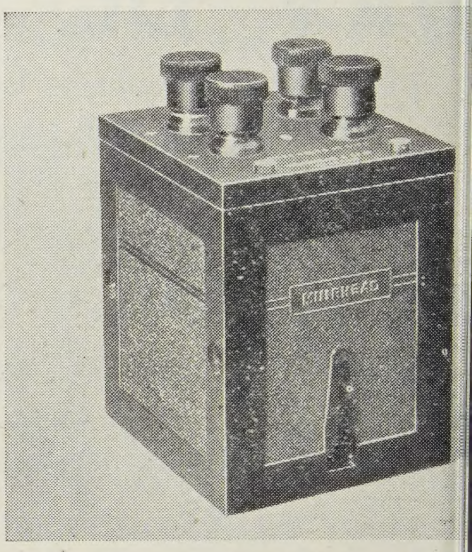

These Weston Standard Cells are of the saturated acid type, and are manufactured in accordance with a specification by the National Physical Laboratory. Single, double and unmounted models are available as listed, and a thermometer for use with the mounted models can be supplied.

SPECIFICATION :

NOMINAL E.M.F.: 1·01824 volts Int. at

TEMPERATURE CO-EFFICIENT: −0·00004 per °C.

ACCURACY : A certificate o giving the E.M.F. at a given temperat 1 part in 10,000 is supplied in all cases, bu fication by the National Physical Labora strongly recommended.

TYPE	DESCRIPTION	WEIGHT		PI
D-402-A	SINGLE CELL (Mounted in bakelite case)	18 oz.	0·51 kg.	£4
D-402-B	DOUBLE CELL (Mounted in bakelite case)	22 oz.	0·63 kg.	£6 1
D-402-C	SINGLE CELL (Unmounted)	2 oz.	0·06 kg.	£2
D-420-A	4 in. THERMOMETER 0-50 °C.	—	—	

* *These prices are subject to any adjustment which may become effective prior to delivery.*

MUIRHEAD

Muirhead & Co. Limited, Elmers End, Beckenham, Kent. *Telephone : Beckenham 0041-2*

FOR OVER 60 YEARS DESIGNERS AND MAKERS OF PRECISION INSTRUMEI

POINTERS FOR DESIGNERS

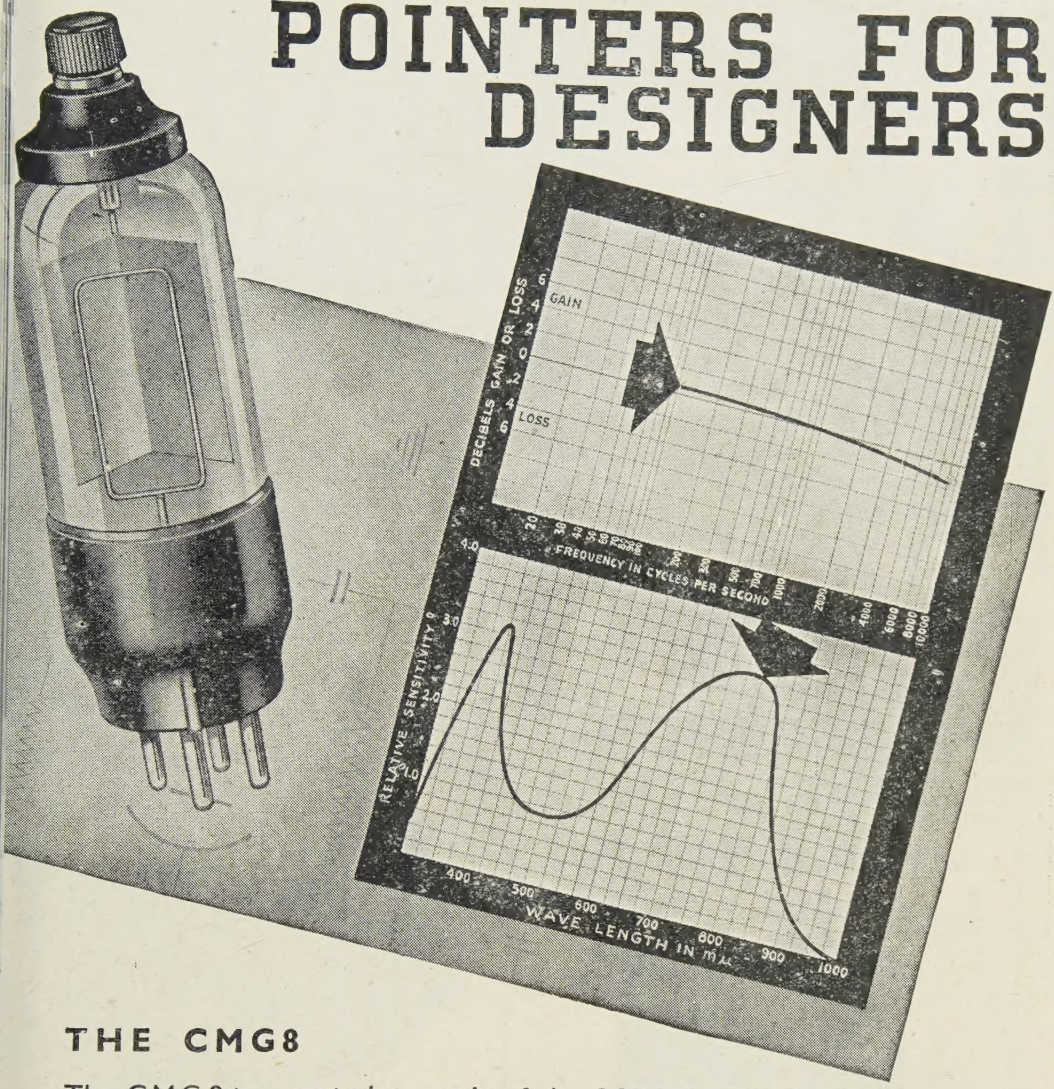

THE CMG8

The CMG 8 is a typical example of the OSRAM range of emission-type photocells which constitute the essential means of converting light changes into electric current. Widely used in sound projectors and industrial apparatus they are non-microphonic and of convenient size. Outstanding features include :—

- Linear response for sound reproduction giving undistorted output.
- High sensitivity to artificial light.

A detailed technical data sheet is available on request.

Osram PHOTO CELLS

G.E.C. CATHODE RAY TUBES

Osram VALVES

Advt. of The General Electric Co., Ltd., Magnet House, Kingsway, London, W.C.2.

LOWEST EVER attenuation & capacitance

CO-AX CABLES for RADIO FREQUENCIES

LOW ATTEN. TYPES	IMPED. OHMS.	ATTEN. db/100ft at 100 Mc/s.	LOADING K.W	O.D.
A1	74	1.7	0.11	0.36"
A2	74	1.3	0.24	0.44"
† A34	73	0.6	1.5	0.88"

LOW CAPAC. TYPES	CAPAC. mmf/ft.	IMPED OHMS.	ATTEN db/100ft 100 Mc/s.	O.D.
C 1	7.3	150	2.5	0.36"
★ PC 1	10.2	132	3.1	0.36"
C 11	6.3	173	3.2	0.36"
C 2	6.3	171	2.15	0.44"
C 22	5.5	184	2.8	0.44"
C 3	5.4	197	1.9	0.64"
C 33	4.8	220	2.4	0.64"
C 44	4.1	252	2.1	1.03"

† Bending Radius 5"
★ Photocell Cable.

TRANSRADIO LTD. 138A CROMWELL ROAD, LONDON, S.W.7.

VITREOSIL MERCURY VAPOUR PUMPS

This new M.V. Fore Pump will operate from an ordinary water filter pump, and when used in conjunction with our Single-Stage or Two-Stage Pump, pressures less than 0·00002 mm Hg are attained.

Write for descriptive leaflet

THE THERMAL SYNDICATE LTD.
Head Office: Wallsend, Northumberland
London Office: 12–14 Old Pye Street, S.W.1

DAWE

INSULATIO TESTE

TYPE 402 B

Directly measures 10,000 Megohms at low voltage

A compact, highly sensitive instrument for m
Insulation Properties and Leakage Resistance
destructive breakdown; also suitable for
Determinations. A guard circuit is provided fo
elimination of surface leakages.

Range : 0.1 MΩ to 10,000 MΩ
Test Potential : Less than 50 volts
Power Supply : Self-contained dry batteries
Dimensions : $4\frac{1}{4}'' \times 7\frac{3}{4}'' \times 4''$ deep

Technical data forwarded on request to :
DAWE INSTRUMENTS LTD., 130 UXBRIDGE ROAD,
LONDON, W.7

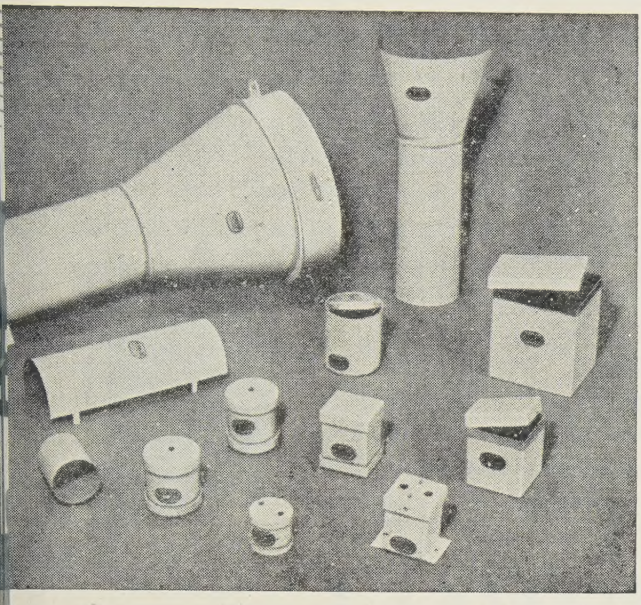

MUMETAL
REGD.

MAGNETIC SCREENS

The high permeability of MUMETAL makes it the outstanding material for the production of all types of magnetic screens. We are in a position to fabricate boxes and shields of practically any shape or size for the screening of delicate instruments and equipment from both uni-directional and alternating magnetic fluxes. A complete range of standard MUMETAL shields is available, examples of which are illustrated. Our technical experts will be pleased to assist in the solution of all screening problems. Your enquiries are invited.

TELCON

TELCON METALS

TELEGRAPH CONSTRUCTION & MAINTENANCE CO. LTD.
Founded 1864

ffice: 22 OLD BROAD ST., LONDON, E.C.2. *Tel: LONdon Wall* 3141
es to: TELCON WORKS, GREENWICH, S.E.10. *Tel: GREenwich* 1040

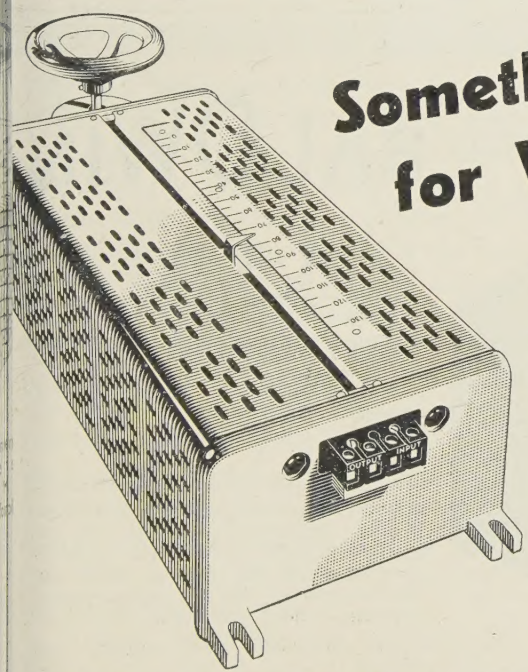

Something NEW for Voltage control

The "Regavolt" is an all-British transformer type regulator of new design and robust construction which make it particularly suitable for heavy industrial use. Special points of performance are: smooth stepless control of voltage, good regulation, high efficiency, and no waveform distortion. Suitable for control of electric furnaces, high voltage testing transformers, speed of electric motors, rectifier equipment, etc.
Write for full details. Booklet 3/3062

BERCO
REGAVOLT
REGULATING TRANSFORMER

BRITISH ELECTRIC RESISTANCE CO. LTD., Queensway, Ponders End, Middlesex
hone: HOWard 1492 Telegrams: "Vitrohm, Enfield"
BR3062-EHI

Any Questions?

To get authoritative answers to questions about photographic apparatus . . materials . . techniques . .

(1) Turn up the relevant Kodak Data Sheets. There are some 150 of these, covering a great range of scientific, industrial and commercial applications of photography.

Or (2) Write to Kodak. Your query will be dealt with by experts, who have the unique resources of the Kodak Research Laboratories at their call.

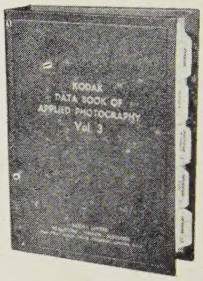

KODAK DATA BOOK OF APPLIED PHOTOGRAPHY 3 VOLUMES . . . 15/-

KODAK

KODAK LTD., KODAK HOUSE, KINGSWAY, LONDON, W.C.2.

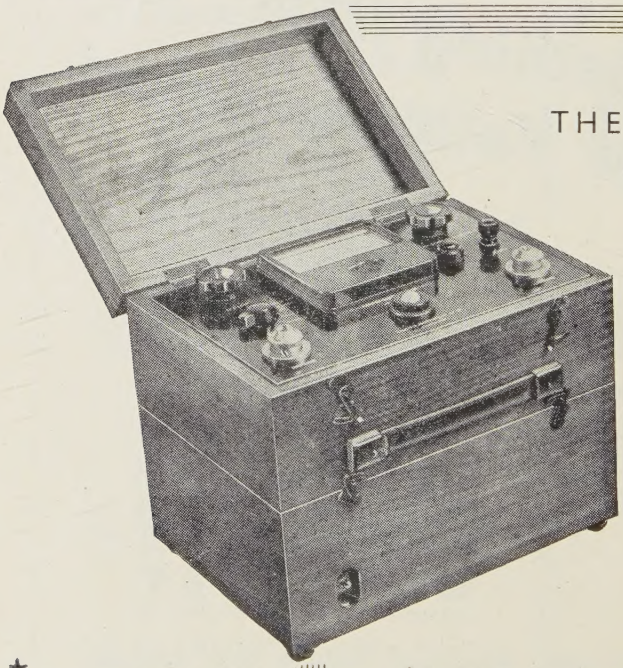

THE BALDWIN

FARMER ELECTROMETER

FOR RADIOLOGICAL WORK

A unique electronic instrument for research and routine testing in Hospital Radium and X-ray Therapy Departments.

It has an input resistance of 10^{16} ohms and an input capacity of less than 1 $\mu\mu$F. Developed primarily for use in Radiological work, where small condensers of the Sievert type are used extensively for the measurement of gamma and X-ray intensities.

Fully descriptive leaflet supplied on request.

★VOLTAGE RANGES
0 - 50
0 - 100
0 - 250

BALDWIN INSTRUMENT COMPANY LTD
BROOKLANDS WORKS, PRINCES ROAD, DARTFORD, KENT.
Telephone: DARTFORD 2989

THE PROCEEDINGS OF THE PHYSICAL SOCIETY

VOL. 60, PART 5 1 May 1948 No. 341

A Quantitative Study of the Expansion Method for Liquefying Helium

BY G. L. PICKARD * AND F. E. SIMON
Clarendon Laboratory, Oxford
* Now at University of British Columbia, Vancouver

MS. received 12 *December* 1947

ABSTRACT. The yield of the Expansion Method for producing liquid helium has been measured for various starting conditions and the results are presented in the form of two diagrams.

In addition some data are given on the volumes and specific heats of compressed helium gas; although these are only of a preliminary nature, they give all the data necessary for the design of such an expansion liquefier.

The entropy diagram has been extended to higher pressures and the actual yield compared with the " ideal " yield of a piston and cylinder arrangement. It appears that the simple expansion method results in an efficiency which is 60% of the ideal when starting from the usual temperature and pressure conditions. The reasons for this high efficiency are discussed.

§ 1. INTRODUCTION

THE principle of the Expansion Method (Simon 1932a, b, 1935, 1936, 1937, Simon and Ahlberg 1933) of liquefying gases is a very simple one. The gas is compressed isothermally into a container C (figure 1) called the expansion chamber, which is pre-cooled in a low temperature bath A to the lowest temperature possible. The container is then isolated by evacuating B and the gas expanded slowly through valve V outside the apparatus. After this expansion a certain proportion of the gas remains as liquid inside the container. Such a method would be quite impossible with most gases, and is only feasible for gases with very low boiling points. The reason is that at ordinary temperatures, say room temperature, the container has always a much higher heat capacity than the gas which it contains. With falling temperature, however, conditions change radically because, first, at constant pressure a given vessel contains more gas at low temperatures, and secondly, the specific heat of solid bodies disappears with the approach to absolute zero.

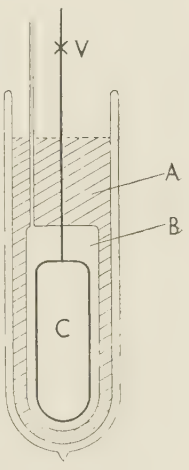

Figure 1.

Table 1 gives the heat capacities of a steel container of 150 cm^3 capacity, designed (with the conventional safety factor) to stand up to 100 atmospheres, together with the heat capacities of the helium which it would contain at two temperatures.

Table 1. Heat capacities (cal/deg.) of steel container and helium

	Room temp.	10° K.
Steel container	50	0·1
Helium at 100 atm.	2	20
Ratio	25	0·005

Thus while at room temperature the container has 25 times the heat capacity of the gas, at 10° it has only $\frac{1}{2}\%$; this represents a change by a factor 5000 of the ratio between the capacities of the container of which the greater part is due to the falling off in the specific heat of the steel. It is still possible to liquefy hydrogen (Simon *et al.* 1935) by this method, but its main application is in the liquefaction of helium.

The method has been used extensively at the Clarendon Laboratory and also in a few other laboratories (for a full list of work see Simon 1940). In most of the experiments carried out, the appropriate low-temperature apparatus has been attached to the expansion chamber. This method of working has many advantages, chiefly that the whole apparatus is surrounded throughout by liquid hydrogen and thus the heat losses are kept very low. An expansion chamber of about 100 cm^3 capacity provides enough helium for an experiment of 10–20 hours' duration, and as a result, expansion chambers larger than about 100 cm^3 have seldom been used. The expansion method is therefore generally regarded as a small scale method, but there is in fact no limitation to the size of an expansion liquefier. Just before the war the first liquefier of this type was built in which liquid helium could be siphoned over from an expansion chamber of 450 cm^3 into an exterior container (Cooke *et al.* 1939). Since the war another such liquefier has been described (Scott and Cook 1947) of a capacity of 400 cm^3, and one of $1\frac{1}{2}$ litre capacity is now under construction at the Clarendon Laboratory. With the widening interest in this method we think it worth while to publish some data, obtained in 1936, from which it is possible to decide upon the best starting conditions. Some earlier experiments on the liquid yields have been described by Simon and Ahlberg (1933) and a preliminary account of the present results was given by Simon in 1936.

The main object of these experiments was to determine the effect of varying starting conditions on the yield of liquid helium, and while doing so, to obtain as much data as possible about the diagram of state and thermal properties of helium, of which little was known at the time in the region of operation of the expansion method. It should be emphasized, however, that these latter experiments have been regarded only as auxiliary and were not carried out with high accuracy.

§ 2. GENERAL ARRANGEMENT

For the experiments an expansion chamber (enclosed in a vacuum case) was fitted with an electrical resistance thermometer and heating coil and the helium was allowed to expand into a large reservoir of known volume. Measurements of the pressure and temperature of the gas in the expansion chamber and of the gas expanded were made at intervals during the expansion. The volume of helium remaining as liquid after expansion to the normal boiling point was measured by heating the cylinder and measuring the volume of gas obtained. A series of seven such experiments from different starting conditions gave sufficient data for the construction of curves showing the relations between

the starting conditions and the yield of liquid obtained. The heating was carried out electrically so as to measure the heat capacity of the helium gas up to about 20° K. before it was let out into the reservoir for measurement.

§ 3. DETAILS OF THE APPARATUS

The expansion chamber was the hemispherically ended cylinder of Hecla AMF steel used in the previous work on hydrogen (Simon *et al.* 1935); it had an internal volume of 144 cm^3 and weighted only 212 gm. The heater and thermometer wires were wound directly on to the cylinder and attached by bakelite varnish, which was not subsequently hardened by baking. The cylinder was then covered with bright aluminium foil to reduce radiation effects. The thermometer coil of No. 47 S.W.G. Eureka wire was of about 500 Ω resistance and the heater coil of No. 40 S.W.G. Eureka wire was of about 200 Ω resistance. The wires were wound in longitudinal zig-zags up and down the side of the cylinder to reduce the risk of their being strained by distension of the cylinder at high pressures.

The single tube to the cylinder was of cupro-nickel and served to support the cylinder within a brass vacuum case, which was immersed in a bath of liquid hydrogen. The temperature of the bath could be reduced to the triple point (14° K.) by reducing the vapour pressure over the liquid. All the necessary connecting tubes for the helium supply etc. were of as small a bore as practicable in order to reduce the dead volume correction. The pressure of the helium in the cylinder was measured by means of a small volume bent-tube manometer and the pressure in the reservoir by a precision bent-tube manometer calibrated against a mercury U-tube manometer.

The resistance thermometer was calibrated from 10°–20° K. using the known vapour pressure–temperature relation for hydrogen after liquefying hydrogen in the cylinder; from 2°–5° K. it was calibrated against the vapour pressure of liquid helium, and in the intermediate region from 5°–10° K. by using the cylinder as the bulb of a helium gas thermometer.

In performing the experiments, the vacuum case, precooled with liquid air, was immersed in a bath of liquid hydrogen and a small quantity of helium gas admitted to permit thermal exchange between the cylinder and the bath. Helium was compressed into the expansion chamber to a pressure of about 160 atmospheres and the temperature of the bath lowered to the desired starting temperature. When thermal equilibrium had been attained the exchange gas was pumped from the vacuum case to isolate the cylinder. The heat inflow along the connecting tube could be neglected during the expansion.

The expansion was effected in stages, the gas being permitted to expand into the reservoir and the pressure and temperature of the gas in the cylinder and in the reservoir measured at each stage. On reaching a pressure of 1 atm. in the cylinder the valve to the reservoir was closed. The specific heat of the helium remaining in the cylinder was measured up to 20° K. and the volume of this helium determined by releasing it into the reservoir. From this volume was calculated how much had been present as liquid at the boiling point after correction for the helium in the form of vapour above the liquid.

The "yield" of liquid was then defined for practical purposes as the percentage of the volume of the cylinder which remained filled with liquid after the expansion. The range of starting conditions covered during the series of expansions enabled

a yield diagram to be constructed showing the relationship between starting conditions and the yield obtained. Furthermore, from the measurements of corresponding pressure, temperature and amount of gas contained in the known volume of the cylinder it was possible to draw a diagram of state for the gas under the conditions of the expansion method.

With the above apparatus it was practicable to use pressures up to 160 atm. and temperatures as low as 14° K., which resulted in yields up to about 45%. It was found impossible to reach lower starting temperatures by pumping the bath alone, and therefore in order to extend the measurements a second apparatus was used. In this apparatus the helium cylinder had a hydrogen chamber attached to it and by reducing the pressure over this hydrogen the temperature of the helium before expansion could be reduced to 11° or 10° K. With this apparatus it was possible to obtain yields up to 80%. The measurements with the second apparatus were rather less accurate than those with the first and no attempt was made to obtain any diagram of state or specific heat results. The effect on the yield of the residual solid hydrogen in the hydrogen chamber was calculated and also checked by experiment. This factor introduced a correction of a few per cent to the yield obtained. The temperatures with this apparatus were measured by means of a simple gas thermometer of the Simon type (Mendelssohn 1931).

With both sets of apparatus the necessary corrections were made throughout for the dead volume of the tube system and a correction was applied to allow for the volumes of the cylinders for thermal contraction. The correction for distension of the cylinder due to the internal pressure was negligible except at the highest pressures.

§4. RESULTS

The experimental data for the pressure–temperature relationships during expansion are represented in figure 2, the curves with roman figures being those

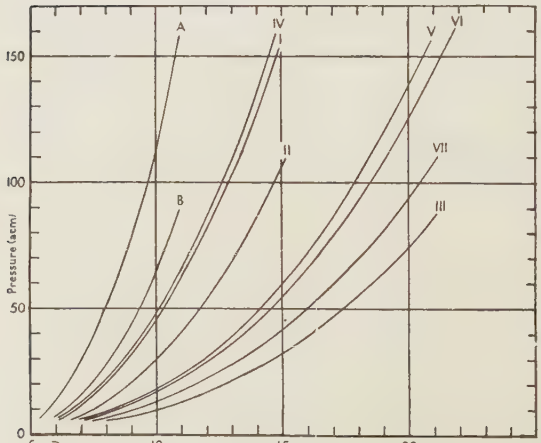

Figure 2. Experimental pressure–temperature data observed during expansions.

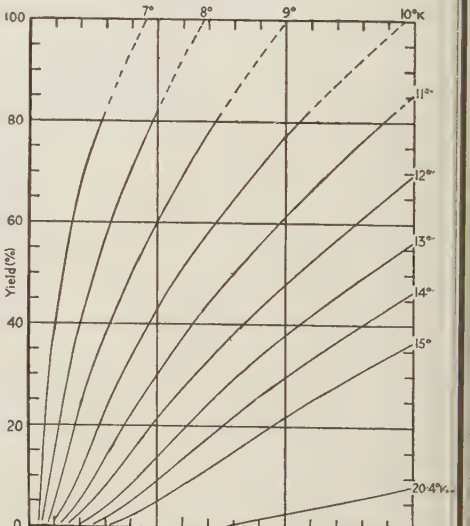

Figure 3. Yield of liquid helium by the expansion method. (Percentage of volume of expansion chamber remaining filled.)

made with the main apparatus, while A and B represent the expansions made with the second apparatus.

The most generally convenient method of plotting the *yield results* is that of figure 3 in which the yield is plotted against the starting pressure for a series of starting temperatures from 7° to 20·4° K. The extent to which the yield is increased by raising the starting pressure and lowering the starting temperature is clearly seen. A comparison between these results and those of Simon and Ahlberg (1933) was made. The curved form of the present yield isotherms is very marked, while Simon and Ahlberg whose experiments were of a less precise nature than the present ones and did not extend to such high yields, represented their yield isotherms as straight lines as a first approximation. A closer inspection of the original experimental results shows that a better representation is given by yield isotherms of similar form to the present ones. With this readjustment the agreement between the earlier results and the present ones is good. Some figures for the yields are given in table 2.

Table 2. Yield of liquid helium obtained by the expansion method expressed as the percentage of the volume of the expansion chamber remaining filled after the expansion

		Starting temperature (° K.)			
		8°	10°	15°	20·4°
Starting	150	>100	100	37	10
pressure	100	>100	76	22	3
(atm.)	50	82	43	5	0

Some of the *diagram of state* data are plotted in figure 4 in the form of atomic volume isotherms at pressures up to 150 atmospheres. Values for the atomic volume are also given in table 3.

Table 3. Atomic volume of helium gas (cm^3)

	Pressure (atm.)						
	5	10	20	30	50	100	150
Temp. °K. 8	88·0	45·5	32·0	28·0	—	—	—
10	137·0	64·5	38·5	31·5	26·5	22·0	19·5
15	240·0	112·0	60·5	43·5	32·0	23·5	21·0
20	—	171·0	85·0	—	39·0	27·0	23·0

The figures in table 3 agree with the data of Zelmanov (1944) within the accuracy of the present measurements (estimated as ±3%) except in the region of 20 atm. pressure and 8°–12° K. where the present figures are about 6% greater than those of Zelmanov.

The *atomic heat* of helium gas at constant volume was measured at various concentrations. These results show a considerable scatter in places and this is attributed to the varying conditions under which the readings were taken. These measurements were made at the end of the experimental "runs" and

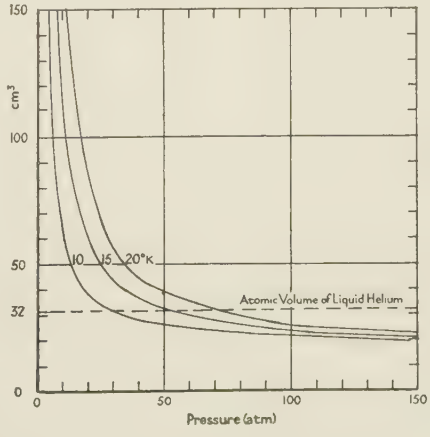

Figure 4. Atomic volume of helium gas.

very often a shortage of liquid hydrogen caused the level in the bath to fall below the upper end of the vacuum case. In consequence the temperature drift of the cylinder increased and varied, due to increased conduction along the supporting tube, and to a reduction in the efficiency of the thermal insulation caused by desorption of gas inside the case. Although the accuracy is not higher than $\pm 3\%$, we think it worth while to give in table 4 the values of the smoothed curves for two different concentrations as hardly any other measurements have yet been made in this region.

Table 4. Atomic heat at constant volume (cal/deg.)

		Temperature (° K.)			
		7°	10°	15°	20°
Density	5	3·2	3·0	$3{\cdot}0_5$	3·1
(gm.atoms/litre)	14	$2{\cdot}7_5$	2·8	$2{\cdot}9_5$	$3{\cdot}0_5$

The only direct measurements in this region which are available from other sources are those of Eucken (1916) at 18° and 22° K. for a concentration of 9.3 gram atoms per litre, which give a value at both temperatures of 3·0 cal/deg.

Some specific heat measurements were made below 7° K. but these are not quoted as they are considered unreliable on account of the phenomenon of bad heat exchange through the helium in the neighbourhood of the critical point. No effect of this nature took place during the expansion because then the heat absorption was homogeneous throughout the whole volume of gas. In view of the fact that temperature equilibrium during the expansion was established in less than 20 seconds at each stage, it was considered that the thermal exchange between the gas, cylinder and wires was good and that poor thermal conductivity of the material of the cylinder could not be responsible for the effects noted above when heating the cylinder and contents after the expansion.

§ 5. DISCUSSION

Figure 3, giving the *yield* isotherms, provides all the information needed for the construction of an expansion liquefier. The data are represented in a somewhat different form in figure 5, in which " isoyields " are plotted as functions of starting pressure and temperature. The shaded areas indicate the regions of zero yield and yield above 100%.

An approximate formula for the (percentage) yield isotherms of figure 3 is

$$\text{Yield} = 5{\cdot}5\, p_{\text{atm.}}/T + 10(12 - T)$$

within the limits $p = 75$ to 150 atm. and $T = 10°$ to 12° K., which covers the region of greatest practical interest. This formula represents the yield isotherms to an accuracy of $\pm 2\%$ yield.

As can be seen from the diagrams, the yield increases considerably with pressure. A practical limit to the pressure is set by the dimensions of the expansion chamber and the connecting

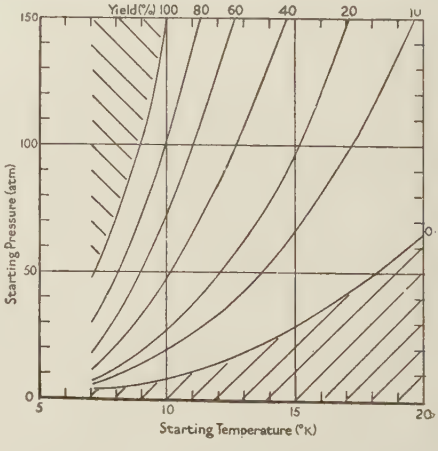

Figure 5. Yield diagram, curves of constant yield.

tube. We generally use pressures between 100 and 150 atm., and as very satisfactory yields can be obtained with these pressures at starting temperatures of the order of 10°–12°, which are easily obtainable, there does not seem to be any point in going to higher pressures. The question whether a combination of low temperature and low pressure, or higher temperature and higher pressures, is preferable, and under what circumstances, has previously been fully discussed by Simon (1940), and we can, therefore, refer to this paper.*

The form of the *diagram of state*, figure 4, presents no unusual features. It is of great interest, however, that at fairly low pressures volumes are shown which are considerably lower than that of the liquid at the boiling point. This is due to the fact that liquid helium is "blown up" by its considerable zero-point energy (Simon 1934) to a volume about four times that which would be predicted from the data of gas kinetics. The fact that at certain starting conditions the gas has a smaller volume than that of the liquid is also the explanation for the result that we can get yields of above 100% (measured as the degree of filling of the vessel).

The *entropy diagram* of helium has been published by Keesom (1942) for a range of temperatures and pressures. An extension of this range is possible by employing the values from the isentropic pressure–temperature curves obtained during the expansions made in the present experiments (figure 5). By this means isobars for pressures up to 160 atm. have been drawn on the entropy diagram; some figures are quoted in table 5. It should be noted that the entropy is given for 1 gram atom and that the zero of entropy has been taken as that of the liquid at the boiling point (4·22°) and 1 atm.

Table 5. Entropy of helium gas (cals/gm. atom °K.)

	Pressure (atm.)						
	160	140	120	100	80	60	40
Temp. °K. 7·5	—	—	—	—	−0·15*	+0·05*	0·45
10	0·20	0·30	0·40	0·50	0·75	1·10	1·65
15	1·45	1·60	1·85	2·10	2·50	3·05	—
20	2·70	2·95	3·20	3·60	4·00	—	—

* Slightly extrapolated.

The "Ideal" Yield

These extended data cannot be regarded as very accurate but are sufficient to permit calculations to be made as to the yields which would be obtained by the operation of an expansion in an ideal piston and cylinder process. For suppose that 1 gram atom of helium is compressed into a cylinder by a piston and that after an ideal adiabatic expansion to 1 atm. pressure has taken place the helium remains in the form of a fraction x as liquid and $(1-x)$ as gas at the normal boiling point. Then if the entropy of the compressed gas at the starting

* In 1939 Van Itterbeek published some data on the liquid yields of a small number of expansions which were considerably higher than in the data given by us. As one of the authors has shown (Simon 1940), there are valid reasons why Van Itterbeek's experiments might have been affected by erroneous determinations of the temperature. Later, Van Itterbeek (1943) published the results of some new determinations at conditions which resulted in a rather low yield; they agree with our values within the limit of error. It should be added that we have now made more than 1000 expansions at the Clarendon Laboratory, in most of which a rough check on the yield was taken, and that we have never found any disagreement with the results of our diagram.

conditions is S_i and those of the liquid and gas at the boiling point are S_l and S_g respectively, we have, since the expansion is an isentropic process,

$$S_i = x S_l + (1-x) S_g.$$

Now if we put $S_l = 0$, then $S_g = 4.65$ entropy units and we have

$$x = 1 - S_i/4.65.$$

To express this as "yield" as defined previously it is necessary to compare the volumes occupied by a fraction x of 1 gm. atom of liquid with that of 1 gm.atom of gas at the starting conditions used. This latter would be the volume of the expansion chamber in a practical liquefier.

Since the atomic volume of the liquid is 32 cm^3, the volume occupied by x gm.atoms is $32x$ cm^3 and if the volume occupied by 1 gm.atom of gas at the starting conditions is V_i then the yield for an ideal expansion is

$$Y_{id} = 32x\,100/V_i\,\% = (32/V_i)(1 - S_i/4{\cdot}65)100\,\%.$$

From this expression it is found that the ideal yield (Y_{id}) may be greater than 100% in the case of good starting conditions for the reason already mentioned, namely that the atomic volume of the compressed gas is very considerably less than that of the liquid. In a practical apparatus of course the maximum yield is 100% as any surplus evaporates at once in the connecting tubes.

It is interesting to compare the observed yields with these ideal yields for given starting conditions. In figure 6 are plotted the values of the ideal yield as calculated above and the observed yield, for starting temperatures of 10°, 15°, 20° K. Naturally the observed yield approximates to the theoretical yield at lower starting temperatures and higher pressures. It is, however, interesting to see how high a percentage of the ideal yield can actually be obtained with such a simple arrangement, about 60% when starting from the usual pressures and temperatures. There are two reasons: firstly, the heat capacity of the containers is practically negligible in comparison with that of the working gas—we have the advantage of working with "mathematical" walls; secondly, pressures as low as 100 atm. are very high "reduced" pressures for helium, as its internal pressure is of the order of 20 atm.; thus when working with helium we have, at 100 atm. pressure, conditions corresponding to about 10 000 atm. pressure for nitrogen, which has an internal pressure about 100 times as great.

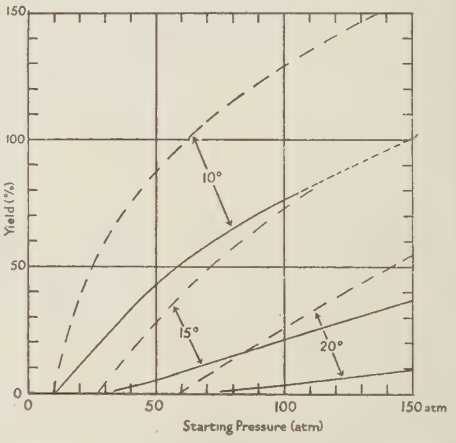

Figure 6. Comparison of ideal and observed yields from expansion method for helium liquefaction.

— — — Ideal yield of cylinder and piston.
——— Observed yield of expansion method.

The data already given enable us to calculate the amount of gas leaving the apparatus during an expansion, which has to be taken up by the gasometer. No diagrams have been prepared, but it should be mentioned that under average working conditions, say 100 to 150 atm. and 10–12°, about half the gas leaves the apparatus during the expansion.

As has been indicated in earlier work (Simon and Ahlberg 1933), an improvement of the yield can be obtained by making use of the Joule-Thomson effect. Our data on the equation of state have been used to calculate the Joule-Thomson inversion curve which is found to be in quite good agreement with the direct experiments of Zelmanov (1940). A calculation shows that in general the yield from a simple expansion is so high that the gain which would result from using the Joule-Thomson effect as well would not be worth the complication of the apparatus and technique which would be necessary.

For the larger expansion apparatus which we are now contemplating at the Clarendon Laboratory, giving a yield of one or more litres per expansion, the position may however be different, and we are studying this matter at the present moment. We shall also postpone a discussion on the efficiency of the method from the point of view of consumption of liquid hydrogen until these larger pieces of equipment are in operation.

REFERENCES

Cooke, A. H., Rollin, B. V., and Simon, F., 1939, *Rev. Sci. Instrum.*, **10**, 251.
Eucken, A., 1916, *Verh. dtsch. phys. Ges.*, **18**, 4.
Keesom, W. H., 1942, *Helium* (Amsterdam), p. 247.
Mendelssohn, K., 1931, *Z. Phys.*, **73**, 494.
Scott, R. B., and Cook, J. W., 1947, *Phys. Rev.*, **72**, 161.
Simon, F., 1932 a, *Z. ges. Kaelte-Ind.*, **39**, 89 ; 1932 b, *Phys. Z.*, **34**, 232 ; 1934, *Nature, Lond.*, **133**, 529 ; 1935, *Proc. Roy. Instn.*, **28**, 155 ; 1936, *Proc. 7th Int. Congr. Refrig.*, **1**, 367 ; 1937, *Physica*, **4**, 886 ; 1940, *Ibid.*, **7**, 502.
Simon, F., and Ahlberg, J. E., 1933, *Z. Phys.*, **81**, 817.
Simon, F., Cooke, A. H., and Pearson, N., 1935, *Proc. Phys. Soc.*, **47**, 678.
Van Itterbeek, A., 1939, *Physica*, **6**, 728 ; 1943, *Ibid.*, **10**, 90.
Zelmanov, J., 1940, *J. Phys. U.S.S.R.*, **3**, 343 ; 1944, *Ibid.*, **8**, 135.

Penetration of Magnetic Field into Superconductors: I. Measurements on Thin Cylinders

By M. Désirant and D. Shoenberg
Royal Society Mond Laboratory, Cambridge

MS. received 13 *December* 1947

ABSTRACT. Absolute values of the penetration depth λ of a magnetic field into a superconductor at different temperatures can be obtained from the relative values indicated by measurements on colloids, if $\Delta\lambda$, the difference between λ at a variable and at a fixed temperature, is known. Various methods of measuring $\Delta\lambda$ are briefly reviewed, and a detailed account is given of one particular method in which $\Delta\lambda$ is deduced from the changes of susceptibility of thin cylinders with temperature. The changes found for mercury cylinders were, within experimental error, inversely proportional to the radii as simple theory demands, and the temperature variation was consistent with that to be expected from the colloid results. The absolute value of λ at 0° K. is estimated as $7{\cdot}6\times10^{-6}$ cm. In the case of tin the values of $\Delta\lambda$ measured by the present method were in rough agreement with those of other methods, but since no colloid results were available, the absolute value of λ remains undetermined. The mercury results are discussed also in relation to critical field measurements on thin films. Some preliminary results bearing on the possible dependence of λ on magnetic field are mentioned ; it is concluded that λ does not vary appreciably in fields up to half the critical value.

§ 1. INTRODUCTION

WHEN a superconductor is in a magnetic field, currents flow on its surface in such a way as to keep the magnetic field out of the interior of the superconductor. These currents require a certain depth in which to flow, and this is also the depth to which the applied magnetic field penetrates the superconductor. If the size of the superconductor is large compared with the penetration depth λ, it behaves to a close approximation as if it had zero magnetic permeability or diamagnetic susceptibility $1/4\pi$. If, however, the size is comparable to or less than λ the superconductor has a weaker diamagnetism.

In the phenomenological theory of F. and H. London (1935) the penetration is described by the differential equation

$$\nabla^2 H = H/\lambda^2 \qquad \ldots\ldots(1)$$

and λ is given in terms of the number, n, of superconducting electrons per unit volume, their effective mass m, and their charge e, by

$$\lambda^2 = mc^2/4\pi ne^2. \qquad \ldots\ldots(2)$$

Although the detailed form of penetration law predicted by (1) has not yet been proved experimentally, equation (2) shows the theoretical importance of λ, in giving the ratio m/n for the superconducting electrons.

The first direct experimental evidence about λ came from measurements of the magnetic properties of small mercury particles in colloids (Shoenberg 1940) and showed that λ was of order 10^{-5} cm. and increased rapidly as the transition temperature was approached. Similar evidence came from measurements of the critical fields of thin mercury films (Appleyard *et al.* 1939), though the interpretation in this case involved certain additional assumptions about the thermodynamics of the destruction of superconductivity and was therefore less certain. The colloid results, though indicating the order of magnitude of λ, could not give a precise absolute estimate since the average particle size was not accurately known, and even if it were, an absolute estimate would involve assuming the truth of (1); they did, however, give a fairly accurate measure of the variation of $\lambda(T)/\lambda(T_0)$ with temperature T, where T_0 is a fixed temperature. If it were possible to measure also $\lambda(T)-\lambda(T_0)$, which we shall denote by $\Delta\lambda$, the combination of such measurements with those of $\lambda(T)/\lambda(T_0)$ would at once give the absolute size of λ.

Fortunately, several methods are possible for measurement of $\Delta\lambda$, and we shall indicate three which have been tried successfully :

(1) The diamagnetic susceptibility χ of a long cylinder of radius r much larger than λ, should be slightly less than the value $\chi_0(=1/4\pi)$ for r infinite. As is obvious from elementary considerations, and also follows from the appropriate solution of (1), we should have

$$\chi/\chi_0 = 1 - 2\lambda/r, \qquad \ldots\ldots(3)$$

and if r is of the order 10^{-3} cm., $2\lambda/r$ should be of order 2%. In principle, accurate measurement of χ should give λ absolutely, but this is very difficult in practice, and, as will be explained later, only relative changes of χ as the temperature is varied can be measured with sufficient accuracy. If we denote $\chi(T_0)-\chi(T)$ by $\Delta\chi$, we have in fact

$$\Delta\chi/\chi \simeq \Delta\chi/\chi_0 = 2\Delta\lambda/r, \qquad \ldots\ldots(4)$$

and so accurate measurements of $\Delta\chi/\chi$ will give $\Delta\lambda$ absolutely. This method

should work also with thin superconducting plates, but some preliminary experiments showed that the results were very sensitive to slight non-parallelism of the plate and the field, and the geometry of the measuring apparatus will have to be improved before reliable results on plates can be obtained. A full account of these experiments will be given in the present paper; a preliminary note has already been published (Désirant and Shoenberg 1947).

(2) The mutual inductance of two coils wound on a superconducting core should decrease slightly as the temperature is lowered, owing to the decrease of λ, and the change should be proportional to $\Delta\lambda$. This method was tried by Casimir (1940), but owing to a technical complication the experiment appeared to give much less temperature variation of $\Delta\lambda$ than was to be expected from the colloid results. A repetition of the experiment, avoiding the technical complication, has been made by Laurmann and Shoenberg and has confirmed the validity of the colloid results, and has also given interesting evidence for anistropy of penetration depth in single crystals. This work will be fully described in the second paper of this series; a preliminary note has already been published (Laurmann and Shoenberg 1947).

(3) Pippard (1947) has used an R.F. method which measures effectively the difference between λ in the superconducting state, and the skin depth δ_n of ordinary eddy currents when superconductivity has been destroyed by a magnetic field. The value of δ_n is not accurately known, but for tin it is almost certainly independent of temperature, so that measurements of $\lambda - \delta_n$ at various temperatures give $\Delta\lambda$ as a function of temperature; the results (which were in fact the first for tin) agree well with those of the other two methods. For mercury, however, δ_n varies with temperature, so that the method cannot be used to give $\Delta\lambda$ until a complete theory of the skin effect at high frequencies has been developed.

Further work is in hand to extend and improve the colloid method of studying λ, and also to investigate the validity of the London's penetration law (equation (1)) and to look for a possible field dependence of λ. This will be dealt with in later papers in this series.

§ 2. EXPERIMENTAL DETAILS

(i) *Method of Measurement*

The method of measuring susceptibility was the same in principle as that used in the colloid experiments, but considerable improvements in sensitivity and accuracy were necessary before it was suitable for the present purpose. An account of these improvements was given at the Physical Society's conference in 1946 (Shoenberg 1947), and only those features of the method important for the present purpose will be described in detail. The principle of the method is to displace the specimen smartly in a uniform magnetic field from the centre of one coil to the centre of a similar oppositely wound coil, connected in series with the first and a ballistic galvanometer. The small change of flux linkage produced by the movement, if the specimen is magnetized, then gives a galvanometer deflection proportional to the magnetic moment of the specimen; two coils, rather than one, are used to minimize the disturbing effects of any fluctuations of current in the solenoid producing the uniform magnetizing field.

The main improvements introduced for the present experiments were (i) to immerse the coil system in liquid helium (instead of liquid nitrogen as in the

colloid experiments) thus enabling a greater number of turns to be used without increasing the circuit resistance, (ii) to use photoelectric amplification of the galvanometer deflection, thus increasing the deflection about 100 times, and (iii) to use a null method in which the magnetic moment of the specimen is compensated by the opposite magnetic moment of a small current in a 5-turn coil surrounding it. The overall sensitivity of the apparatus was about 3×10^5 mm. per C.G.S. unit of uncompensated magnetic moment, and the zero instability was of order 1 mm. in low magnetic fields and of order 1 cm. in a field of 300 gauss.

In order to understand how the measurements were actually carried out we shall now describe the null method in greater detail. As shown in figure 1, the current in the 5-turn coil is taken from across a fixed resistance a in the solenoid circuit and is therefore a fraction $a/(R+a+b)$ of the solenoid current, where R is the resistance in the decade box which controls the fraction, and b the resistance of the 5-turn coil and its leads. When the decade box is set so that the magnetic moment of the specimen is compensated, we have

$$Aai/(R+a+b) = \chi V k i, \quad \ldots\ldots (5)$$

where χ is the susceptibility of the specimen defined as I/H, V is its volume, k the field per unit current of the solenoid, i the solenoid current, and A the area turns of the 5-turn coil. Thus independently of the magnetic field-strength, the value of χ is inversely proportional to $R+a+b$. Our conditions were such that R was a few hundred ohms when the specimen was superconducting, while a was about 5 ohms and b about 1 ohm. As the liquid helium fell, the resistance of the leads and, therefore, b increased by about 0·3 ohm, and this change was allowed for where its effect was more than 0·1%.

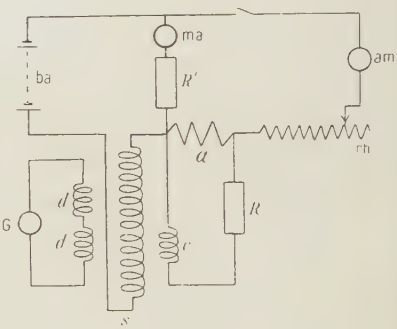

Figure 1. Schematic circuit diagram.

ba	80 volt battery supply.
ma	milliammeter.
am	ammeter.
G	galvanometer system.
rh	rheostats controlling current in *s*.
s	long solenoid ; 92·4 gauss/amp.
R'	resistance box controlling compensating current of earth's vertical field.
R	resistance box controlling current in *c*.
d d	multi-turn coil in 2 opposite halves (22 000 turns in each h[illegible] located symmetrically at centre of *s*.
c	5-turn coil movable from top to bottom half of *d*.
a	fixed resistance (5·2 ohm).

It will be noticed that equation (5) assumes implicitly that the whole magnetic moment of the specimen is due to the solenoid field. In practice there are two sources of magnetic moment independent of i; first the earth's vertical field is present in addition to the solenoid field, and secondly there may be small residual moments due either to ferromagnetic impurities or to frozen-in moments arising from previous magnetization cycles of the superconductor. Ferromagnetic effects may be very nearly eliminated by a suitable cycle of operations above the transition temperature of the superconductor; it was found that if a negative field of order 1000 gauss was switched on and off an appreciable negative remanence was obtained and this could then be eliminated by switching a positive field of about 300 gauss on and off. Provided no negative fields were used and positive fields did not exceed 300 gauss the remanence remained zero subsequently. Frozen-in moments were eliminated by always

warming the specimen above its transition temperature before a new series of measurements was started. Finally the earth's vertical field was compensated as well as possible by passing through the solenoid an additional current which was not controlled by the main rheostats and did not pass through the resistance a or the ammeter. This compensation was achieved by making the specimen superconducting and adjusting R' (figure 1) until with no current in a the deflection was zero for pulling the specimen.

The limitation to complete elimination of the various effects just discussed was the zero instability of the galvanometer. Since it was not possible to detect reliably deflections smaller than about 1 mm., appreciable errors could still be caused where the measurement was in very low solenoid fields. Suppose that the residual uncompensated effects are such as would correspond to a magnetic moment of the specimen x (which by itself would give a deflection comparable to the zero instability) then equation (5) must be replaced by

$$Aa/(R+a+b)=\chi Vk+x/i \qquad \ldots\ldots(6)$$

and we see that such uncompensated effects can be allowed for by plotting $1/(R+a+b)$ against $1/i$ and extrapolating to zero $1/i$. This was in fact always done, and as will be seen from the examples shown in figure 2, a linear plot is indeed obtained; the value of $1/(R+a+b)$ for zero $1/i$ is proportional to the true value of χ, and the slope of the graph is a measure of x, the uncompensated extraneous effect. Confirmation of the validity of this procedure was obtained by deliberately increasing x (by deliberate uncompensation of the earth's field) and as can be seen from figure 2 a steeper graph is obtained but still passing through the same point on the axis of $1/(R+a+b)$. In the actual measurements we always made x as small as possible, and it is satisfactory that the linear plots were all nearly horizontal and about as often with positive as with negative slopes.

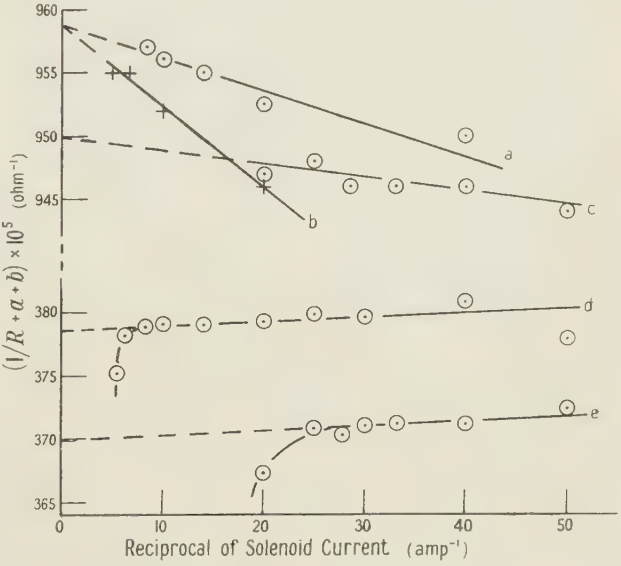

Figure 2. Illustrating extrapolation method of deducing true value of $1/(R+a+b)$.

(a) S5 : 2·16° K., (b) S5 : 2·16° K., but earth's vertical field slightly uncompensated, (c) S5 : 3·649° K., (d) H5 : 4·044° K., (e) H5 : 4·127° K.

A correction for paramagnetism of the specimen mounting has to be added to each intercept on the $1/(R+a+b)$ axis. This is 15·2 for (a) and (b), 9·0 for (c), 9·9 for (d) and 9·6 for (e). The turning down of the curves (d) and (e) corresponds to the falling off of the susceptibility as the field approaches the critical field.

The exact setting of R to give zero galvanometer deflection proved rather difficult owing to the appearance of "double kicks" close to the balance position. These "double kicks" arise from the fact that the galvanometer has a finite period and so does not provide completely effective integration of the E.M.F.S. developed in the coil. Even when the

net moment of the specimen and its surrounding coil is zero, this zero moment is obtained effectively as the sum of slightly positive and slightly negative contributions (due to the detailed geometry of the arrangement), and so the galvanometer gets impulses first one way and then the other.

The exact "profile" of the double kick corresponding to the balance point is difficult to assess, and it was found that the best accuracy could be obtained by interpolation, noting the galvanometer deflections for several values of R definitely below and above the balance value, and plotting the deflections against $1/(R+a+b)$. To reduce the effect of zero instability several readings were taken for each value of R and an average taken. A typical graph is shown in figure 3, and it will be seen that the value of $1/(R+a+b)$ corresponding to zero deflection can be assessed with an accuracy of a few parts in a thousand. The precision increases of course as the magnetic moment, and hence the uncompensated galvanometer deflections, become larger, though a limit is reached when the zero instability begins to grow with the applied field.

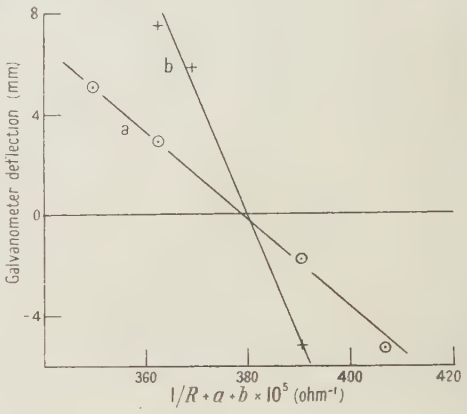

Figure 3. Illustrating interpolation of $1/(R+a+b)$ to zero galvanometer deflection. H5, 4·044° K. (a) solenoid current 20 ma., (b) 50 ma. The interpolated values appear as two of the points on (d) of figure 2.

As can be seen from equation (6) our procedure finally gives a value of $\chi Vk/Aa$, but since k and A could be determined with an accuracy only of order 1% and V only with an accuracy of order 5% (see below), the method is not suitable to give absolute values of χ with sufficient accuracy to measure the small deviation from χ_0 (see equation (3)). Moreover, equation (6) requires slight correction, if, as was the case in most of our measurements, the specimen is appreciably longer than the 5-turn coil; the sensitivity of the double coil method falls off if the specimen does not move exactly from the centre of one coil to the centre of the other, and since evidently this cannot be true for all points of a long specimen, the specimen and compensating coil produce different effects per unit magnetic moment if they occupy different lengths. This correction can be estimated by auxiliary experiments and amounts to nearly 10% for the longest specimens. Fortunately all these uncertainties are irrelevant if we are interested only in relative changes of χ with temperature, for $\Delta\chi/\chi$ does not involve the calibration constants at all, provided that the temperature changes do not alter any of the constants. The only possibility of a change of calibration constants with temperature arose from possible slight movement of the Dewar vessel in which the coils were mounted as the helium vapour pressure was changed; such movement would have altered the relative positions of specimen and coils and hence the calibration constants, but auxiliary measurements showed that this effect was negligible. Thus the values of $\Delta\chi/\chi$ could be measured with an accuracy of a few parts in a thousand.

Since the measured value of χ includes the magnetic effects of the specimen mounting (mostly glass and distrene), it was essential to determine these separately, in case they too varied with temperature. This was done by measuring in a

field high enough to destroy superconductivity completely, and the residual effect was found to be paramagnetic, with an effective susceptibility (i.e. per unit volume of the superconductor) of the order of a few per cent of that due to the superconductor. It did indeed vary with temperature, roughly according to Curie's law, so that this correction was quite important; it has been made in all the results quoted below.

(ii) *Temperature Measurement*

All temperatures quoted were deduced from the vapour pressure of the helium bath by means of the 1932 Leiden scale.

(iii) *The Specimens*

The specimens were prepared by filling fine capillaries with spectroscopically pure mercury or tin. In order to obtain enough total volume a large number of these filled capillaries were bundled together so that they were parallel to each other; and separated from each other by about 10 radii. In one case (H2) the necessary volume was obtained by winding a long length of capillary into a spiral with the turns well separated. In the case of the spiral (H2) and of one of the bundles (S5) the field was perpendicular to the length of the superconductor. It should be noted that with this arrangement χ_0 is $1/2\pi$ instead of $1/4\pi$, but equation (3) is unaffected. The gain in sensitivity is offset by the fact that fields only half as large can be used before superconductivity begins to be destroyed. Full magnetization curves of H2 and S5 were taken for the purpose of studying the intermediate state; the results of these measurements are discussed elsewhere (Désirant and Shoenberg 1948). In the case of the other two specimens (H5 and H6) the field was parallel to the cylinder lengths. Details of the specimens are summarized in table 1. The radii quoted were worked out from the values of $\chi Vk/Aa$ deduced from the susceptibility measurements after making due allowance for the various corrections mentioned above, and assuming an approximate value of λ in using equation (3) for χ. This was considered more accurate than direct measurement, since measurements with a travelling microscope were difficult, and weighing was also difficult in view of the large numbers of capillaries and the small masses involved. The radii deduced in this way did in fact agree with those estimated by travelling microscope well within the limits of error of the latter method. The microscope readings were useful in indicating the order of magnitude of the variation of radii between the individual capillaries; the estimated mean deviation was 7% of the radius for H5 and H6, and about 20% for S5. Strictly speaking the radius deduced from V is $(\overline{r^2})^{\frac{1}{2}}$ while that required in deducing $\Delta\lambda$ from the experiment is $\overline{r^2}/\overline{r}$, which is slightly different if the mean deviation of r is taken into account. Assuming a Gaussian distribution of the radii, it is easily shown that the difference is negligible for H5 and H6, but amounts to 3% for S5. The corrected value of r for S5 is shown in table 2.

§ 3. EXPERIMENTAL RESULTS

For each specimen measurements were made at several temperatures from close to the transition temperature (T_c) down to about 2·1° K., and from the changes of $1/(R+a+b)$ which is proportional to χ, values of $\lambda(T)-\lambda(2{\cdot}1^\circ\text{K.})=\Delta\lambda$ were deduced. The exact rather than the approximate form of equation (4) was used for this purpose, using our final estimate of $\lambda(2{\cdot}1^\circ\text{K.})$ to correct χ to χ_0

Table 1

Specimen	Radius r cm. $\times 10^4$	Description	$T°$ K.	$1/(R+a+b)$ $\times 10^5$	$\Delta\lambda$ cm. $\times 10^6$	$\Delta\lambda/\lambda(2{\cdot}1)$ from colloids
H2	22·8	Pyrex capillary	2·14	303·7±0·5		
		spiral filled with	3·691	302·1±0·5	6·1±3	0·52
		with mercury.	3·968	300·6±0·5	11·9±3	1·25
		About 6·4 mg.	4·046	300·6±1·0	11·9±6	1·83
		HS.10 763	4·085	296·9±1·5	25·5±8	2·34
H5	15·55	Bundle of 98	2·16	396·4±0·5		
		pyrex capillaries.	3·928	392·7±0·5	7·2±2	1·03
		Mean length	4·000	391·0±0·5	10·5±2	1·45
		18·3 mm.	4·088	387·4±1·0	17·5±3	2·38
		About 19 mg.				
		HS.11 023.	1·72	396·9±0·5		
			(2·14)	(396·8±0·5)		
			3·699	393·8±1·0	5·9±3	0·52
			4·046	390·8±0·5	11·6±2	1·82
			4·046	391·8±1·0	9·7±3	1·82
			4·127	384·6+1·0 −15·0	23·8+31 −3	3·97
			(2·14)	(394·8±0·5)		
			3·19	394·1±0·5		
			4·044	388·5±0·5	12·3±2	1·82
			4·127	379·5±0·5	29·8±2	3·97
			4·045	266·7±0·5		
H6	9·03	Bundle of 198	4·129	255·8+5·0 −0·5	See below	
		pyrex capillaries.				
		Mean length				
		18·6 mm.	(2·14)	277·5±0·5		
		About 13 mg.	3·19	276·6±0·5		
		HS.11 023	4·000	270·1±1·0	11·8±3	1·45
			4·048	269·4±1·0	12·9±3	1·87
			4·085	265·0±0·5	20·0±2	2·33
			(4·129)	258·7+6·0 −1·0	30·1±2 −11	4·04

Notes to table 1.

(i) The different series of values represent experiments on different occasions ; the slightly different values of $1/(R+a+b)$ at 2·1° K. in different series are due to slight differences in the exact geometry of the specimen relative to the measuring apparatus. The values of $1/(R+a+b)$ for different specimens are not exactly proportional to the masses, since different coils c were used on different occasions.

(ii) Of the two readings at 4·046° K. on H5, the first was taken before the low temperature reading and the second after.

(iii) The first of the readings on H5 at 4·127° K. has such large limits of error that it has been ignored in the calculations.

(iv) The first series of readings on H6 was accidentally cut short, but the difference between the 4·045° K. and 4·129° K. readings has been transferred to the next series to give an estimate of $\Delta\lambda$ at 4·129° K.

Table 2

Specimen	Radius r cm. $\times 10^4$	Description	$T°$ K.	$1/(R+a+b)$ $\times 10^5$	$\Delta\lambda$ cm. $\times 10^6$	$\Delta\lambda$ cm. $\times 10^6$ (Pippard)	$\Delta\lambda$ cm. $\times 10^6$ (Laurmann and Shoenberg)
S5	17·8	209 pyrex	2·16	974·0±1			
		capillaries	3·009	971·4±2	2·3±2	1·2	2·4
		in 5 layers,	3·555	965·1±1	8·1±1	6·2	7·5
		field applied	3·598	963·2±2	9·9±2	7·3	9·2
		transversely.	3·649	958·6±2	14·0±2	9·9	12·3
		Mean length	3·667	949 ±8	22·7±7	11·2	13·9
		7·9 mm.					
		About 11 mg.					
		JM.12 966					

by means of equation (3)*. The results of the various series of measurements for mercury and tin are collected in tables 1 and 2; the errors indicated as ± are rough estimates of probable error based on the individual extrapolations (similar to those of figure 2) which yield the appropriate values of $1/(R+a+b)$. In a few cases it was not possible to take accurate readings at 2·1° K., and in such cases an estimated value of $1/(R+a+b)$ at 2·1° K. has been put in the table for the purpose of calculating $\Delta\lambda$. These estimates (shown in brackets in table 1) were made from the value at the nearest temperature used, on the basis of the colloid results assuming an approximate absolute value of λ, or by interpolation, and the error involved is small, since the λ–T curve is nearly flat over a wide range (e.g. below 3·7° K. for mercury).

The usual order of experiment was to measure at successively lower temperatures, and it was necessary to make sure that the observed changes of $1/(R+a+b)$ were genuinely due to changes of penetration depth rather than to some stray effect which was associated with the passage of time (e.g. falling of the liquid helium level in the Dewar vessel). For this purpose, in one experiment (on H5) the measurements at 4·048° K. were repeated after those at 2·1° K. had been taken; as can be seen from table 1, no significant difference was found, thus confirming that the observed changes were indeed only due to the temperature changes.

In order to derive an absolute value of λ for mercury our results must now be compared with those from the colloid measurements (Shoenberg 1940). From the latter we have derived values of $\Delta\lambda/\lambda(2{\cdot}1^\circ\text{K.})$ at each temperature used in the present experiments, and these are shown in the last column of table 1. The comparison assumes† that T_c for our specimens was the same (4·17° K.) as for the colloid specimen, but actually this assumption was not very carefully verified, since its importance was realized only later. From such few measurements of critical field as were made, however, it is unlikely that T_c differs from 4·17° K. by more than 0·01° K. The simplest method of deriving $\lambda(2{\cdot}1^\circ\text{K.})$ is to plot the observed values of $\Delta\lambda$ from the present experiments against those of $\Delta\lambda/\lambda(2{\cdot}1^\circ\text{K.})$ from the colloid results. This has been done in figure 4, and it will be seen that within the limits of experimental error the relation is a linear one. This confirms the validity of equation (4), since there is no systematic difference between the points for specimens of different radii, and also the consistency of the present results with the colloid measurements.

The slope of the best straight line through the points of figure 4 gives $\lambda(2{\cdot}1^\circ\text{K.})$ in absolute measure, and a least squares calculation using weights inversely proportional to the errors shown in table 1 gave $\lambda(2{\cdot}1^\circ\text{K.}) = 7{\cdot}9\times10^{-6}$ cm. with a standard deviation of $0{\cdot}3\times10^{-6}$ cm. Extrapolation to absolute zero by means of the colloid results then gives $\lambda(0^\circ\text{K.}) = 7{\cdot}6\times10^{-6}$ cm. This estimate may well be in error by a greater amount than indicated by the small standard deviation, since the calculation cannot, of course, allow for possible systematic errors in the colloid results, for possible differences in T_c between the present specimens and the colloid (which might introduce a systematic error) and for unsuspected systematic errors in the present experiments. In figure 5 the values of $\Delta\lambda$ are

* In the case of tin, $\lambda(2{\cdot}1^\circ\text{K.})$ was assumed to be 5×10^{-6} cm. for this purpose, but since the correction is only about ½%, the uncertainty in this assumption is unimportant.

† It is probable that for small changes of T_c, λ remains the same function of $T_c - T$, so if T_c is different for two specimens, the observed values of T must be adjusted in order to compare values of λ.

shown plotted against $\Delta T = T_c - T$, (assuming $T_c = 4{\cdot}17°$ K.) together with a graph of the colloid results assuming $\lambda(2{\cdot}1°\text{ K.}) = 7{\cdot}9 \times 10^{-6}$ cm. The broken-line curve comes from the results of Appleyard *et al.* (1939) which are discussed below.

The results for tin cannot be treated in the same way as those for mercury, since no colloid measurements are as yet available. They may, however, be compared with those of Pippard (1947) and with those of Laurmann and Shoenberg (1947). In making such a comparison due allowance must be made for the fact that S5 had a transition temperature $T_c = 3{\cdot}738°$ K. while the specimens of the other two experiments had $T_c = 3{\cdot}711°$ K., for each temperature of measurement of S5 we therefore show in table 2 the value of $\Delta\lambda$ obtained in each of the other two experiments at a temperature $0{\cdot}028°$ K. lower. It will be seen that except at the highest temperature (where owing to the limited range of fields available the accuracy was rather poor), the results agree fairly well with those of Laurmann and Shoenberg, but are a little higher than those of Pippard. It is possible that this discrepancy is associated with anisotropic effects, but it will be convenient to defer a detailed discussion of this point to paper II.

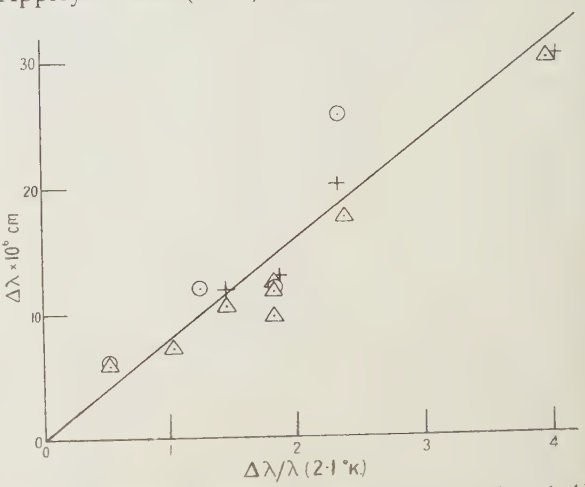

Figure 4. Relation between $\Delta\lambda$ from present work and $\Delta\lambda/\lambda$ deduced from colloid experiments. ⊙ H2, △ H5, + H6.

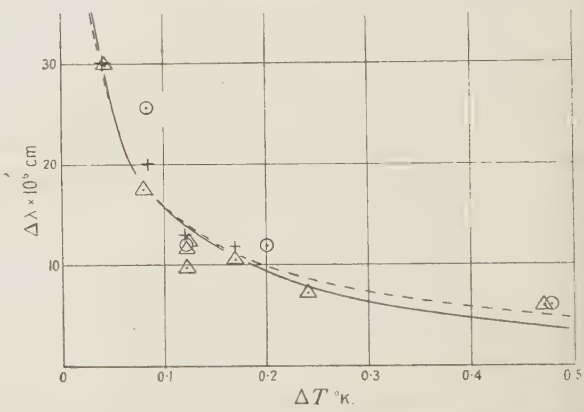

Figure 5. Relation between $\Delta\lambda$ and ΔT (assuming $T_c = 4{\cdot}17°$ K.). ⊙ H2, △ H5, + H6. Full curve deduced from colloids assuming $\lambda(2{\cdot}1°\text{ K.}) = 7{\cdot}9 \times 10^{-6}$ cm. Broken curve from thin film measurements of critical field explained in text.

§ 4. RELATION BETWEEN PENETRATION DEPTH AND CRITICAL FIELD

As has already been mentioned, information about penetration depth may be obtained also from the measurements of critical fields of thin mercury films by Appleyard *et al.* (1939). The interpretation is complicated by the necessity of allowing for a possible difference between the surface tensions α_n and α_s at a boundary between an insulator and the normal and superconducting phases respectively. If the film thickness is not too small, Ginsburg (1945) has shown thermodynamically that the critical field h of a film of thickness $2r$ is given by

$$h/H_c = 1 + (\lambda + \beta)/r, \qquad \ldots\ldots(7)$$

where $$\beta = 8\pi(\alpha_n - \alpha_s)/H_c^2 \quad \ldots\ldots (8)$$

and H_c is the critical field of the bulk metal. Equation (7) is valid, however, only if $(\lambda+\beta) \ll r$, while most of the thin films of Appleyard *et al.* had $r \lesssim \lambda+\beta$. For such thin films the thermodynamic theory can be developed only by assuming a detailed form of penetration law, and Ginsburg in fact assumed the exact validity of the Londons' law (1); he assumed further that the concept of a surface tension still applies even when $r \lesssim \lambda+\beta$, which would seem to require some justification. On the basis of these assumptions Ginsburg calculated from the thin film data a curve of λ against T which disagrees seriously with that of figure 5. The lack of agreement suggests that Ginsburg's assumptions are probably unjustified.

The analysis of their results made by Appleyard *et al.* suggested that within experimental accuracy $h\,H_c$ was a function of a single temperature dependent parameter divided by r. They identified this parameter with the penetration depth λ, but in view of the complications just discussed, it is safer to suppose that it has some other meaning and we shall denote it by λ'; for thick films, for instance, λ' should be the same as $\lambda+\beta$. If we assume $\lambda'(2{\cdot}1^\circ\text{K.}) = 10{\cdot}8\times10^{-6}$ cm.*, we find that the curve of $\Delta\lambda' = \lambda'(T) - \lambda'(2{\cdot}1^\circ\text{K.})$ against ΔT (the broken line of figure 5) agrees fairly well with the colloid curve of $\Delta\lambda$ against ΔT. This suggests that $\lambda'-\lambda$ is fairly independent of temperature, and if, speculatively, we identify $\lambda'-\lambda$ with β, this result might be taken to mean that β is about 3×10^{-6} cm. at high and low temperatures, rising to about 4×10^{-6} cm. at $3{\cdot}7^\circ$ K.

§ 5. POSSIBLE FIELD DEPENDENCE OF λ

An interesting possibility, first suggested by Ginsburg (1947), is that the penetration depth may depend on the strength of the applied magnetic field. Most of our measurements were made at low fields, and up to about $\frac{1}{2}H_c$ there was certainly no appreciable effect of this kind. A few measurements were, however, made at higher fields and we did find that χ began to fall off appreciably; some typical curves of $\frac{1}{2}r\Delta\chi/\chi$ against H/H_c for H5 and H6 at $4{\cdot}05^\circ$ K. and $2{\cdot}16^\circ$ K. are shown in figure 6, and similar effects were found in longitudinal tin specimens. If these changes of χ are interpreted as due to changes of λ with field, the values of $\frac{1}{2}r\Delta\chi/\chi$ would represent those of $\lambda(H)-\lambda(0)$; since this quantity is greater for the thinner specimen H6 than for H5, this does not seem to be a satisfactory interpretation, though it should be emphasized that these measurements were not very accurate, and it is just possible that the differences between H5 and H6 are due to experimental error. Probably the observed effects are at least partly due to some

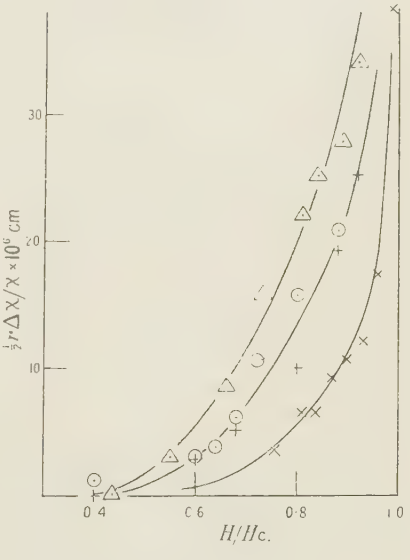

Figure 6. Relation between $\frac{1}{2}r\Delta\chi/\chi$ and H/H_c.
+ H5 $4{\cdot}046^\circ$ K. × H5 $2{\cdot}14^\circ$ K.
⊙ H5 $4{\cdot}047^\circ$ K., on another occasion.
△ H6 $4{\cdot}045^\circ$ K.

* Appleyard *et al.* gave $\lambda'(2{\cdot}1^\circ\text{K.}) = 12\times10^{-6}\pm2\times10^{-6}$ based on the values of h/H_c for their thickest films, so our assumption is not inconsistent with their results.

slight destruction of superconductivity starting at irregularities or at the ends of the cylinders. A similar effect was found by Laurmann and Shoenberg in their repetition of the Casimir experiment, and there the apparent increase of λ was always associated with the appearance of resistive losses. Although evidently this question requires further investigation, we may say from the present experiments that there is no appreciable increase of λ up to $\frac{1}{2}H_c$, and that for higher fields an increase cannot be excluded, though there is no proof of its existence.

It may be noted that if in fact λ does increase with field, this would invalidate the argument on which equation (7) is based, and would further complicate the interpretation of critical field measurements, such as those of Appleyard *et al.*

ACKNOWLEDGMENTS

We wish to thank Mr. A. B. Pippard for many helpful suggestions and discussions, and Mr. J. M. Lock for help in preparing the diagrams.

REFERENCES

Appleyard, E. T. S., Bristow, J. R., London, H., and Misener, A. D., 1939, *Proc. Roy. Soc.* A, **172,** 540.

Casimir, H. B. G., 1940, *Physica*, **7,** 887.

Désirant, M., and Shoenberg, D., 1947, *Nature, Lond.*, **159,** 201 ; 1948, *Proc. Roy. Soc.* A, in press.

Ginsburg, V., 1945, *J. Phys. U.S.S.R.*, **9,** 305 ; 1947, *Ibid.*, **11,** 93.

Laurmann, E., and Shoenberg, D., 1947, *Nature, Lond.*, **160,** 747.

London, F. and H., 1935, *Proc. Roy. Soc.* A, **149,** 71.

Pippard, A. B., 1947, *Nature, Lond.*, **159,** 434.

Shoenberg, D., 1940, *Proc. Roy. Soc.* A, **175,** 49 ; 1947, *International Conference on Fundamental Particles and Low Temperatures*, Vol. II (Physical Society), p. 85.

The Rate of Growth of Current and the Behaviour of the Cathode Spot in Transient Arc Discharges

By K. D. FROOME

1851 Senior Student, Department of Physics, Imperial College, London

Communicated by G. P. Thomson; *MS. received* 25 *November* 1947

ABSTRACT. The factors are discussed which control the initial rate of increase of current in the arc-like discharge obtained when a condenser of several microfarads is discharged through a small tube containing rarefied gas. It is suggested that at higher pressures ionization probably proceeds " thermally ", but that at lower pressures ionization takes place by direct electron collision, the cathode spot having a negligible retarding effect except possibly at very low pressures. The current density of emission from the cathode spot is at all times enormous, appearing sometimes greater than 10^6 amperes per cm^2 and very seldom less than 10^5 amperes per cm^2 even for a discharge prolonged until it has the appearance of a normal arc. It is suggested, therefore, that the value (Druyvesteyn and Penning 1940) of the emission current density of about 10^4 amperes per cm^2 usually accepted for normal vacuum arcs is in error (Froome 1946, 1947). The rapid movement of the cathode spot and rate of growth of current exclude the possibility of the cathode emission being derived thermionically, while the very high current densities observed favour field emission.

§ 1. INTRODUCTION

ALTHOUGH the transient arc obtained by condenser discharge through a tube filled with gas at reduced pressure is widely used for high speed photography (for list of references see Henry 1944), a systematic study of the factors determining the growth of current seems to have been neglected. The discharge will be termed for convenience an "arc" since it needs, in common with a normal arc, a cathode spot for its maintenance, although it differs considerably in other respects from a normal arc, especially during its initial stages. In this work a condenser of a few microfarads, charged to some 360 volts, is connected directly across the tube, the discharge being started by applying a brief high-tension pulse to an electrode wrapped round the outside of the tube, adjacent the cathode. The discharge tube usually has an electrode spacing of about 18 mm. The paper consists of two parts : firstly the study of current rise when the impedance of the leads between condenser and tube is a minimum except for a small inductance in series with a small resistance included in the cathode lead for measuring purposes; secondly the study of the cathode spot by a simple Kerr cell technique, where sometimes a fairly large resistance has been added to the leads in order that the transition to a normal arc can be studied.

§ 2. THE RATE OF CURRENT RISE

Discussion will be limited to studies of times of the order of 10^{-7} second, since the effects of possible cathode vaporization and of impurities arising from this seem negligible in such times. It is not proposed, in this section, to trace the current rise above 100 amperes or so, although the current may rise to over 1000 amperes in a microsecond if the external impedances are kept very low.

To measure such times a cathode-ray tube is used on a repetitive system so that a fair sensitivity of Y-shift is obtained. This should not be less than 1 cm. shift for 30 v. applied; otherwise too much of the condenser voltage will be taken up in the measuring circuit. The trace is photographed with an F 3·5 lens. With the tubes and condenser voltages used there is a variable delay of the order of $\frac{1}{10}$ to 1 microsecond, occasionally as much as 100 microseconds, between the application of the triggering pulse and the start of the arc. Further, if a cathode spot does not form during this time, a glow discharge may strike, but not an arc. The probability of the formation of an unwanted glow discharge can be reduced by making the electrode area small, and the cathode of metal of low work function, or of mercury; this does not upset the discharge if an arc forms, for in this case ionization follows a narrow intense channel. Because of this delay, an independent linear time base is useless for measuring durations of 10^{-7} sec. or less unless the photographic writing speed of the cathode-ray tube is such that the current at any time in the discharge tube can be measured on a single trace. This demands a cathode-ray tube operating at an anode voltage of at least 5000, and a faster lens, implying too great a sacrifice of deflection sensitivity. Thus the method adopted was to allow the voltage (or a fraction of it) across the discharge tube to supply the X-deflection, and to record the rate of growth of current, and the current, on the Y-shift. If a double-beam tube is used these can be recorded simultaneously, but if a single beam tube is used, then two exposures must be superimposed.

This method was found to be very satisfactory, for once an arc starts, the relation between the potential difference across the discharge tube and the current or rate of

growth of current in it is always the same, so that the trace obtained, even after several thousand superimposed flashes, is quite sharp. The cathode-ray tube beam is turned to full brilliancy for a time a little longer than the duration of the discharge plus the variable delay already mentioned.

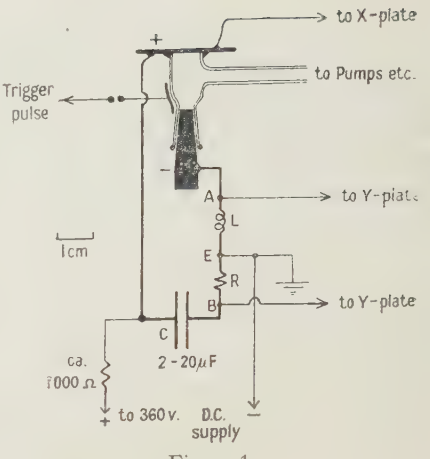

Figure 1.

Figure 1 shows a typical discharge tube and the measuring circuit employed for these current rise experiments. L is a small inductance (about 10^{-7} henry) in series with a small resistance R (about 1 ohm) in the cathode lead of the discharge tube. The junction of these, E, is earthed, so that the potential across L or R can be applied to the Y plate of the cathode-ray tube, and thus di/dt and i can be found if the values of L and R are known. Hence the area under a graph of dt/di against i gives a time scale, since

$$t = \int_1^i (dt/di)\, di.$$

The minimum detectable current is about 1 amp. and for convenience we shall measure time from this point. This method will resolve 10^{-8} second.

Figure 2 shows the recurrent single-sweep linear time-base and pulse generator, the time base portion being used in the second half of this investigation. It provides the triggering pulse to the discharge tube, as well as switching on the cathode-ray tube beam to full intensity for a time equal to that of the linear sweep. This can be varied between 3 and 10 000 μsec. in 8 steps. It is used on a VCR.97 with anode voltage of 2500, the most sensitive plates being used for Y deflection. The linear sweep is used for the set up of figure 1.

In figure 2, the thyratron V1, is used to trigger the whole sequence of events. It can be used as a slow relaxation oscillator, or triggered singly by a pulse applied through C2, or synchronized to a sub-multiple of the mains frequency by closing S1. This latter alternative is used when a large number of recurrent traces is needed, R8, R2 being adjusted for a repetition speed of about 10 per sec. Single triggering is used for the Kerr cell shutter investigations described later. When V1 has "fired", it triggers the thyratron V3, which discharges one of the time-base condensers C15–C22 at constant current through the beam tetrode V2, thus providing a single high-speed linear sweep for supplying the cathode-ray tube X-deflection if required. V2 should have a screen potential of about 400 v. in order that this may be large compared with the potential drop across V3 when in the conducting state. After V3 had fired, it was found that it would not recover until one of the tetrode screen decoupling condensers C6–C8 had been discharged. It was also found that for a GTIC thyratron the resistance R21 and small condensers C13 were needed to assist recovery. These should be as small as possible. It is thus apparent that the tetrode screen decoupling condenser C6–C8 must be of such a value as not to discharge appreciably during the linear part of the sweep—but must do so before V1 produces a further triggering pulse to V3.

During the time of linear discharge a small negative square-wave pulse appears across R22; this is amplified by V4, and the resulting positive square-wave pulse

fed to the cathode-ray tube grid through C31, thus turning this tube to full brilliance for the duration of the linear discharge. It can also be used to trigger the Kerr cell circuit described later. The thyratron V5 can be triggered after V3 through the variable delay network D2 by this positive pulse from V4, or it can be triggered before V3, the triggering of V3 then being delayed by the variable lag D1, depending on the position of the switch S2. When V5 fires, the condenser C33 is discharged through the primary of a small induction coil, thus producing the high

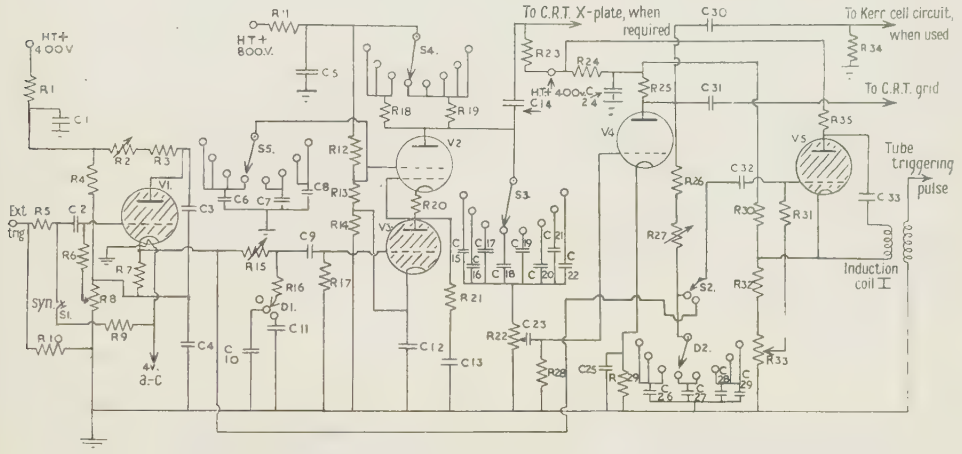

Figure 2.

Resistances (R)		Condensers (C)		Valves	
R1, 11, 14, 15, 17, 24, 25, 33	10,000 Ω	C1, 24	8 μF.	V1, V3, V5	Type GTIC
2	250,000 Ω	2, 3, 6, 9, 14, 19, 23, 29, 30, 31, 32	0·1 μF.	2	Type 6L6
3, 6	200,000 Ω	4, 7	0·5 μF.	4	Type 6J5
4	89,000 Ω	5, 8, 22	4 μF.		
5, 12, 13, 19, 31	100,000 Ω	10, 15, 27	0·001 μF.		
7, 16	1,000 Ω	11, 17, 28	0·01 μF.		
8	5,000 Ω	12, 25	20 μF.		
9	22,000 Ω	13	0·005 μF.		
10, 23, 28, 34	1 MΩ	16	0·003 μF.		
18	300,000 Ω	18	0·03 μF.		
20, 21	30 Ω	20, 33	0·25 μF.		
22	100 Ω	21	1 μF.		
26	50,000 Ω	26	0·0002 μF.		
27	3 MΩ				
29	500 Ω				
30	80,000 Ω				
32	4,200 Ω				
35	69,000 Ω				

tension pulse which finally triggers the discharge tube under investigation. The delay networks D1, D2, are needed to ensure that the discharge tube arc starts whilst the cathode-ray tube beam is at full brilliance. The 8-position switches S3, S4, S5, D2 are ganged.

Figures 3, 4, 5 show some experimental results for a tube of 18·5-mm. electrode spacing, connected across a condenser of 2 μF., initially charged to 360 v., at various pressures and natures of gas filling.

It is seen that at about 2 mm. Hg pressure there is a marked difference in the rates of current rise for air, helium and argon filling. With helium the current rises to 50 amp. in about 10^{-7} sec., whereas with air it takes about $2\frac{1}{2}$ times as long.

Even so, the speed with which the current increases is very great for both, suggesting that whatever is the emission process operating at the cathode, it can build up extremely rapidly. This emitting area or "cathode spot" will be discussed next, before attempting theoretical estimates of the current rise to be expected. It has not been found that the nature of the cathode has a significant effect on the current rise, provided measurements (such as the above) are made before extensive vaporization takes place from it. These results of figures 3–5 have been obtained

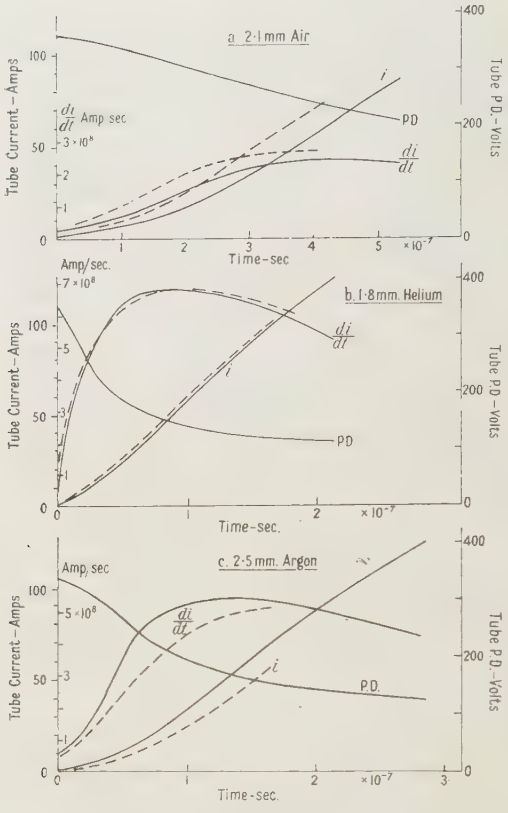

Figure 3.

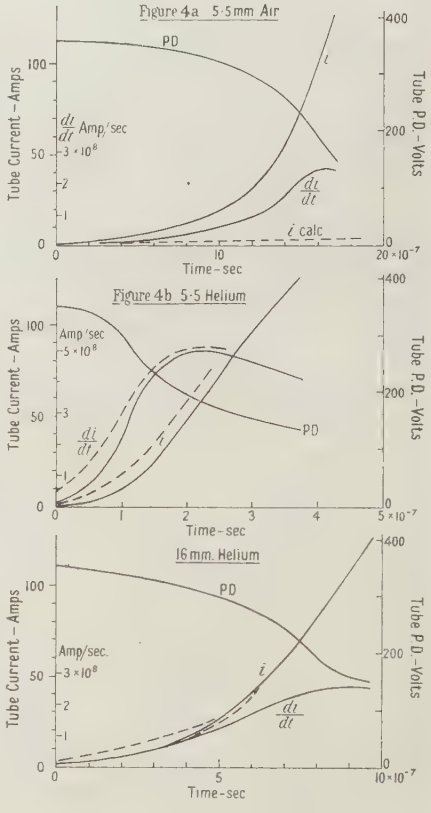

Figures 4 & 5.
Figure 4: 5·5 mm. Figure 5: 16 mm.

with a sodium cathode with enough lead added to render it sufficiently hard for machining on a lathe. Before use the protective layer of oxide which forms on the surface is removed, the cathode quickly inserted into the discharge tube, and the discharge run for some thousand flashes so that the cathode spot can further clean the cathode under it.

§ 3. THE BEHAVIOUR AND SIZE OF THE CATHODE SPOT

A study of the cathode spot during a transient condenser discharge is important for two reasons. Firstly, the nature of the cathode spot is liable to influence the rate of growth of current. Secondly, if the arc is prolonged by addition of a resistance of several ohms in the lead between condenser and discharge tube, until it has the characteristics of a normal vacuum arc, then the small size of the tube

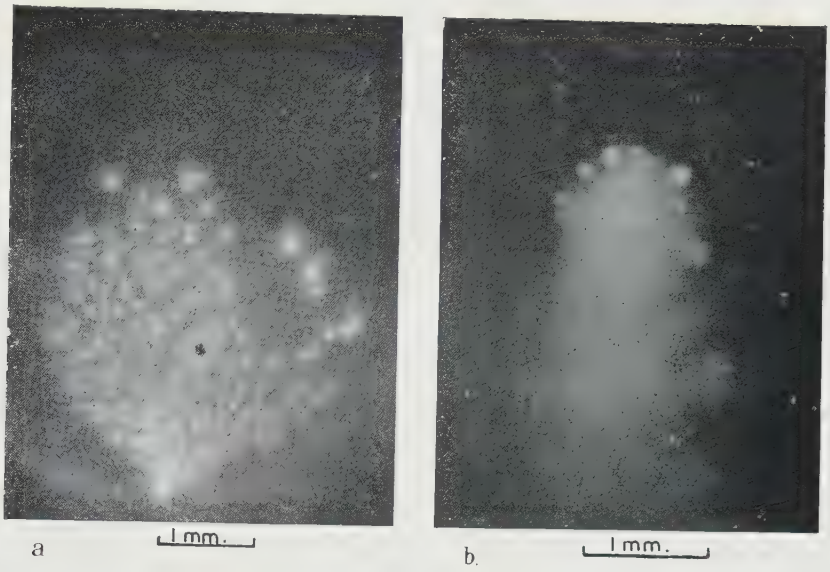

Figure 8.

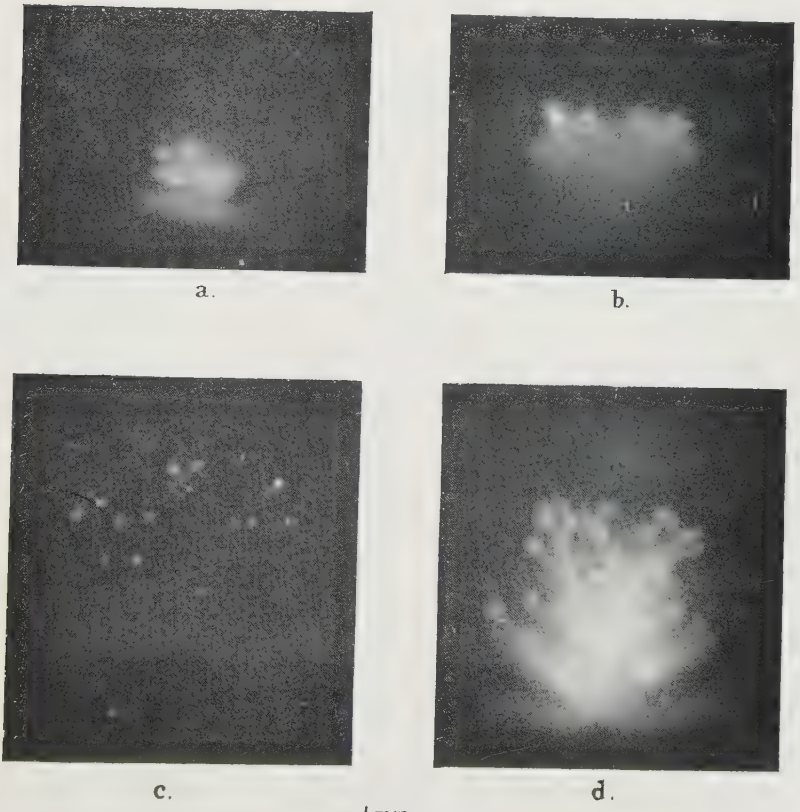

Figure 9.

To face page 428

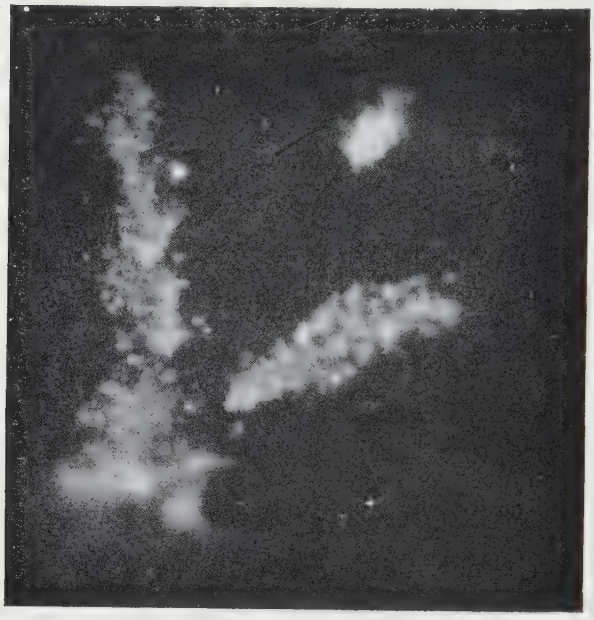

Figure 11a.

Figure 11b.

Figure 12a.

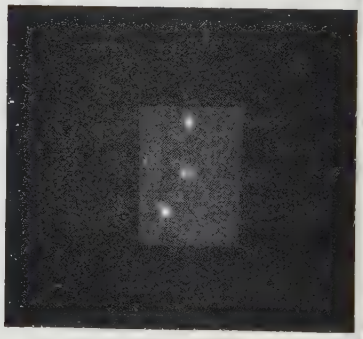

Figure 12b.

1 mm.

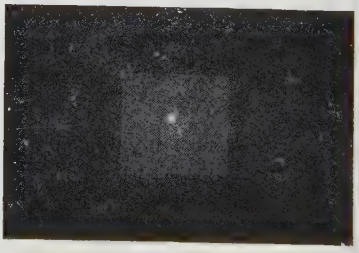

Figure 13.

enables the cathode spot to be studied under much better conditions than in a tube designed for continuous running at comparable currents.

A Kerr cell shutter has been used to take low power photomicrographs of the discharge-tube cathode at any stage during the condenser discharge. These are taken singly, on ciné film, and subsequently enlarged until the final overall magnification is about 20 diameters. The ciné film technique is of value when short exposures of moving objects are needed (Froome and Jarrett 1943, 1944).

Figure 6 shows the circuit diagram of the Kerr cell shutter, which is triggered via a delay circuit by the positive pulse from the amplifier valve V4. The optical arrangement for photographing a tube with a mercury cathode is shown in figure 7. In this particular tube the distance from the top of the cathode to the optical flat covering the tube was about 25 mm.

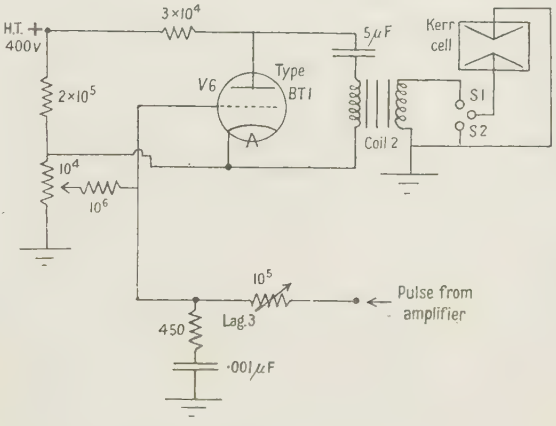

Figure 6.

When the thyratron V6 (figure 6) is triggered, the 5-μF. condenser is discharged into the primary of induction coil 2. The resulting high tension developed across the secondary then sparks over the spark gap S1, opening the Kerr cell shutter until S2 sparks over, when the shutter closes once more. The spark gaps S1, S2, must be arranged so that light from S1 adequately illuminates S2. Both S1 and S2 can be varied by screw adjustments. By judiciously varying S1 and S2, exposures can be obtained ranging from about $\frac{1}{10}$ to 40 μsec. When it is desired to use this apparatus, the cathode-ray tube X-sweep is provided by the linear time-base already described, the length of exposure, time of exposure after initiation of discharge tube arc, and arc current being observed on the screen, either visually or by photography. If exposures less than about 3 μsec. are required, only visual observation can be used, since there is a variable delay of at least 1 μsec. between the application of the triggering pulse to the discharge tube and the development of the arc, even when operating under optimum conditions. There is a similar degree of uncertainty in the sparking over of the gap S1 of figure 6. If longer exposures are used (as when studying prolonged arcs) the cathode-ray tube can be photographed by repeating the whole process a sufficient number of times. In this case, of course, the film of the Kerr cell shutter is exposed for one condenser discharge only. There is also a variation in the exposures given by the

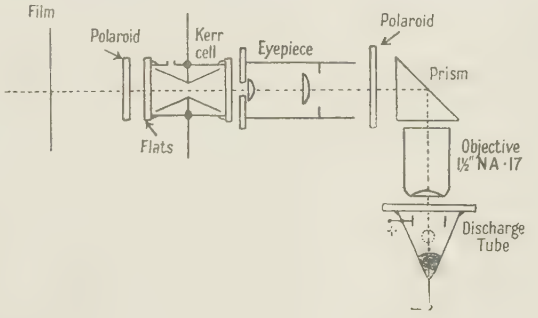

Figure 7.

Kerr cell shutter for any given setting of the gaps S1 and S2, but the exposure actually obtained on the ciné film can always be observed sufficiently accurately on the cathode-ray tube screen. In practice, exposures have usually been made as short as possible consistent with adequate exposure of the ciné film, except when it was desired to show movement of the cathode spot during a fairly long exposure. Some results for various cathodes will now be discussed; these are all characteristic of a large number of similar photographs. It was not found that the pressure of the gas filling of the discharge tube had any significant effect on the appearance of the cathode spot; in all cases in this investigation the tubes have therefore been run at conditions of optimum ease of triggering.

Mercury cathode

Figure 8 (*a*) shows a photomicrograph of the mercury cathode during the whole of one discharge of 20 μF. initially at 300 v. The external impedances between condenser and discharge tube were made a minimum, the L and R of figure 1 being reduced to 3×10^{-8} H. and 0·05 Ω respectively, and the total residual inductance of the condenser and leads about 10^{-7} H. Under these conditions the discharge lasts some 7 μsec. and the current reaches a peak of 1400 amp. about half-way through this time. It is found that the cathode emitting area always produces a similar, but not identical, photograph. The "spot" usually forms on the mercury surface adjacent to the tube wall, and expands outwards covering the area shown. For different discharges this area is approximately constant in size, but varies in shape. Figure 8 (*b*) shows a Kerr cell picture of an identical discharge with an exposure of about 10^{-7} second, taken with tube current at the maximum. It is now apparent that the area exposed in figure 8 (*a*) is caused by much smaller, rapidly moving emitting areas, the current density of emission from these being, for this stage of the discharge, greater than 10^6 amp/cm^2. Reducing the maximum current by reducing the initial condenser voltage merely seems to reduce the area of emission. Before discussing this further, we will examine the behaviour of the "spot" when the arc is prolonged to about 90 μsec. (thus reducing the peak current) by adding a resistance of 1·6 Ω between condenser and discharge tube. Figure 10 shows the tube current and voltage drop plotted against time for such a discharge. It also shows the positions A, B, C of the Kerr cell exposures corresponding to the photographs in figure 9 (*a*), (*b*), (*c*), respectively.

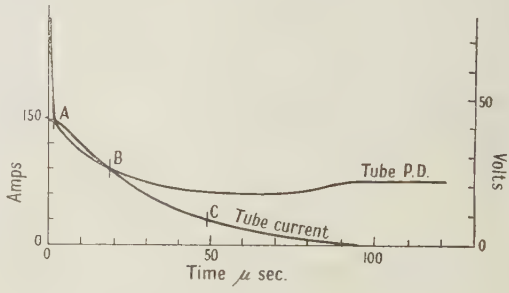

Figure 10.

Figure 9 (*a*) shows the cathode spot for the first 5 μsec. of the discharge. Figure 9 (*b*) shows a longer exposure of 7 μsec. taken about 18 μsec. from the start, and figure 9 (*c*) shows an 8 μsec. exposure taken about 50 μsec. from the start, when the arc has apparently become a "normal arc". Figure 9 (*d*) shows the cathode for the whole of one flash. It is easy to see how this picture is built up from (*a*)–(*c*). In figure 9 (*a*) the "spot" appears similar (though on a smaller scale) to that of the minimum impedance discharge of figure 8 (*a*), probably consisting of a very small, nebulous, rapidly moving area. In figure 9 (*b*), the

"spot" has moved further over the mercury surface away from the tube wall, is spreading out, and developing into a number of separate unit-like spots. The fine streaks shown indicate these moving radially outwards from the discharge starting point. In (*c*), the unit-spot formation is complete, the current being carried by some 15–20 spots each presumably emitting about 2 amp. From this point the motion of the spots is random; they remain in a group, but at relatively large distances apart. The current density of emission is probably at least 10^5 amp cm^2. In this case the average diameter of the spots appears to be about $\frac{1}{20}$ mm. After this spot-formation is complete, no further change takes place; the number of spots merely falls with falling current. This suggests that the usually accepted value of the cathode spot emission current density for mercury arcs is at least an order low. Further photographs, with the Kerr cell shutter, of 50 amp. and 100 amp. normal arcs, $\frac{1}{100}$ sec. after their initiation, confirm this (Froome 1946). There can be little doubt that an arc is "normal" after this interval.

Sodium cathode

Figure 11 (*a*) shows the appearance of a freshly scraped sodium cathode for the whole of one minimum impedance discharge, under electrical conditions identical with those obtaining for the discharge shown in figure 8. This photograph shows an unusual, but not rare, occurrence in that the arc struck simultaneously in three cathode "spots". Figure 11 (*b*) shows an exposure of 10^{-7} sec. taken at the maximum of an identical discharge with the arc current at 1400 amp. Again it is found that the emitting area at any instant is only a fraction of the whole area traversed and that the emission current density is in excess of 10^6 amp/cm^2 at this stage.

The result of prolonging the discharge by the addition of a series resistance of 7 Ω between condenser and tube is seen in figure 12 : figure 12 (*a*) shows the appearance of the cathode for the whole of one flash and figure 12 (*b*) shows a 2 μsec. Kerr cell exposure of the cathode, taken 120 μsec. from the time of arc initiation, with the arc current at 12 amp. The unit-spot formation illustrated for a mercury cathode in figure 9, also takes place for a sodium cathode; the number of emitting spots has dwindled to three (figure 12 (*b*)). Hence, a current density well in excess of 2×10^5 amp/cm^2 is found, although the arc appears "normal" at this stage, having a potential drop of some 20 v. and a negative characteristic.

Copper cathode

An important difference was noted between copper cathodes and mercury and sodium cathodes : for mercury or sodium the cathode "spots" were brilliantly visible during the very high current minimum impedance discharges and the early stages of prolonged discharges, whereas the copper cathode "spot" was not, and in fact was often apparently non-existent. It was found, however, that a clean, polished cathode was marked after one such flash in a manner not unlike the photographs of figures 8 (*a*) or 11 (*a*). This suggested that the cathode emission process was not significantly different, but that at the estimated velocity of the emitting area for mercury or sodium (about 10^5 cm sec. for a 1400-amp. "spot") the copper cathode was not vaporized and thus the "spot" was much less brilliant. By making the conventional supposition that one-tenth the arc current was carried by positive ions, and assuming a cathode fall (see later) of about 20 v., calculation shows that a mercury cathode could be easily vaporized in the time of about

10^{-7} sec. that the cathode spot takes to move on to fresh territory, while copper would not even be heated to red heat. It has been seen, however, that for a prolonged discharge with mercury or sodium cathodes, the unit-spots formed after the arc has become "normal" move more slowly (of the order of 10^3 cm/sec.) and hence it might be expected that for a similar discharge with copper cathode these unit-spots should appear once the copper in their neighbourhood became incandescent or vaporized. This was in fact found: after some 30 μsec. very brilliant unit spots became visible. They moved more slowly than for mercury and sodium, and were considerably brighter in appearance, presumably due to incandescence of the copper. Their size was again very small, indicating emission current densities of at least 2×10^5 amp cm^2, their numbers falling with decreasing current. Each spot carried about 3–5 amp.

Figure 13 shows these spots with an exposure of 4 μsec. with the arc current at 9 amp., 150 μsec. after the start of a discharge prolonged as for the sodium cathode spot photographs of figure 12. An approximate treatment for estimating the cathode temperature rise under the spot is as follows:

Assume that the temperature of the surface, initially θ_0, is instantaneously raised to θ_1. Then θ_x at a distance x from this surface is given by an equation of the form

$$\frac{\theta_x - \theta_1}{\theta_0 - \theta_1} = \frac{2}{\sqrt{\pi}} \int_0^y \exp(-y^2)\, dy,$$

where $y = x/2\sqrt{(ht)}$ and $h = k/\rho s$, k is the thermal conductivity of the cathode material, ρ its density, s its specific heat, and t the time.

Most of the heat will be concentrated in a distance x given by $\frac{1}{2}x(kt/\rho s)^{-\frac{1}{2}} \simeq 1$. Thus for copper $x = 2\sqrt{(0{\cdot}9t/9 \times 0{\cdot}1)} = \frac{2}{3} \times 10^{-3}$ cm. and for mercury $x = 2\sqrt{(0{\cdot}02t/14 \times 0{\cdot}03)} = 1{\cdot}4 \times 10^{-4}$ cm., if $t = 10^{-7}$ sec., the time taken for the spot to move to fresh territory. We now assume that all the energy supplied to the cathode from the time the spot forms on it, will be used in heating the volume of material of depth x under it.

The input energy to this region is about 2×10^6 w/cm^2 if the cathode fall is 20 v. and the positive ion current is one-tenth the electron current, the electron current density being about 10^6 amp/cm^2.

Thus the temperature reached by the copper in this time is found to be 75° c. The temperature that would be reached by the mercury if there were no boiling is 770° c.

Conclusions on cathode spots

(i) At all times the emission current density is enormous, ranging between 10^5 to well in excess of 10^6 amp/cm^2. (ii) The initial rapid movement of the emitting area precludes all possibility of the emission being derived thermionically. (iii) Intense luminosity of the cathode spot is a secondary effect, only caused if the positive ions falling on the cathode (under the "spot") are able to vaporize it or render it incandescent. It seems probable that the mottled effects of figures 8 (*a*) and 11 (*a*) are due to an unevenness in the velocity of the emitting area, as though it were constantly slowing down and gathering speed, the cathode "spot" appearing brighter when moving more slowly. (iv) Previous measurements of cathode spot current density based upon its markings on the cathode over a long period of time are probably unreliable. It may be that Slepian's (1942) "low current density arc" had a very high cathode current density carried by a large number of small,

rapidly moving areas. (v) The very high cathode current density encountered for both high current arcs and arcs prolonged to normality with mercury, sodium, or copper cathodes, favour Langmuir's original theory (1923) that normal arcs with cathodes of these metals have their cathode emission derived by field emission. Current densities of the order of those herein described, make this theory more plausible than hitherto.

§ 4. THEORETICAL IMPLICATIONS

Discussion in this paper is limited to the simplest calculation of rate of growth of current, time is measured from the point when the current has reached 1 amp. When this has occurred there is a conducting path of positive ions and electrons bridging anode and cathode, but the potential difference applied across the tube is still substantially that across the condenser. Inside the discharge tube this potential difference will be formed of three parts, that due to cathode fall, that due to anode fall, and that due to the necessity of maintaining an electric field inside the plasma or ionized gas between anode and cathode. It is well known that the cathode fall for normal arcs is roughly equal to or less than the ionization potential of the gas filling and this assumption will be made for the arcs examined here, for increasing or decreasing the current does not alter the cathode fall of normal arcs appreciably. If, as seems most likely, field emission is the process by which electrons leave the cathode at the cathode spot, this process does not demand a particularly high cathode fall, and the current rise (as far as this process is concerned) will be equal to the speed at which the necessary positive ion space charge sheath can be built up at the cathode. The anode fall arises from the need for a rate of ionization slightly greater just near the anode than in the plasma. The same density of ionization is needed at the anode as in the plasma, but there is a slow drift of positive ions away from the anode, so that the anode fall is needed to make good such losses. Again, if we assume an anode fall equal to the gas ionization potential, adequate ionization can be produced. On these hypotheses we see that some 20–50 v. of the initial overall voltage of approximately 360 are absorbed by the combined anode and cathode falls.

We shall assume that the remainder is applied to the plasma and calculate the rate of growth of current, on this hypothesis, from the rate of plasma ionization to be expected if ionization takes place by direct electron collision. In general, discussion is restricted to times of the order of 10^{-7} sec., for vapour from the cathode and positive ions moves a negligible distance in this time. Recombination of ions is also neglected. If it is also assumed that the ionized gas between anode and cathode is a genuine" plasma", i.e. that it consists of equal densities of positive ions and electrons, the calculation is simple, for then space charge effects may be neglected. Potential measurements by means of probes placed along the tube indicate that at any instant the plasma field is approximately equal to the tube potential difference divided by the electrode spacing (table 1).

If we then assume that in the plasma ionization initially takes place only by direct electron collision, the equations of continuity are (Thomson 1933)

$$\frac{\partial n_-}{\partial t} + \frac{\partial}{\partial x}(n_- u_-) = \alpha n_- u_-, \qquad \ldots\ldots(6)$$

$$\frac{\partial n_+}{\partial t} - \frac{\partial}{\partial x}(n_+ u_+) = \alpha n_- u_-, \qquad \ldots\ldots(7)$$

n_-, n_+ = density of electrons, positive ions,
u_-, u_+ = drift velocity of electrons, positive ions,
α = ionization efficiency (i.e. the number of ion pairs produced per electron per cm. of advance).
x refers to distance from the cathode.

If $n_+ = n_-$,
$$\frac{\partial}{\partial x}(n_- u_-) = -\frac{\partial}{\partial x}(n_+ u_+) = 0, \qquad \ldots\ldots(8)$$

and
$$\partial n_-/\partial t = \alpha n_- u_-, \qquad \ldots\ldots(9)$$

or, if the discharge path is not of unit cross-section, $\partial N/\partial t = \alpha N U$, where U now refers to electron drift velocity, and N is the actual number of ions present per unit length. Hence,
$$N = N_0 \exp\left(\int_0^t \alpha U \, dt\right),$$

where N_0 is the initial number of ions present. But $NqU = i$, where i = current and q = electron charge, whence
$$i = N_0 q U \exp\left(\int_0^t \alpha U \, dt\right). \qquad \ldots\ldots(10)$$

Table 1

	Helium			Argon		
Gas pressure (mm. Hg)	15	8	0·5	8	3	0·5
Initial condenser voltage	310	310	310	310	310	310
X_p (v/cm.)	39·2	37·0	23·1	46·1	41·5	34·6
d (cm.)	3·0	3·0	3·0	3·0	3·0	3·0
$X_p d$	117	111	69·3	138	125	104
Tube p.d. at $(di/dt)_{max}$ (v.)	155	155	108	193	180	135

X_p is the gradient in the plasma at $(di/dt)_{max}$; d is the electrode spacing.

NOTE.—The plasma potential gradient is obtained from the main differences in potential indicated by four identical " floating " probes equally spaced along the body of the tube. The tube used had a mercury cathode. The circuit impedances were slightly different from those used in the measurements of figures 3, 4, 5.

In conditions of no space charge the electric field and current in the tube at any time are independent of the position in the tube, i.e. X, U, and α are independent of x.

If in equation (10) we measure time from the moment when $i = 1$ amp., we get
$$1 = N_0 U_0, \qquad \ldots\ldots(11)$$

whence
$$i = (U/U_0) \exp\left(\int_0^t \alpha U \, dt\right),$$

and $U = KX$ where K is the electron mobility in an electric field X. The equation we have to solve is thus
$$i = (X/X_0) \exp\left(\int_0^t \alpha U \, dt\right). \qquad \ldots\ldots(12)$$

Unfortunately it cannot be assumed that X, and hence α, are constant with time since the inductive drop of voltage in the leads and the resistive drop cause X to change rapidly with time.

If the capacity of the condenser is assumed to be large, so that a negligible charge flows out of it during the early stages of the discharge in which we are most interested, we can put
$$X = d^{-1}(V_0 - 2V_i - L(di/dt) - iR), \qquad \ldots\ldots(13)$$

where d is the electrode spacing, V_0 the initial applied voltage, V_i the ionizing potential of the gas (assumed cathode and anode fall), L the total inductance and R the total resistance of the leads.

α also varies with X/P where P is the residual gas pressure. For various values of X/P, α has been fairly accurately evaluated by several workers (Druyvesteyn and Penning 1940), so that equation (12) can be solved by a laborious numerical integration. In obtaining numerical results one is hampered by uncertainty in the values for the electron mobility K found by other workers. It appears to have been measured only at values of X/P lower than those used here, and although it is fairly constant over the measured range, some error may be introduced by extrapolation; this is, however, not likely to be great enough to alter seriously the conclusions reached.

In figures 3–5 it is seen that the current rises at rates expected on the above hypotheses over a limited pressure range. At higher pressures (e.g. 5·5 mm. air) the measured rises are more rapid than expected : some additional form of ionization must be operative, the most probable being some "thermal" mechanism. This appears to have appreciable effect at values of X/P lower than about 10 for helium, 30 for argon, and 40 for air. Ionization by direct collision will account for the measured current growths for values of X/P probably up to at least 150 for these gas fillings. It must be emphasized that these results are obtained for pressure ranges of 2 to 40 mm. Hg for helium, 2 to 6 mm. for air, and 2 to 30 mm. for argon. A substantial triggering pulse is needed at the higher pressure end of these measurements, but once the arc has started, this pulse has never been found to have effect upon the current–time characteristics of the resulting discharge. Within these limits the cathode spot appears to have no effect.

ACKNOWLEDGMENTS

The writer is indebted to Prof. Sir George P. Thomson, F.R.S., for many valuable discussions, to Dr. M. Blackman for suggestions on the heating of the cathode, to Mrs. K. D. Froome for assistance in the preliminary experimental work and preparation of diagrams, and to B. A. Jarrett for considerable advice.

REFERENCES

Druyvesteyn, M. J., and Penning, F. M., 1940, *Rev. Mod. Phys.*, **12,** 88.
Froome, K. D., 1946, *Nature, Lond.*, **157,** 446 ; 1947, *Ibid.*, **159,** 129.
Froome, K. D., and Jarrett, B. A., 1943, *J. Roy. Photog. Soc.*, **83,** 352 ; 1944, *J. Roy. Micr. Soc.*, **64,** 136.
Henry, P. S. H., 1944, *J. Sci. Instrum.*, **21,** 135.
Langmuir, I., 1943, *Gen. Elect. Rev.*, **26,** 731.
Slepian, J., 1942, *J. Appl. Phys.*, **13,** 113.
Thomson, J. J. and G. P., 1933, *Conduction of Electricity through Gases* (Cambridge : University Press), Vol. 2, p. 512.

Blue and Ultra-Violet Bands of K_2

By S. P. SINHA

Imperial College, London

MS. received 9 *July* 1947

ABSTRACT. Bands of K_2 have been photographed in absorption in the region λ 4510–λ 3940 A. in the first order of a 21-ft. concave grating with a dispersion of about 1·28 A. per mm. The bands measured fall into two systems, one lying between λ 4510 and λ 4220 A. and the other between λ 4160 and λ 3940 A. They can be represented by the following equations :

$$\lambda\,4510\text{–}\lambda\,4220\ \text{A.}: \quad \nu = 22970{\cdot}0 + 60{\cdot}60(u') - 0{\cdot}20(u'^2) - 92{\cdot}64(u'') + 0{\cdot}354(u''^2),$$

$$\lambda\,4160\text{–}\lambda\,3940\ \text{A.}: \quad \nu = 24627{\cdot}7 + 61{\cdot}60(u') - 0{\cdot}90(u'^2) + 0{\cdot}0010(u'^3) - 0{\cdot}00030(u'^4) - 92{\cdot}64(u'') + 0{\cdot}354(u''^2),$$

where $u = v + \frac{1}{2}$.

The upper states of the two systems are considered to dissociate into $4\,^2S + 5\,^2P$ and $4\,^2S + 3\,^2D$ atoms respectively.

§1. INTRODUCTION

POTASSIUM is known to possess a number of systems of bands in the infra-red, visible and the ultra-violet region. The infra-red bands were first photographed by McLennan and Ainslie (1923) and their vibrational analysis has been carried out by Ritschl and Villars (1928) and by Crane and Christy (1930). The vibrational structure of the red system has been studied by Fredrickson and Watson (1927), and by Crane and Christy (1930) in absorption and by Loomis and Nusbaum (1932) who used the technique of magnetic rotation, while the rotational structure of this system has been studied by Loomis (1931). A vibrational analysis of the blue bands has been made by Weizel and Kulp (1930) from the data of Walter and Barratt (1928) and by Yamamoto (1929). Several systems of bands have been reported in the ultra-violet region by Chakraborti (1936), Yoshinaga (1937) and Sinha (1945, 1945 a). In general the analyses of the ultra-violet bands provided by the various authors do not appear satisfactory in as much as the systems look fragmentary. A somewhat similar situation existed in case of the ultra-violet bands of Na_2, but it has now been shown that the bands which were analysed into five different systems by Weizel and Kulp (1930) constitute in reality two systems only (Sinha 1947). The present investigation has therefore been undertaken with a view to improving the existing data and obtaining a more satisfactory analysis of the bands of K_2 in the blue and ultra-violet region. The work has so far been carried out only in the region λ4500–λ3900 A., although bands have been reported in previous works to wavelengths as low as λ2900 A. Work is in progress, however, in the latter region.

§2. EXPERIMENTAL

The bands have been studied in absorption. The absorption vessel consisted of a cylindrical steel tube, 65 cm. long and 2·5 cm. in internal diameter, provided with water-cooled glass or quartz windows. The central portion of the tube (30 cm. in length) could be electrically heated from outside to temperatures up to 1000° C. Potassium, freed from the oil in which it was stored by scraping off the outer layer of the oxide and washing two to three times in ether containing a few per cent. of alcohol, was put into a steel tube which was

then pushed to the centre of the absorption tube. The absorption tube was evacuated with a Cenco hyvac pump and filled with nitrogen at a pressure of a few cm. of mercury. The presence of nitrogen prevents rapid distillation of the metal to cooler parts when the tube is heated. A pointolite lamp was used to give continuous radiation. When used in proper orientation, the continuum given by it was free from band structure.

Preliminary investigations to determine the conditions under which the bands appeared most satisfactorily in different regions were first investigated with a low dispersion spectrograph. It was found that with a given amount of nitrogen gas inside the absorption tube, a higher temperature was generally needed to produce the systems the smaller the wavelength. Thus when the total pressure of nitrogen and potassium vapour in the tube, as indicated by a manometer connected to it was 10–15 cm. Hg, the blue bands appeared satisfactorily at about 550° C. (within the system a slightly higher temperature was needed to obtain the long wavelength end and a slightly lower temperature to obtain the short wavelength end satisfactorily), and the bands between λ 4160 and λ 3940 A. at about 700° C. Using these values of temperature and pressure, the spectrum was next photographed in the first order of a 21-ft. concave grating (Eagle mounting), having a dispersion of about 1·28 A. per mm. The iron arc spectrum has been used for comparison.

§3. APPEARANCE OF THE BANDS AND MEASUREMENTS

The bands appear in two distinct regions: (i) λ 4510–λ 4220 A. and (ii) λ 4160–λ 3940 A. They are all degraded to the red. The heads appear much better

Table 1. K_2 bands: λ 4510–λ 4220 A.

λair (A.)	Int.	v', v''	$\nu_{obs}-\nu_{calc}$ (cm^{-1})	λair (A.)	Int.	v', v''	$\nu_{obs}-\nu_{calc}$ (cm^{-1})
4505·3	1	2,10	1	4343·5	10	1,0	0
4500·0	2	1,9	3	4338·1	5	3,1	2
4495·1	3	0,8	0	4332·3	7	2,0	0
4487·8	2	2,9	3	4327·1	4	4,1	2
4482·8	2	1,8	1	4320·9	7	3,0	2
4477·7	4	0,7	0	4316·2	4	5,1	1
4470·6	3	2,8	2	4310·0	7	4,0	0
4465·6	3	1,7	−1	4304·8	4	6,1	3
4460·3	5	0,6	−1	4299·0	8	5,0	1
4453·7	2	2,7	0	4294·5	5	7,1	2
4448·2	3	1,6	0	4288·4	8	6,0	1
4442·6	6	0,5	0	4284·0	4	8,1	2
4436·5	4	2,6	−1	4277·6	6	7,0	1
4430·8	4	1,5	−1	4273·6	6	9,1	1
4425·5	6	0,4	−2	4269·8	3	11,2	1
4419·3	4	2,5	−1	4267·2	4	8,0	1
4413·3	3	1,4	0	4263·6	4	10,1	0
4407·7	5	0,3	−1	4259·5	2	12,2	1
4401·8	4	2,4	0	4256·8	3	9,0	2
4395·9	4	1,3	0	4253·0	2	11,1	2
4390·2	5	0,2	−1	4249·6	3	13,2	1
4378·4	6	1,2	0	4243·4	3	12,1	−1
4372·9	7	0,1	−2	4236·7	2	11,0	1
4367·8	5	2,2	1	4229·8	1	15,2	1
4361·0	6	1,1	0	4223·0	1	14,1	3
4355·1	8	0,0	−1				
4349·7	6	2,1	0				

marked in the former region than in the latter. Lines due to rotational structure appear over the entire region, but the branches cannot be identified at all owing to overlapping and closeness of structure.

Measurements of the heads of the bands are given in tables 1 and 2. Intensities given are visual estimates on a scale of 1–10; they have been estimated in different regions (separated by horizontal lines in the tables) from different spectrograms.

Table 2. K_2 bands: λ4165–λ3940 A.

λair (A.)	Int.	v', v''	$\nu_{obs}-\nu_{calc}$ (cm^{-1})	λair (A.)	Int.	v', v''	$\nu_{obs}-\nu_{calc}$ (cm^{-1})
4164·7	1	5,10	−1	4063·5	4	3,2	−1
4161·0	1	—	—	4059·9	4	5,3	3
4159·1	1	4,9	−1	4059·0	4	7,4	−2
4155·4	2	6,10	0	4057·9	5	2,1	−2
4153·2	2	3,8	−1	4054·8	4	4,2	−3
4149·4	2	5,9	−2	4033·5	6	3,0	−1
4146·0	3	7,10	−4	4031·1	4	5,1	−2
4144·3	3	4,8	−2	4029·3	2	—	—
4138·2	3	3,7	0	4024·9	6	4,0	−3
4137·5	3	8,10	4	4022·8	4	6,1	−2
4134·6	4	5,8	1	4016·3	5	5,0	−2
4133·1	4	2,6	0	4014·4	5	7,1	0
4131·1	4	7,9	6	4008·0	5	6,0	−2
4127·6	5	1,5	1	4004·9	3	—	—
4125·6	4	6,8	2	3999·6	5	7,0	0
4123·6	5	3,6	−1	3995·1	4	14,3	−3
4122·7	6	0,4	1	3992·6	4	12,2	−1
4121·9	4	—	—	3991·6	5	8,0	1
4119·8	5	5,7	0			10,1	1
4115·1	3	—	—	3989·6	3	15,3	−4
4113·8	4	4,6	3	3986·2	3	13,2	2
4112·8	8	1,4	0	3984·7	5	11,1	1
4110·5	4	6,7	4	3984·1	4	9,0	2
4108·6	6	3,5	−1	3980·8	4	—	—
4107·3	7	0,3	2	3979·8	4	14.2	2
4104·7	4	5,6	3	3978·9	4	—	—
4103·0	6	2,4	0	3978·0	5	12,1	0
4101·7	4	—	—	3976·7	4	10,0	−3
4099·1	5	4,5	0	3975·8	3	—	—
4097·4	7	1,3	1	3974·3	3	15,5	0
		6,6	−3				
4095·7	4	—	—	3972·1	3	13,1	1
4093·9	5	3,4	−2	3970·3	3	11,0	0
4092·3	8	0,2	−2	3969·6	3	16,2	−6
4090·2	4	5,5	0	3966·0	3	14,1	−2
4087·5	6	2,3	2	3964·6	3	12,0	−6
4084·7	4	4,4	−2	3963·2	2	17,2	0
4082·7	10	1,2	−1	3960·6	3	15,1	0
4081·4	5	6,5	2	3957·2	3	13,0	1
4078·2	6	3,3	1	3955·3	2	16,1	−7
4075·5	5	5,4	0	3951·6	1	14,0	−2
4073·0	4	2,2	−1	3946·3	1	15,0	−5
4069·1	2	4,3	2	3941·3	1	—	—
4067·0	8	1,1	1				
		6,4	−1				
4065·1	3	—	—				

§4. VIBRATIONAL ANALYSIS AND MOLECULAR CONSTANTS

All the bands measured fall into two systems, one lying between λ4510 and λ4220 A. and the other between λ4160 and λ3940 A. We will, for convenience,

call them the blue and the first ultra-violet systems respectively. The assignments of vibrational quantum numbers are given in tables 1 and 2 and the arrangements in v', v'' schemes in tables 3 and 4 respectively.

Table 3. Deslandres' scheme for the blue system of K_2 bands

v' \ v''	0	1	2	3	4	5	6	7	8	9	10	Mean diff.
0	22955	22862	22772	22681	22590	22503	22414	22327	22240			
	61	62	61	61	62	60	61	60	60			60·9
1	23016	22924	22833	22742	22652	22563	22475	22387	22301	22216		
	60	60	61		60	59	59	60	61	60		60·0
2	23076	22984	22894		22712	22622	22534	22447	22362	22276	22190	
	61	59										60·0
3	23137	23045										
	58	59										58·5
4	23195	23104										
	59	58										58·5
5	23254	23162										
	58	61										59·5
6	23312	23223										
	58	56										57·0
7	23370	23279										
	58	57										57·5
8	23428	23336										
	57	57										57·0
9	23485	23393										
	(57)	55										56·0
10	—	23448										
	(55)	58										56·5
11	23597	23506	23414									
		53	56									54·5
12		23559	23470									
		57	55									56·0
13		23616	23525									
		57	(55)									56·0
14		23673	—									
			(55)									55·0
15			23635									
Mean diff.	91·6	90·5	91·0	90·5	88·7	88·3	87·3	86·0	85·5	86·0		

Table 4. Deslandres' scheme for the first ultra-violet system of K_2 bands

v' \ v''	0		1		2		3		4		5		6		7		8		9		10		Mean diff.
0					24429	68	24340	16	24249														
									59														
					58		59		24308	88	24220												58·7
1	*		24581	†6	24487	88	24399	16	58														
			55		58		59		24366				24188										
2	*		24636	16	24545	48	24458	92															57·5
					57		54		54				56										
3	24785		*		24602	06	24512	92	24420	88	24332	88	24244	98	24158	48	24071						55·3
	53				56		56		55		57		58				52						
4	24838		*		24655	53	24568	93	24475	98	24389	88	24302				24123		24037				54·9
	54						54		55		53		53				56		56				
5	24892	92	24800				24622	92	24530	88	24442	88	24355	68	24266	48	24179	98	24093	88	24005		54·4
	51	92	51						51		53		54		55		53				53		
6	24943	92	24851						24581	98	24495	88	24409	88	24321	68	24232				24058		52·6
	52	92	52						49												54		
7	24995	92	24903						24630										24198	98	24112		51·7
	50																				50		
8	25045																				24162		50·0
	48																						
9	25093																						48·0
	46																						
10	25139		25045																				46·0
	41		44																				
11	25180		25089																				42·5
	45		42																				
12	25225		25131	92	25039																		43·5
	38		38		40																		
13	25263		25169	06	25079																		38·7
	36		38																				
14	25299		25207				25024																37·0
	34		35				37																
15	25333		25242				25061																35·3
	32		33				32																
16	25365	06	25275		25184	16	25093	16															32·3
							32																
17							25125																32·0
Mean diff.	92·2		91·6		88·7		91·8		87·2		87·0		87·7		87·6		86·0		86·9				

(a) *Blue system*

As mentioned before, the blue bands were analysed by Yamamoto (1929) and by Weizel and Kulp (1930). The analysis of the former appears more satisfactory and is in good agreement with the present one.

All the blue bands measured in the present case can be represented by the equation

$$\nu = 22970{\cdot}0 + 60{\cdot}60u' - 0{\cdot}20u'^2 - 92{\cdot}64u'' + 0{\cdot}354u''^2 \quad \ldots\ldots(1)$$

where $u = v + \frac{1}{2}$.

The terms in u'' are those from the work of Loomis and Nusbaum (1932). The values of $\nu_{obs} - \nu_{calc}$ given in table 1 indicate fairly good agreement between the observed positions of the band heads and those calculated from equation (1).

The heat of dissociation for the upper state calculated from the above formula by applying Birge and Sponer's extrapolation rule is 4560 cm^{-1}. This enables us to calculate ν_{atom}, the energy of the dissociated atoms, given by the expression, $\nu_{atom} = \nu_{0,0} + \boldsymbol{D}' - \boldsymbol{D}''$, where the symbols used have the usual significance. Now $\nu_{0,0} = 22955$ cm^{-1}, $\boldsymbol{D}' = 4560$ cm^{-1} and $\boldsymbol{D}'' = 4130$ cm^{-1}, and therefore $\nu_{atom} = 23385$ cm^{-1}. Further, from the study of line spectra data for potassium, we have $4^2S - 5^2S = 21025$ cm^{-1}, $4^2S - 3^2D = 21540$ cm^{-1} and $4^2S - 5^2P = 24710$ cm^{-1}. Comparison of these with the above value of ν_{atom} shows that the upper state of the blue system dissociates into 4^2S and 5^2P atoms of K.

(b) *The first ultra-violet system*

Bands in this region have previously been reported by Yoshinaga, who regards them as belonging to two different systems, one lying in the region λ4160–λ4050 A. and the other in the region λ4040–λ3960 A.; his systems are fragmentary and comparison of his measurements with table 4 indicates that all the bands which he measured in this region could be included in a single system. It appears that the presence of the λ4045·6 A. line of the P series of K which obscures some bands between λ4040 and λ4050 A. led him to consider the bands as belonging to two different systems. The region of overlap of the bands by the broadened P series line is indicated by asterisks in table 4.

The bands measured in the present investigation can be represented by the following equation:

$$\nu = 24627{\cdot}7 + 61{\cdot}60u' - 0{\cdot}90u'^2 + 0{\cdot}0010u'^3 - 0{\cdot}00030u'^4 - 92{\cdot}64u'' + 0{\cdot}354u''^2, \quad \ldots\ldots(2)$$

where $u = v + \frac{1}{2}$ as before.

The terms in u'' have been retained, as before, from the work of Loomis and Nusbaum. Values of $\nu_{obs} - \nu_{calc}$ given in table 2 indicate fairly good agreement between the observed frequencies and those calculated from equation (2).

The value of $\boldsymbol{D}'$ cannot in this case be obtained from Birge and Sponer's extrapolation rule. It has therefore been determined from figure 1, which gives a plot of T' (i.e. $\nu_{0,0}, \nu_{1,0}, \nu_{2,0}, \ldots$) against $\Delta T'$ (i.e. $\nu_{0,0} - \nu_{1,0}, \nu_{1,0} - \nu_{2,0} \ldots$). T'_{max}, the value of T' corresponding to $\Delta T' = 0$, is equal to 25590 cm^{-1}, and since $\nu = 24612$ cm^{-1}, $\boldsymbol{D}'$ is approximately 980 cm^{-1}.

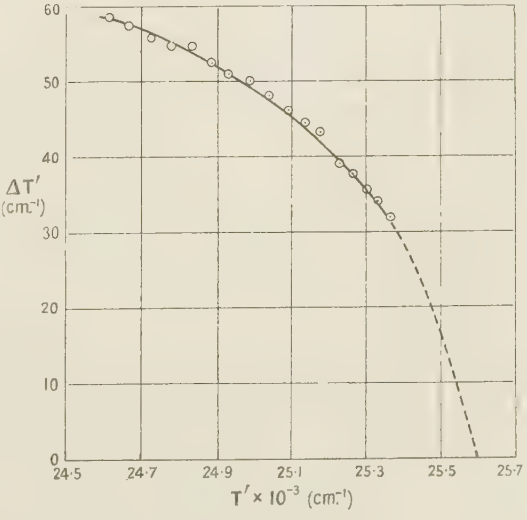

Figure 1.

$\Delta T'$–T' curve for λ4160–λ3940 bands of K_2.

The energy of the dissociated atoms can be determined from the relation, $\nu_{atom} = T'_{max} - \boldsymbol{D}''$ and is equal to 21455 cm^{-1}. Comparing this value of ν_{atom} with the separations of the excited atomic K levels from its ground 4^2S level, given above, it may be concluded that the dissociation products for the excited state of this system of K_2 bands are 4^2S and 3^2D atoms of K.

Vibrational constants for the five states of K_2 are summarized in table 5. The constants ν_e, ω_e, $x_e\omega_e$, $y_e\omega_e$, $z_e\omega_e$ are those in the expression (3) and are given in cm^{-1},

$$\nu = \nu_e + \omega_e u_e - x_e\omega_e u^2 + y_e\omega_e u^3 - z_e\omega_e u^4, \qquad \ldots\ldots(3)$$

where $u = v + \frac{1}{2}$.

Table 5. Vibrational constants for the ground and the excited states of K_2

States	ν_e	ω_e	$x_e\omega_e$	$y_e\omega_e$	$z_e\omega_e$	D	Dissociation products
$^1\Sigma_g^+$	—	92·64	0·354	—	—	4135	$4\,^2S + 4\,^2S$
$^1\Sigma_u^+$	11683·6	69·09	0·153	—	—	5510	$4\,^2S + 4\,^2P$
$^1\Pi_u$	15378·0	75·00	0·388	0·00437	0·00018	1780	$4\,^2S + 4\,^2P$
$^1\Sigma_u^+$(?)	22970·0	60·60	0·20	—	—	4560	$4\,^2S + 5\,^2P$
	24627·7	61·60	0·90	0·0010	0·00030	980	$4\,^2S - 3\,^2D$

§5. CONCLUSION

The ground state of K_2 is $^1\Sigma_g^+$, due to two atoms of potassium in the normal 4^2S state. The next two states are $^1\Sigma_u^+$ and $^1\Pi_u$ states formed from 4^2S and 4^2P atoms. Transitions between these and the ground state are responsible for the infra-red and the red systems of bands of K_2. The next higher molecular states revealed in absorption experiment are those involved in the blue and the ultra-violet systems studied in the present investigation. The upper state of the blue system has been shown to be due to $4^2S + 5^2P$ atoms and from analogy with the states due to $4^2S + 4^2P$ atoms, it may be concluded that this state is of $^1\Sigma_u^+$ type. The blue system should thus be due to $^1\Sigma_u^+ \leftarrow {}^1\Sigma_g^+$ transition and the bands should be single headed and should only have two branches. The general appearance of the bands suggests that they are single headed, but confirmation is impossible since the dispersion used was insufficient to enable resolution of two separate heads. An attempt was made to employ sufficient dispersion so as to see clearly the branches possessed by the bands. This has not, however, succeeded. The upper state of the next system, i.e. the first ultra-violet system, is regarded as due to $4^2S + 3^2D$ atoms of potassium. It is, however, also equally probable that it may be due to $4^2S + 5^2S$ atoms. At wavelengths lower than λ 3900 A. several systems of bands have been proposed by different workers (referred to earlier), but only one system appears extensive (λ 3900–λ 3700 A.). It is not, however, possible to make a correct estimate of $\boldsymbol{D}'$ even for this system, and thereby to determine the states of the atoms into which its upper state dissociates. If however, we suppose that this state dissociates into $4^2S + 5^2P$ atoms, the value of $\boldsymbol{D}'$ required for this purpose would be about 2000 cm^{-1}, and the state would be $^1\Pi_u$ in character. A comparison with the value of dissociation energy of $^1\Pi_u$ state from $4^2S + 4^2P$ atoms given in table 5 indicates that the above value of $\boldsymbol{D}'$ is not unlikely. Investigations are in progress to clarify the position with regard to the bands of this system and of other systems at lower wavelengths.

ACKNOWLEDGMENTS

Finally, it is a great pleasure to express my gratitude to Assistant Professor R. W. B. Pearse, D.Sc., for his valuable guidance in the work. My thanks are also due to the University of Patna, India, for the award of their Birla scholarship, which has enabled me to carry out the work.

REFERENCES

CHAKRABORTY, B. K., 1936, *Ind. J. Phys.*, **10**, 155.
CRANE, W. O., and CHRISTY, A., 1930, *Phys. Rev.*, **36**, 421.
FREDRICKSON, W. R., and WATSON, W. W., 1927, *Phys. Rev.*, **30**, 428.
LOOMIS, F. W., 1931, *Phys. Rev.*, **38**, 2152.
LOOMIS, F. W., and NUSBAUM, R. E., 1932, *Phys. Rev.*, **39**, 89.
MCLENNAN, J. C., and AINSLIE, D. S., 1923, *Proc. Roy. Soc.* A, **103**, 304.
RITSCHL, R., and VILLARS, D., 1928, *Naturwissenschaften*, **16**, 219.
SINHA, S. P., 1945 a, *Curr. Sci.*, **14**, 230 ; 1945 b, *Thesis for Ph.D.*, Patna Univ., India ; 1947, *Proc. Phys. Soc.*, **59**, 610.
WALTER, J. M., and Barratt S., 1928, *Proc. Roy. Soc.* A, **119**, 257.
WEIZEL, W., and KULP, M., 1930, *Ann. Phys., Lpz.*, **4**, 971.
YAMAMOTO, H., 1929, *Jap. J. Phys.*, **5**, 153.
YOSHINAGA, H., 1937, *Proc. Phys. Math. Soc., Japan*, **19**, 847.

Ultra-Violet Bands of Li_2

By S. P. SINHA
Imperial College, London

MS. received 1 *August* 1947

ABSTRACT. The ultra-violet bands of Li_2 have been photographed in absorption on a quartz spectrograph, using lithium vapour in argon at a pressure of half an atmosphere, at temperatures between 900 and 1100° C. Bands appear between λ 3500 and λ 3100 A. The band heads, which have been measured between λ 3450 and λ 3130 A., can be represented by the equation :

$$\nu = 30658{\cdot}5 + 231{\cdot}5u' - 1{\cdot}5u'^2 - 351{\cdot}6u'' + 2{\cdot}6u''^2.$$

where $u = v + \frac{1}{2}$.

The upper state of this system of bands is considered to dissociate into $2\,^2S + 3\,^2P$ atoms of lithium.

§1. INTRODUCTION

THERE are two systems of Li_2 bands in the visible region: (i) λ 7700–λ 6550 A. and (ii) λ 5600–λ 4500 A. These have been studied by Wurm (1929), Harvey and Jenkins (1930), Loomis and Nusbaum (1931) and others, and are due to $^1\Sigma_u^+ \leftarrow {}^1\Sigma_g^+$ and $^1\Pi_u \leftarrow {}^1\Sigma_g^+$ transitions. Li_2 has also some bands in the ultra-violet region between λ 3500 and λ 3100 A. which have been considered to belong to four different systems (Vance and Huffman 1935). These systems, however, appear fragmentary. Moreover, the corresponding bands of Na_2—the λ 3600–λ 3200 A. system—formerly regarded as due to several systems of bands have now been shown to constitute a single system (Sinha 1947). It has therefore been considered necessary to re-photograph the lithium ultra-violet bands and attempt a fresh analysis.

§2. EXPERIMENTAL

The details of the absorption tube used in the present investigation have been described earlier in connection with the ultra-violet bands of K_2 (Sinha 1948). Lithium, freed from the oil in which it was stored, was placed at the centre of the tube and heated electrically from outside to temperatures up to 1100° C. The source of continuous radiation was a 6-v. 18-amp. tungsten lamp which gave a fairly intense continuum down to λ3100 A. A quartz spectrograph (E_1) was used to photograph the bands.

In the case of sodium and potassium, experience had shown that the presence of a certain amount of a gas like nitrogen, which did not react chemically with the metal, was almost a necessity to obtain a satisfactory photograph of the ultra-violet bands, and nitrogen was invariably used. The main function of the gas is probably to prevent a rapid distillation of the metal to cooler parts of the absorption tube. With lithium, however, it was found that as soon as the metal was heated, all nitrogen introduced inside the chamber was absorbed by it and the pressure was reduced to its initial value. Under these conditions, although the visible bands appeared, there was no more than a trace of the ultra-violet bands, nor was there any spectroscopic evidence of the formation of a lithium–nitrogen compound. Nitrogen had, therefore, to be discarded and argon used. This was not absorbed by hot lithium and in its presence the Li_2 bands appeared quite satisfactorily in the ultra-violet region. When the pressure, as read on a manometer connected to the absorption chamber, was about 40 cm. Hg, the bands appeared well developed at temperatures between 900 and 1100° C. (estimated from the colour of the furnace).

§3. APPEARANCE OF THE SPECTRUM AND MEASUREMENTS

The bands, which appear between λ3500 and λ3100 A., are all degraded to the red. Lines due to rotational structure can be seen throughout the region, but it is not possible to draw any conclusion with regard to the number of branches they have, unless the bands can be photographed at a higher dispersion without much overlapping. It is equally difficult to say whether they are single-headed; for even if they were double-headed, the heads would lie too close together to be seen distinctly resolved at the dispersion employed. The iron arc has been used for comparison. Wavelengths of the band heads are given in table 1; intensities given are visual estimates on a scale of 1–10.

§4. VIBRATIONAL ANALYSIS AND MOLECULAR CONSTANTS

All the band-heads measured are found to belong to a single system. The vibrational quantum numbers assigned to them are given in table 1, and table 2 gives their arrangement in a Deslandres scheme. The heads can be represented by the equation:

$$\nu = 30658{\cdot}5 + 231{\cdot}5(u') - 1{\cdot}5(u'^2) - 351{\cdot}6(u'') + 2{\cdot}6(u''^2),$$

where $u = v + \frac{1}{2}$.

The terms in u'' are those of Loomis and Nusbaum (1931). Values of $\nu_{obs} - \nu_{calc}$ given in table 1 indicate that the representation of the band heads by the above equation is satisfactory.

The value of the energy of dissociation for the upper state, calculated from Birge and Sponer's rule, is about 9000 cm^{-1}; the value thus calculated can be

Table 1. Li_2 ultra-violet bands

λair (A.)	Int.	v', v''	νobs−νcalc	λair (A.)	Int.	v', v''	νobs−νcalc
3442·8	2	1,5	1	3266·3	2	2,1	0
3431·2	4	0,4	−3	3253·1	10	1,0	3
3416·3	1	2,5	0	3229·6	2	2,0	2
3404·4	4	1,4	−3	3219·9	1	4,1	0
3392·1	6	0,3	−2	3206·9	6	3,0	−1
3378·5	4	2,4	−3	3197·2	1	5,1	3
3365·8	3	1,3	−1	3184·2	6	4,0	1
3353·6	10	0,2	−1	3175·3	2	6,1	4
3340·5	2	2,3	−2	3162·0	5	5,0	3
3327·8	2	1,2	1	3154·5	2	7,1	3
3315·6	9	0,1	0	3140·8	4	6,0	−1
3290·5	4	1,1	1	3133·8	2	8,1	1
3277·6	6	0,0	2				

Table 2. Arrangement of Li_2 ultra-violet bands in Deslandres' scheme

v' \ v''	0		1		2		3		4		5	Mean diff.
0	30501	348 349	30152	341 342	29810	338 339	29472	336 337	29136			
	230		230		231		230		229			230
1	30731	348 349	30382	341 342	30041	338 339	29702	336 337	29365	327	29038	
	224		225				225		225	327	225	224·8
2	30955	348	30607				29927	337	29590	327	29263	
	219											219
3	31174											
	222											222
4	31396	348	31048									
	220		220									220
5	31616	348	31268									
	214		213									213·5
6	31830	349	31481									
			211									211
7			31692									
			208									208
8			31900									
Mean diff.		348·5		341·5		338·5		336·7		327		

accepted only with great reserve, since the calculation involves a large range of extrapolation.

§5. ISOTOPE EFFECT

Lithium has two isotopes, ^{6}Li and ^{7}Li and their relative abundance is in the approximate ratio 1 to 12. It would therefore appear that although it may not be possible to see bands due to $^6Li_2$, strong bands of $^6Li^7Li$ may possibly be seen under favourable conditions. The separation between the heads of bands due to $^6Li^7Li$ and $^7Li_2$ may theoretically be calculated from the expression

$$\nu^i - \nu = (\rho - 1)[\omega_v'(u') - \omega_v''(u'')],$$

where $\rho = \sqrt{(\mu/\mu^i)} = 1{\cdot}041$ approximately, and the superscript i refers to the $^6Li^7Li$ molecule. Calculation from the above expression indicates that, of the bands of $^7Li_2$ molecule which have appeared strongly on the plate, the 0,4 0,3 0,2 and 0,1 bands will have the components due to $^6Li^7Li$ on their long-wave side, i.e. on the side on which their own rotational fine structure will extend, and it will therefore be difficult to detect them. For the remaining strong bands, i.e. the 1,0 3,0 and 4,0 bands, the isotope components will lie on the short-wave side and may possibly be detected. Faint heads separated from the strong

heads of 3,0 and 4,0 bands by 24 and 35 cm^{-1} have been detected on the plate, the corresponding calculated values being 25 and 34 cm^{-1} respectively.

§6. DISSOCIATION PRODUCTS

The energy of the dissociated atoms from the excited state of the ultra-violet system can be calculated from the expression: $\nu_{atom} = \nu_{0,0} + \boldsymbol{D}' - \boldsymbol{D}''$, where the terms used have the usual significance. Since $\nu_{0,0} = 30500$ cm^{-1}, $\boldsymbol{D}' = 9000$ cm^{-1} and $\boldsymbol{D}'' = 9200$ cm^{-1} (Loomis and Nusbaum 1931), we have $\nu_{atom} = 30300$ cm^{-1} Also from Li line spectrum data, we have $2^2S - 3^2S = 27205$ cm^{-1}, $2^2S - 3^2P = 30926$ cm^{-1} and $2^2S - 3^2D = 31283$ cm^{-1} A comparison of these with the above value of ν_{atom} suggests that the excited state dissociates into $2^2S + 3^2P$ atoms.

§7. DISCUSSION

Altogether three systems of bands due to Li_2 are now known, two of which are in the visible and one in the ultra-violet. The visible systems have been definitely established to be due to transitions between the ground $^1\Sigma_g^+(2^2S + 2^2S$ atoms) and the excited $^1\Sigma_u^+$ and $^1\Pi_u$ ($2^2S + 2^2P$ atoms) states. Theoretical considerations indicate that the next higher excited states to which transitions from the ground $^1\Sigma_g^+$ state are permitted will be the following: (i) $^1\Sigma_u^+$ state from $2^2S + 3^2S$ atoms, (ii) $^1\Sigma_u^+$ and $^1\Pi_u$ states from $2^2S + 3^2P$ atoms and (iii) $^1\Sigma_u^+$ and $^1\Pi_u$ states from $2^2S + 3^2D$ atoms. Since, from simple considerations of Heitler-London theory, all these states would be stable, we should observe five systems of bands in the region under present investigation. A somewhat similar discrepancy between the number of systems expected from considerations of Heitler-London theory and the number observed has been noted also in Na_2 and K_2. For each of these molecules three systems of bands have been found, two of which are believed to be due to $^1\Sigma_u^+$, $^1\Pi_u(m^2S + (m+1)^2P) \leftarrow {}^1\Sigma_g^+(m^2S + m^2S)$ and one due to transition from the ground $^1\Sigma_g^+$ state to an excited state dissociating into $m^2S + m^2D$ atoms ($m = 3$ for Na_2 and for K_2). Of these three systems, that towards the long-wave side, i.e. the $\lambda 3600$–$\lambda 3200$ A. system of Na_2 and the $\lambda 4500$–$\lambda 4200$ A. system of K_2, appears more intensely developed than the other two, and also appears at a lower temperature than is needed for the others. From analogy with these, it is considered probable that the Li_2 $\lambda 3500$–$\lambda 3100$ A. system corresponds to the Na_2 $\lambda 3600$–$\lambda 3200$ A. or to the K_2 $\lambda 4500$–$\lambda 4200$ A. system, and its upper state dissociates into $2^2S + 3^2P$ atoms. The systems of Li_2 bands corresponding to the other two systems of Na_2 or K_2 bands will require higher temperatures for their development and cannot be observed with the present steel absorption tube.

A few additional band-heads have been measured by Vance and Huffman which have led them to consider that there are three more systems of bands in the region investigated. Present observations, however, provide no evidence of the existence of these bands. Since Vance and Huffman have not published the intensities of the bands which they measured, it is difficult to account for this discrepancy.

ACKNOWLEDGMENTS

The author wishes to acknowledge his indebtedness to Assistant Professor R. W. B. Pearse, D.Sc., for his kind help and valuable suggestions, and to Patna University, India, for the grant of their Birla scholarship.

REFERENCES

HARVEY, A., and JENKINS, F. A., 1930, *Phys. Rev.*, **35**, 789.
LOOMIS, F. W., and NUSBAUM, R. E., 1931, *Phys. Rev.*, **38**, 1447.
SINHA, S. P., 1947, *Proc. Phys. Soc.*, **59**, 610 ; 1948, *Ibid.*, **60**, 436.
VANCE, J. E., and HUFFMAN, J. R., 1935, *Phys. Rev.*, **47**, 215.
WURM, K., 1929, *Z. Phys.*, **59**, 35.

Ultra-Violet Bands of NaK

BY S. P. SINHA
Imperial College, London

MS. received 1 *August* 1947

ABSTRACT. Bands due to NaK, in the region λ 3820 to λ 4080 A., have been photographed in absorption in the first order of a 21-ft. concave grating and their vibrational analysis carried out. The constants for this system are (in cm^{-1})

$$\nu_e = 25\,201,\ \omega_e' = 95{\cdot}85,\ x_e\omega_e' = 0{\cdot}94,\ \mathbf{D}' = 2320$$

$$\omega_e'' = 123{\cdot}29,\ x_e\omega_e'' = 0{\cdot}40,\ \mathbf{D}'' = 5025.$$

The system is regarded as arising from transitions from the ground $^1\Sigma^+$ state to an excited state dissociating into Na 3 ^2S + K 3 ^2D atoms.

§1. INTRODUCTION

THERE are three systems of bands of NaK in the infra-red and the visible regions: (i) λ 9150–λ 7200 A., (ii) λ 6150–λ 5600 A., and (iii) λ 5300–λ 4700 A. They have been studied by Ritschl and Villars (1928) and by Loomis and Arvin (1933, 34). Some bands in the ultra-violet region, extending from λ 4020 to λ 3540 A., attributed to NaK have been reported by Walter and Barratt (1928). Two different analyses of the ultra-violet bands have been proposed; one by Uchida (1929) and the other by Weizel and Kulp (1930). Since the data given by Walter and Barratt were obtained on an instrument of rather low dispersion and the two analyses of these data are widely divergent, it has been considered desirable to re-photograph the bands with a higher dispersion and attempt a fresh analysis.

§2. EXPERIMENTAL

The bands have been photographed in absorption. The details of the apparatus used are the same as for the ultra-violet bands of K_2 (Sinha 1948). Preliminary investigations were made on a small-dispersion instrument to study the conditions under which the NaK bands appeared satisfactorily in different regions. The observation of these bands is more difficult than for Na_2 or K_2 because they may be masked by bands due to these molecules if they have very strong absorption bands in any particular region. The difficulty may be overcome to a certain extent by adjusting the relative proportion of sodium and potassium in the absorption chamber. For example, in attempting to photograph NaK bands in a region likely to be overlapped by Na_2 bands, only a small proportion of sodium should be used. Thus, in the green and the yellow regions, both Na_2 and NaK are known to give bands; the former had to be suppressed in order to obtain NaK bands only and the trial experiments showed

that this was very effectively done by photographing the absorption spectrum of a sample of potassium in which the only sodium was that present as impurity. The bands appeared very satisfactorily at a temperature of about 500 to 600° C. when the pressure inside the absorption chamber, obtained by introducing nitrogen, was about 5 cm. Hg. Although the *D* lines appeared quite strongly in absorption, no trace of Na_2 bands was found. To photograph the ultra-violet bands of NaK, since overlapping by K_2 bands was expected, only a small proportion of potassium was used in the mixture. The bands appeared at a temperature of about 650° C. when the pressure of nitrogen inside the tube was about 15 cm. Hg. The method would be more difficult in a region where both Na_2 and K_2 bands were present, but the relative intensities of the bands as a function of the relative concentrations of sodium and potassium could be studied as a means of deciding which belonged to Na_2, which to K_2 and which to NaK.

The bands were then photographed on high-dispersion instruments. For the visible bands, a tungsten lamp (6 V., 18 amp.) was used as a source of continuum and photographs were taken on a glass Littrow spectrograph (dispersion about 8 A. per mm. at λ6000 and 4 A. per mm. at λ4500). The ultra-violet bands were photographed in the first order of a 21-ft. concave grating (dispersion 1·3 A. per mm.) using a 500 c.p. pointolite lamp to give the continuum.

§3. APPEARANCE OF THE SPECTRUM AND MEASUREMENTS

(a) *Visible systems*

As noted above the visible systems have been studied by a number of workers, but since no satisfactory photograph of these bands has been published nor any satisfactory description given, it is considered worth while to publish the spectrograms which might prove useful for purposes of identification.

The visible band-systems of NaK, taken on a glass Littrow spectrograph, are reproduced in the plate facing p. 452. For the yellow system (strip (*a*)) between λ6150 and λ5600, the temperature was 500° C. and the pressure (by introducing nitrogen) 5 cm. Hg; the bands are all degraded to the red, and the heads can be clearly detected. The absorption seems stronger between λ5800 and λ5600 than at longer wavelengths. The λ5300–λ4700 system (strips (*b*) and (*c*)) appear at about 600° C.; the bands are all degraded to the red. Rotational structure can be seen over the entire region, but the dispersion employed is small for its study.

Measurements and assignments of vibrational quantum numbers are given in tables 1 and 2; they agree with those due to Loomis and Arvin (1934). The intensities given are visual estimates on a scale of 10.

Table 1. NaK bands between λ5650 and λ5970

λ_{air} (A.)	Int.	v', v''	λ_{air} (A.)	Int.	v', v''	λ_{air} (A.)	Int.	v', v''
5640·8	4	14,0	5745·4	9	7,0	5935·1	3	0,1
5650·4	5	13,0	5763·4	7	6,0	5954·2	3	1,2
5665·3	6	12,0	5783·0*	6	5,0	5973·0	2	2,3
5676·0	3	18,2	5802·6	7	4,0	5997·0	3	1,3
5680·8	8	11,0	5823·5	6	3,0	6022·1	2	0,3
5696·2	8	10,0	5845·2	7	2,0	6040·5	2	1,4
5711·7	9	9,0	5869·5*	5	1,0	6066·2	3	0,4
5728·2	10	8,0	5912·0*	4	1,1			

* Bands not measured by Loomis and Arvin (1934).

Table 2. NaK bands between λ4730 and λ5260

λair (A.)	Int.	v', v''	λair (A.)	Int.	v', v''	λair (A.)	Int.	v', v''
4702·7	4	16,0	4847·4	10	7,0	5032·4	4	2,3
4717·8	4	15,0	4866·0	8	6,0	5052·6	4	1,3
4733·1	4	14,0	4876·8	10	7,1	5063·5	3	2,4
4748·5	4	13,0	4894·5	8	6,1	5083·8	4	1,4
4764·1	5	12,0	4913·5	8	5,1	5105·4	3	0,4
4779·7	6	11,0	4932·2	8	4,1	5115·0	2	1,5
4796·2 *	7	10,0	4943·2	5	5,2	5136·3	3	0,5
4813·0	8	9,0	4962·4	7	4,2	5167·5	2	0,6
4819·3	7	12,2	4982·2	7	3,2	5198·9	1	0,7
4830·3	10	8,0	5001·8	6	2,2	5230·5	1	0,8
4836·5	8	11,2	5011·9	5	3,3	5261·8	1	0,9

* Band not measured by Loomis and Arvin (1934).

(b) *Ultra-violet system*

Photographs taken on a small quartz instrument indicate that at wavelengths lower than λ3800 A. only bands of Na_2 occur, and no additional bands attributable to NaK can be detected. There is, however, a patch of what appears at this dispersion to be continuous absorption between λ3820 and λ4000 A.; this is considered to be due to NaK. It cannot belong to Na_2 which is known not to have any bands in this region, nor can it be attributed to K_2, for although K_2 has bands in this region, they would not appear without the stronger system of K_2 between λ4500 and λ4200, and this is absent from the spectrum. The spectrum was finally photographed in the first order of a 21-ft. concave grating. The strong bands lie in the region λ3870–λ4010 A., while fainter ones extend to λ3820 A. and to λ4080 A. The bands are all degraded to the red.

The wavelengths measured are given in table 3. The iron lines were used for comparison. Intensities given are visual estimates on a scale of 10.

Walter and Barratt's measurements include bands down to λ3540 A. attributed to NaK; their measurements indicate that there are two strong patches of bands, one between λ3550 and λ3650 A. and the other between λ3820 and λ3990 A. Of these, only the latter has been observed in the present investigation and attributed to NaK; in the former region, no bands except those of Na_2 have been observed. It is possible that the strong patch of bands between λ3550 and λ3650 noted by Walter and Barratt as NaK bands might in fact belong to Na_2. This suggestion receives support from the fact that all their bands in this region can be fitted in the vibrational scheme of the first ultra-violet system of Na_2 bands and they lie over the Franck-Condon parabola. Table 4 gives the classification of these bands. Weizel and Kulp's arrangement does not include these bands at all. Uchida has included them in his arrangement but the intensity distribution, as given by him, does not appear satisfactory.

§4. VIBRATIONAL ANALYSIS AND DETERMINATION OF MOLECULAR CONSTANTS

The quantum numbers assigned to the ultra-violet bands are given in tables 3 and 5. Nearly all the bands measured can be represented by the equation

$$\nu = 25\,201 + 95{\cdot}85(u') - 0{\cdot}94(u'^2) - 123{\cdot}29(u'') + 0{\cdot}40(u''^2),$$

where $u = v + \frac{1}{2}$, and the terms in u'' are those of Loomis and Arvin (1934); the differences between the observed values and those calculated from the above equation are given in table 3.

Table 3. NaK bands in absorption: $\lambda 4080$–$\lambda 3820$.

λair (A.)	Int.	v', v''	νobs−νcalc
4079·60	1	4,9	0
74·48	1	3,8	3
62·91	1	0,5	−3
60·61	1	4,8	−1
55·43	1	3,7	2
51·49	1	2,6	−2
47·21	2	1,5	−3
41·08	2	4,7	1
37·05	2	3,6	2
32·24	2	2,5	−2
28·12	2	1,4	−4
23.52	1	0,3	−2
17·20	2	3,5	0
13·02	2	2,4	−3
08·49	2	1,3	0
04·00	2	0,2	−2
3997·85	2	3,4	1
93·62	1	2,3	−2
88·63	3	1,2	−5
84·33	4	0,1	−1
78·71	4	3,3	2
74·12	4	2,2	0
69·47	4	1,1	1
64·93	4	0,0	0
		4,3	0
59·90	6	3,2	0
54·86	6	2,1	0
51·36	4	5,3	0
45·80	4	4,2	−2
43·12	2	15,9	1
		10,6	8
40·25	5	3,1	4
		12,7	−2
37·75	2	6,3	2
35·68	4	2,0	0
34·31	4	—	—
31·90	3	5,2	4
		8,4	−3
27·00	4	4,1	2
24·85	5	7,3	6
21·19	4	3,0	5
		12,6	1
19·82	4	6,2	−2
		9,4	−3
18·47	4	14,7	−5
16·21	3	16,8	−6
13·59	3	11,5	−5
13·15	4	8,3	−1
12·40	2	—	—
10·55	4	13,6	0
08·80	4	—	—

λair (A.)	Int.	v', v''	νobs−νcalc
3907·91	10	4,0	−3
		10,4	−1
06·31	4	17,8	−5
03·83	4	12,5	−3
01·85	4	9,3	−5
00·29	4	14,6	−3
3898·39	6	16,7	−6
96·33	5	11,4	−1
94·26	8	8,2	1
93·05	4	13,5	−3
89·21	3	10,3	0
		15,6	3
88·62	8	7,1	−1
		17,7	−5
85·80	8	12,4	−5
83·85	3	—	—
82·14	3	6,0	1
		9,2	4
81·48	4	14,5	2
80·13	6	16,6	−3
79·19	4	11,3	−1
76·21	8	8,1	−1
75·15	6	13,4	−5
71·51	4	10,2	−2
		15,5	1
70·05	4	7,0	0
		17,6	0
68·90	2	19,7	3
67·80	3	12,3	−5
66·17	2	—	—
63·96	4	9,1	3
		14,4	0
61·96	3	16,5	−1
59·94	3	11,2	0
58·26	4	8,0	−3
56·96	4	13,3	−5
54·00	3	15,4	−6
3852·91	3	10,1	0
51·79	3	17,5	4
49·93	1	—	—
48·73	2	—	—
46·73	2	9,0	−3
		14,3	−4
43·83	2	16,4	2
42·36	2	11,1	−3
40·60	2	—	—
39·08	1	—	—
36·04	2	15,3	0
34·04	1	12,2	2
		17,4	5
32·08	1	—	—
28·55	1	—	—
25·81	1	18,4	−2

The heat of dissociation $\boldsymbol{D}'$ can be calculated from Birge and Sponer's extrapolation rule. Its value for the upper state is 2320 cm^{-1}. The value for the ground state, $\boldsymbol{D}''$, as given by Loomis and Arvin is 5025 cm^{-1}. With

Table 4. Bands between λ3550 and λ3650, reported by Walter and Barratt as due to NaK, arranged here as part of the first ultra-violet system of Na_2

λair (A.)	Int.	v', v''	$\nu_{obs}-\nu_{calc}$	λair (A.)	Int.	v', v''	$\nu_{obs}-\nu_{calc}$
3538	1	1,8	−5	3603	2	4,14	15
3545	1	3,10	−5	3607	1	0,11	3
3553	2	0,8	−8	3612	4	2,13	8
3561	2	3,11	10	3622	6	5,16	− 4
3569	4	0,9	12	3632	4	2,14	− 5
3577	4	2,11	0	3641	4	6,18	−13
3586	4	5,14	2	3650	2	2,15	− 6
3595	2	2,12	2	3654	1	5,18	0

The values of ν_{calc} have been obtained from the equation representing the Na_2 ultra-violet bands between λ 3600 and λ 3200 measured recently on a 21-ft. concave grating (unpublished).

Table 5. Deslandres' scheme for the ultra-violet bands of NaK

v'' / v'	0	1	2	3	4	5	6	7	8	Mean diff.
0	25214	25091	24968	24847		24606				
1		25185	25064	24943	24819	24701				94·3
2	25400	25278	25156	25033	24912	24793	24675			92
3	25495	25372	25246	25127	25006	24886	24764	24652	24536	92·7
4	25582	25458	25336	25214				24739	24620	87
5	25671	25548	25426	25300						89
6	25752	25632	25504	25388						82·8
7	25832	25709	25592	25473						82·5
8	25911	25791	25671	25548	25426					78·8
9		25873	25752	25622	25504					78·8
10		25947	25822	25704	25582					76
11		26018	25900	25778	25658					74·6
12			25975	25852	25727	25609	25495	25372		72·9
13				25920	25798	25680	25565			70
14				25989	25870	25756	25632	25512		70·8
15				26061	25940	25822	25701	25582		69·4
16					26009	25886	25768			67
17					26075	25955	25832			66
Mean diff.	122·3	122·1	121	121·4	118·7	119·4	118·5	117·5		
(Loomis & Arvin)	(122·9)	(122·1)	(121·3)	(120·5)	(119·7)	(118·9)	(118·1)	(117·3)		

$\nu_{0,0} = 25215$ cm^{-1}, the energy of the dissociated atoms in the excited state, given by $\nu_{atom} = \nu_{0,0} + \boldsymbol{D}' - \boldsymbol{D}''$, is equal to 22 510 cm^{-1}. Since K4 $^2S - 5\,^2S = 21\,025$ cm^{-1} and K4 $^2S - 3\,^2D = 21\,530$ cm^{-1}, and states of Na or other states of K are still farther apart than these, we may reasonably conclude from the above value of ν_{atom} that the dissociated atoms in the excited state are Na3 ^2S and K5 ^2S or 3 ^2D. It is satisfactory to note that the value of ν_{atom} calculated from the observed data is higher than the value required from considerations of atomic levels. This can be understood, because the value of $\boldsymbol{D}'$ from the Birge-Sponer extrapolation is generally higher than the true value of heat of dissociation for such molecules (Gaydon 1946). It is, however, difficult to decide whether the K atom after dissociation in the upper level is in 3 ^2D or 5 ^2S state. If we assume that the above values of $\nu_{0,0}$ and $\boldsymbol{D}''$ are correct, then in order that the K atom should be in 3 ^2D or 5 ^2S state, the value of $\boldsymbol{D}'$ should be 1345 cm^{-1} or 835 cm^{-1} respectively. Of these, in view of the above calculated value of $\boldsymbol{D}'$, 2320 cm^{-1}, the former seems more plausible. Hence, it may be concluded that the products of dissociation are Na3 ^2S + K3 ^2D atoms.

§ 5. DISCUSSION

The ground state of the NaK molecule will be due to Na3 ^2S and K4 ^2S atoms, and will be a $^1\Sigma^+$ state. Excited states will be obtained if we consider either the sodium or the potassium atom to be raised to higher energy levels. The energy levels of Na and K beginning from the lowest atomic level are in order as follows: Na3 ^2S or K4 ^2S, K4 ^2P, Na3 ^2P, K5 ^2S, K3 ^2D, Na4 ^2S . . . . Ordinarily we expect that in molecules like Na_2, K_2 or NaK, the lowest molecular state dissociates into atoms in their lowest states, and the next higher molecular state into atoms in the next higher excited states and so on. Hence the molecular states resulting from normal and excited atoms of Na and K will lie roughly in the following order: $^1\Sigma^+$, $^3\Sigma^+$ (from Na3 ^2S + K4 ^2S); $^1\Sigma^+$, $^3\Sigma^+$, $^1\Pi$, $^3\Pi$ (from Na3 ^2S + K4 ^2P); $^1\Sigma^+$, $^3\Sigma^+$, $^1\Pi$, $^3\Pi$ (from Na3 ^2P + K4 ^2S); $^1\Sigma^+$, $^3\Sigma^+$ (from Na3 ^2S + K5 ^2S) and $^1\Sigma^+$, $^3\Sigma^+$, $^1\Pi$, $^3\Pi$, $^1\Delta$, $^3\Delta$ (from Na3 ^2S + K3 ^2D) . . . . . In transitions from the ground state, which is $^1\Sigma^+$, we are concerned only with the $^1\Sigma^+$ and $^1\Pi$ states. Comparing the latter with similar states in Na_2, K_2 or known state of NaK, we conclude that the $^1\Sigma^+$ will be lower than the $^1\Pi$ state. We should, therefore, have the following systems of bands beginning from the long wavelength side:

Systems 1 and 2: $^1\Sigma^+$, $^1\Pi$ (Na3 ^2S + K4 ^2P) $\leftarrow$ $^1\Sigma^+$
Systems 3 and 4: $^1\Sigma^+$, $^1\Pi$ (Na3 ^2P + K4 ^2S) $\leftarrow$ $^1\Sigma^+$
System 5: $^1\Sigma^+$ (Na3 ^2S + K5 ^2S) $\leftarrow$ $^1\Sigma^+$
Systems 6 and 7: $^1\Sigma^+$, $^1\Pi$ (Na3 ^2S + K3 ^2D) $\leftarrow$ $^1\Sigma^+$. . . . .

Of these, systems 1, 2 and 4 are the infra-red, the orange and the green systems studied by Loomis and Arvin (1934). System 3 has not been observed and is believed to be overlapped by strong Na_2 bands. It does not seem possible to say whether system 3 would lie at wavelengths longer than those of system 2 or at shorter wavelengths. Loomis and Arvin seem inclined to think that the excited $^1\Sigma^+$ state of system 3 is fairly deep and that the bands of this system would, therefore, lie in the red region where they are obscured by red bands of Na_2.

The present system of bands can correspond either to system 5 or to system 6. The energy states of K5 ^2S or K3 ^2D are rather too close together to permit

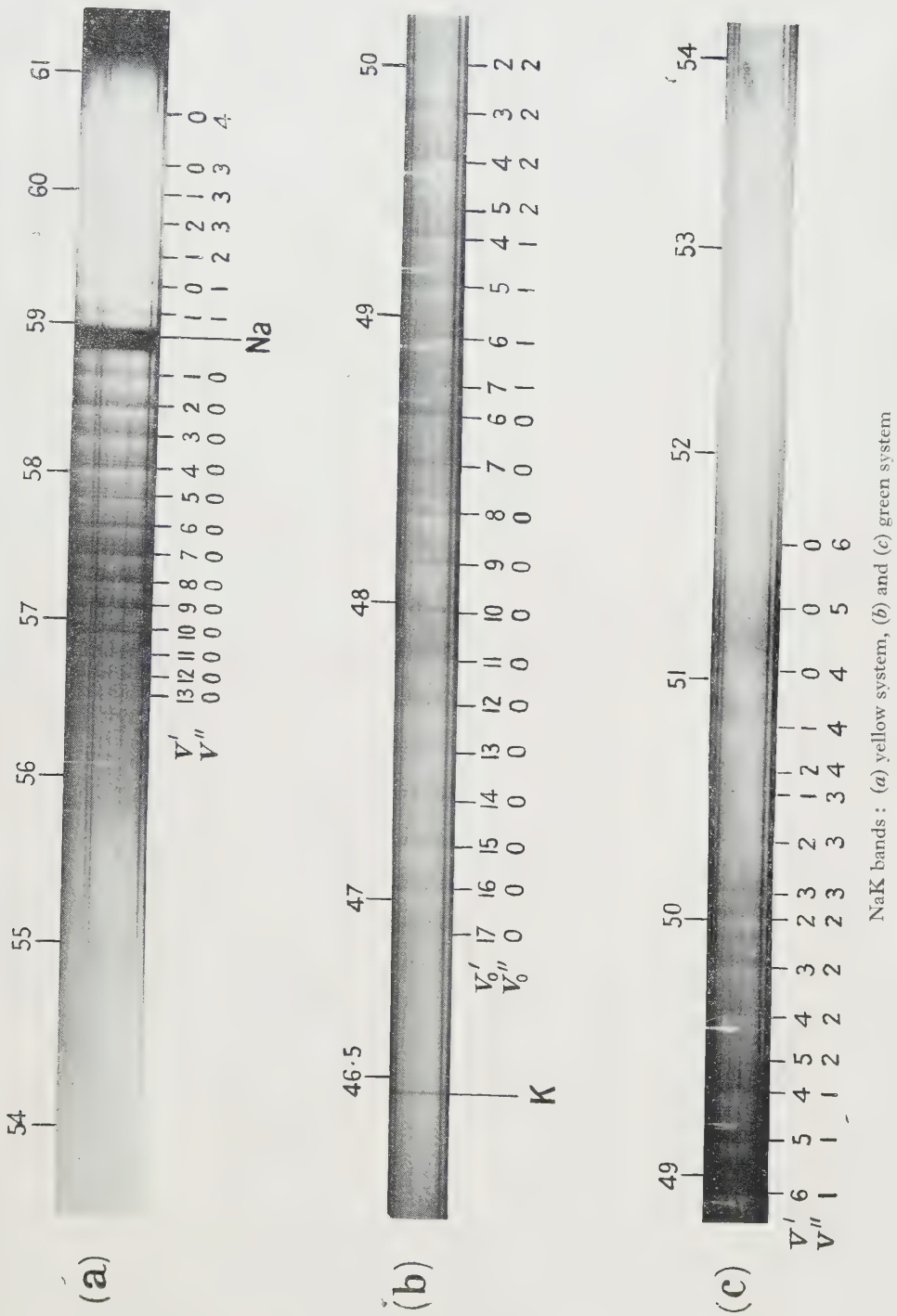

NaK bands : (*a*) yellow system, (*b*) and (*c*) green system

To face page 452

of an unambiguous decision with regard to the dissociation products of the upper state of this system. If we, however, consider the probable error involved in D' we arrive at the conclusion (as shown before) that the dissociated atoms are Na $3\,^2S + \mathrm{K}\,3\,^2D$. This will imply that the bands corresponding to system 5, which will lie at wavelengths longer than those for system 6, are missing. If we consider that like other $^1\Sigma^+$ states, the excited $^1\Sigma^+$ state involved in system 5 is fairly deep so that the bands of this system will lie somewhere in the green region, it is possible that these NaK bands may not be observed at all, having been obscured by strong bands of the green system of Na_2.

ACKNOWLEDGMENTS

The author wishes to acknowledge his indebtedness to Assistant Professor R. W. B. Pearse, D.Sc., for his kind help and valuable suggestions, and to Patna University, India, for the grant of their Birla Scholarship.

REFERENCES

GAYDON, A. G., 1946, *Proc. Phys. Soc.*, **58**, 525.
LOOMIS, F. W., and ARVIN, M. J., 1933, *Phys. Rev.*, **44**, 126 ; 1934, *Ibid.*, **46**, 286.
RITSCHL, R., and VILLARS, D., 1928, *Naturwissenschaften*, **16**, 219.
SINHA, S. P., 1948, *Proc. Phys. Soc.*, **60**, 436.
UCHIDA, Y., 1929, *Jap. J. Phys.*, **5**, 145.
WALTER, J. M., and BARRATT, S., 1928, *Proc. Roy. Soc.* A, **119**, 257.
WEIZEL, W., and KULP, M., 1930, *Ann. Phys., Lpz.*, **4**, 971.

An Extension of Kapitza's Theory of δ-radiation

By R. M. SILLITTO
The University, Edinburgh

Communicated by N. Feather ; MS. received 20 *August* 1947

ABSTRACT. The Kapitza theory of δ-radiation is modified by the introduction of a parameter b specifying the radius of the initial temperature distribution. It is shown that a value for b inferred from the columnar ionization theory of Jaffé leads to estimates of the number of δ-electrons, most probable energy of the δ-electrons, and the duration of the emission process, which are in satisfactory agreement with experimental results for platinum. It is also shown that this satisfactory agreement holds only for quite a small range of values of b.

§ 1. INTRODUCTION

KAPITZA'S theory (1923) of the δ-radiation from solid bodies bombarded by α-particles supposes that the energy lost by an α-particle traversing a solid produces a local heating of the body, that the diffusion of this heat through the body can be described in terms of macroscopic constants (e.g. the thermal conductivity and specific heat), and that those parts of the surface which are heated emit electrons according to Richardson's thermionic equation. These thermionic electrons are supposed to constitute the δ-radiation.

It is assumed by Kapitza that the initial heat is localized along a mathematical line coincident with the track of the α-particle. If we denote distance from this line by r, the initial temperature distribution is thus

$$(T)_{t=0} = \infty, \quad r = 0;$$

$$(T)_{t=0} = 0, \quad r > 0.$$

The temperature distribution at time t, obtained from the equation of heat conduction (assuming purely radial transfer), is expressed in terms of r, the specific heat c, the thermal conductivity k, the density d, and the energy lost per centimetre by the α-particle Q. In principle the macroscopic constants c, k and d should not be used to describe phenomena localized in a space small compared with the spacing of the atoms in the solid; also it would be preferable to assume that the initial temperature distribution occupies a finite volume. Such a modification of the analysis becomes obviously necessary if, in Kapitza's treatment, we write Richardson's equation in the form $N = A'T^2 e^{-\phi/T}$ instead of $N = AT^{\frac{1}{2}} e^{-\phi/T}$; for otherwise, with this change, the number ν of δ-electrons per α-particle becomes

$$\nu = -(A'Q^2/8\pi kcd)\mathrm{Ei}(0) = \infty.$$

The argument of the exponential integral function is proportional to the negative reciprocal of the maximum temperature occurring at $r = 0$; for ν to be finite this temperature must be finite, and hence the initial distribution must occupy a finite volume.

§ 2. THE TEMPERATURE DISTRIBUTION

In Jaffé's theory (1913) of the columnar ionization produced in fluids by α-particles, it is assumed that the initial ion density has a cylindrically symmetrical distribution proportional to $\exp(-r^2/b^2)$. This assumption has been justified on theoretical grounds by Lea and Kara-Michailova (1940) who show that b is independent of the energy of the ionizing particle. It is found experimentally that the distribution parameter b is, to a first approximation, inversely proportional to the density of the fluid, and independent of its nature. We shall assume that the initial temperature distribution produced by the passage of an α-particle through a solid * is also of the form $\exp(-r^2/b^2)$, and, further, that an estimate of the magnitude of b can be obtained from the proportionality relation which applies for fluids. It thus appears that for platinum (see below) we may take $b \simeq 7 \times 10^{-8}$ cm, or 7 Å., a value which is perhaps large enough to allow the macroscopic constants to have some relevance. (It should be observed, however, that in the application of the columnar ionization theory to fluids it is found that the numerical results obtained are very sensitive to variation of b and the practice is to choose a value of b which leads to results in agreement with experiment. In the discussion which follows it will appear that the result of the calculation of the number of δ-electrons is similarly very sensitive to variations of b.)

* There must obviously be a certain, though extremely short, time lag between the passage of the α-particle and the establishment of a physically recognizable temperature distribution; it is perhaps in the recognition of this point that the method of the present paper differs significantly from that of Kapitza.

For the initial temperature distribution we now write

$$(T)_{t=0} = T_0 + (Q/\pi cdb^2)\exp(-r^2/b^2) \qquad \ldots\ldots(1)$$

where T_0 is the temperature of the target before the entry of the α-particle. It follows that, at time t,

$$T = T_0 + \frac{Q}{\pi cd(4kt/cd + b^2)} \cdot \exp\left(-\frac{r^2}{4kt/cd + b^2}\right). \qquad \ldots\ldots(2)$$

§ 3. THE NUMBER OF δ-ELECTRONS

If the α-particle enters the solid normal to the surface, and we assume that (2) gives the temperature distribution on the surface, the total δ-emission is obtained by combining (2) with

$$\nu = \int_0^\infty \int_0^\infty \pi A' T^2 e^{-\phi/T} dr^2 dt \qquad \ldots\ldots(3)$$

and evaluating the integral. Following Kapitza we change this to an integral over surface elements $d\omega$ in the (r^2, t) plane for which T is constant. The analysis is considerably simplified if we drop the constant T_0 of equations (2) and (3), and consider the range of temperature variation as being from 0 to $T_{\max}$ (say) rather than from T_0 to $T_0 + T_{\max}$. If T_0 represents room temperature, say 300° K. and $T_{\max}$ is of the order of 10^4 °K. (see below), no significant error is introduced by this approximation. We then find that

$$d\omega = \left\{\frac{Q^2}{8\pi^2 kcdT^3} - \frac{cdb^4}{8kT}\right\} dT$$

and hence

$$d\nu = \frac{A'}{8k}\left\{\frac{Q^2}{\pi cd}\frac{e^{-\phi/T}}{T} - \pi cdb^4\, T e^{-\phi/T}\right\} dT. \qquad \ldots\ldots(4)$$

When $t = 0$, $r = 0$, we have $T = T_{\max} = T_{\mathrm{m}} = Q/\pi cdb^2$, so that

$$\nu = \frac{A'Qb^2}{8k}\int_0^{T_{\mathrm{m}}}\left\{\frac{T_{\mathrm{m}}}{T}\cdot e^{-\phi/T} - \frac{T}{T_{\mathrm{m}}}\cdot e^{-\phi/T}\right\} dT. \qquad \ldots\ldots(5)$$

If $\theta = -\phi/T$, $\theta_{\mathrm{m}} = -\phi/T_{\mathrm{m}}$, (5) becomes

$$\nu = \frac{A'\phi Qb^2}{8k}\int_{-\infty}^{\theta_{\mathrm{m}}}\left(\frac{1}{\theta_{\mathrm{m}}} - \frac{\theta_{\mathrm{m}}}{\theta^2}\right)\frac{e^\theta}{\theta} d\theta$$

giving

$$\nu = \frac{A'\phi Qb^2}{8k}\left\{\left(\frac{1}{\theta_{\mathrm{m}}} - \frac{\theta_{\mathrm{m}}}{2}\right)\mathrm{Ei}(\theta_{\mathrm{m}}) + \left(1 + \frac{1}{\theta_{\mathrm{m}}}\right)\frac{e^{\theta_{\mathrm{m}}}}{2}\right\}. \qquad \ldots\ldots(6)$$

For the α-rays from polonium falling at the beginning of their range on a platinum target, $Q \simeq 2 \times 10^{-10}$ cal/cm. For Pt, du Bridge gives $A' = 1{\cdot}02 \times 10^{23}$ electrons/sec. cm² deg², and $\phi = 7{\cdot}28 \times 10^4$ °K. Taking $c = 0{\cdot}05$ cal/gm., corresponding to a temperature in the neighbourhood of 2×10^3 °K., we find $T_{\mathrm{m}} = 1{\cdot}21 \times 10^4$ °K. From (6), therefore, we obtain $\nu = 11$ electrons/α-particle.

Experimental values for ν lie between about 0·5 and 15; a value between 5 and 10 seems most probable.

§ 4. THE ENERGY OF THE δ-ELECTRONS

As indicated by Kapitza, (4) may be regarded as specifying the "distribution in temperature" of the emitted electrons. The equation may be rewritten as

$$d\nu = \frac{A'Qb^2}{8k}\left\{\frac{T_{\mathrm{m}}}{T}e^{-\phi/T} - \frac{T}{T_{\mathrm{m}}}e^{-\phi/T}\right\} dT \qquad \ldots\ldots(4')$$

which clearly vanishes when $T=0$ or T_m. dv must therefore have a maximum at some intermediate value of T, which can be found by differentiating the expression with respect to T, and equating to zero. There results the equation

$$T^3+\phi T^2+T_m^2T-\phi T_m^2=0 \qquad \ldots\ldots(7)$$

whose solution may be called the "most probable temperature" of the emitted electrons, and written T_p. The ratio T_p/T_m is found to depend on b, and to vary between 0·8 and 0·9 as b varies from 6 to 9 A. With $b=7$ A. we find $T_p/T_m=0{\cdot}87$, and hence $T_p=1{\cdot}05\times10^4$ °K. If we denote the most probable energy of the electrons by E_p, we should have in this case $E_p=0{\cdot}90$ ev., and should therefore expect the energy spectrum of the secondary electrons to show a peak in the neighbourhood of 0·9 ev., while the mean energy should be in the neighbourhood of 1·3 ev. In practice the majority of the secondary electrons appear to have energies in the range 0–2 ev.

§ 5. THE DURATION OF THE δ-EMISSION PROCESS

From equation (2), it follows that the time taken for the temperature excess (i.e. $T-T_0$) at the centre of the distribution to fall to $1/n$ of its value at $t=0$ is

$$\tau=(cdb^2/4k)(n-1). \qquad \ldots\ldots(8)$$

If we set $n-1=100$ we should obtain an effective upper limit to the duration of the secondary emission process; numerically this gives

$$\tau=0{\cdot}78\times10^{-12}\text{ sec.}$$

Work on electron multipliers (Greenblatt and Miller 1947) shows that the secondary emission takes place in a time less than 5×10^{-11} sec.

§ 6. THE DISTRIBUTION PARAMETER b

The results obtained thus far, using a value of b inferred from the columnar ionization theory, are in satisfactory agreement with experiment. It is a matter of some interest to investigate the dependence of the results on the magnitude of b. Table 1 illustrates the variation.

Table 1

b (A.)	6·0	6·5	7·0	7·5	8·0	8·5	9·0
v	32·0	21·0	11·0	4·9	2·3	0·99	0·35
E_p (ev.)	1·15	1·02	0·90	0·80	0·71	0·64	0·56
τ ($\mu\mu$ sec.)	0·57	0·67	0·78	0·89	1·01	1·14	1·28

v appears to vary rather rapidly with b; the best value for b does indeed appear to be about 7 A. The separation of Pt atoms in the lattice is approximately 2·5 A.; the uncertainty allowed in choosing a value of b to fit the experimental data appears therefore to be considerably less than the lattice spacing.

ACKNOWLEDGMENT

The author is indebted to Professor N. Feather, F.R.S., for his interest in this work and for his guidance in the preparation of this note.

REFERENCES

Greenblatt, M. H., and Miller, P. H., Jr., 1947, *Phys. Rev.*, **72**, 160.
Jaffé, G., 1913, *Ann. Phys., Lpz.*, **42**, 303.
Kapitza, P. L., 1923, *Phil. Mag.*, **45**, 989.
Lea, D. E., and Kara-Michailova, E., 1940, *Proc. Camb. Phil. Soc.*, **36**, 101.

Angular Distribution in Internal Pair Creation

By G. K. HORTON
Department of Mathematical Physics, University of Birmingham

Communicated by R. E. Peierls ; MS. received 15 *November* 1947

If, in a nuclear process, gamma rays are emitted with an energy exceeding one million electron volts, electron–positron pairs may be created in the field of the emitting nucleus. The process is exactly analogous to internal conversion with the creation of a pair replacing the ejection of an atomic electron.

It is well known that nuclear transitions differ in character (as do atomic transitions) and that they can be classified as electric and magnetic dipole, quadrupole etc. transitions with different selection rules for angular momentum and parity applying to each type. We shall show that the statistics of the angles between the directions of the electron and positron emitted in internal pair creation provides a method of distinguishing between the different types of transition without requiring the comparison between counts of gamma quanta and electrons. Magnetic dipole radiation is indistinguishable from electric quadrupole radiation by this method and they are in any case likely to appear mixed in a nuclear transition. (The selection rules that go with them are not mutually exclusive).

This method offers an alternative to the well known procedure in which the ratios of the conversion coefficients from the K, L . . . etc. shells are used. At higher energies where the method here proposed becomes applicable, such a procedure may become difficult as then the conversion electrons from different shells differ relatively little in energy.

External pair creation can occur only in the presence of a field of force (usually the electrostatic field of a nucleus) which takes up excess momentum; the spontaneous transformation of a photon into a pair is not compatible with conservation of both energy and momentum. Hence the probability of the production of external pairs is proportional to the square of the atomic number Z. In internal pair creation, on the other hand, the photon is absorbed so close to the emitting nucleus that in the distance it has travelled before creating a pair, the uncertainty principle does not allow its momentum to be determined exactly, or in other words, the neighbourhood of the emitting nucleus, acting as a source of radiation, still makes itself felt, even apart from the nuclear electrostatic field. As a result, internal pair creation is as important for light as for heavy elements (cf. Jaeger and Hulme 1935) and for the former one may assume the components of the emitted pair to be free.

Such calculations were carried out by Oppenheimer and Nedelski (1933) and Rose and Uhlenbeck (1933). (Exact calculations carried out later by Jaeger and Hulme (1935) justified the approximations made in the earlier calculations at least qualitatively.) Rose and Uhlenbeck give results for the number of pairs for which the positive and negative electrons have energies E' and E'' respectively and are emitted in directions forming an angle θ with each other. This number is given as a function of E' and θ for each value of the total energy in the case

of electric dipole and quadrupole transitions. For the magnetic dipole transitions only the total number of pairs regardless of angle is given as a function of E'.

I have carried out a similar calculation for the angular distribution in the case of magnetic dipole transitions. The number of pairs for which θ lies within an interval $d\theta$ and in which E' lies between $\epsilon' mc^2$ and $(\epsilon'+d\epsilon')mc^2$ is found to be:

$$P(\epsilon',\theta)d\epsilon' \sin\theta d\theta = \frac{\alpha p' p''}{2\pi\gamma(\epsilon'\epsilon''+1-\boldsymbol{p}'.\boldsymbol{p}'')^2}\left\{\begin{array}{l}(\epsilon'\epsilon''+2)-3\gamma^{-2}(\epsilon'\epsilon''+1)^2\\ -\boldsymbol{p}'.\boldsymbol{p}''[1-4\gamma^{-2}(\epsilon'\epsilon''+1)]\\ -\gamma^{-2}(\boldsymbol{p}'.\boldsymbol{p}'')^2\end{array}\right\} d\epsilon' \sin\theta d\theta,$$

where
$$\alpha=\frac{e^2}{\hbar c},\quad |\boldsymbol{p}'|=(\epsilon'^2-1)^{\frac{1}{2}},\quad |\boldsymbol{p}''|=(\epsilon''^2-1)^{\frac{1}{2}}$$
$$\boldsymbol{p}'.\boldsymbol{p}''=|\boldsymbol{p}'||\boldsymbol{p}''|\cos\theta,\quad \gamma=h\nu/mc^2,$$

$h\nu$ being the disintegration energy and $\epsilon''=\gamma-\epsilon'$ is the energy of the positron in units of mc^2. E' and E'' include the rest energy.

As it is difficult to determine experimentally the total number of gamma quanta emitted by an assembly of excited nuclei, it is not easy to measure the absolute probability of internal pair production per emitted gamma quantum (Jaeger and Hulme 1935). Another type of experimental procedure would be to measure the number of pairs as a function of the angle θ between the two components of the pair. A comparison with the calculated results, discussed in this paper, will then show the multipolarity of the gamma ray. In order to facilitate this comparison we give graphs for the three cases, magnetic and electric dipole and electric quadrupole transitions.

Figure 1 shows, for two given total energies, the number of pairs produced per disintegration, in equal intervals of $\cos\theta$, as a function of $\cos\theta$. Equal intervals of $\cos\theta$ correspond to constant solid angle and are convenient for counting experiments in which the solid angle subtended by each counter will usually be independent of the relative position of the two counters.

Figures 2 and 3 show the number of pairs produced, per disintegration, against $\cos\theta$, for given electron–positron energies. We have shown only two representative cases, one in which the electron carries half the energy, the other in which one carries most. It is easy to see from these two cases the qualitative behaviour for other energy distributions.

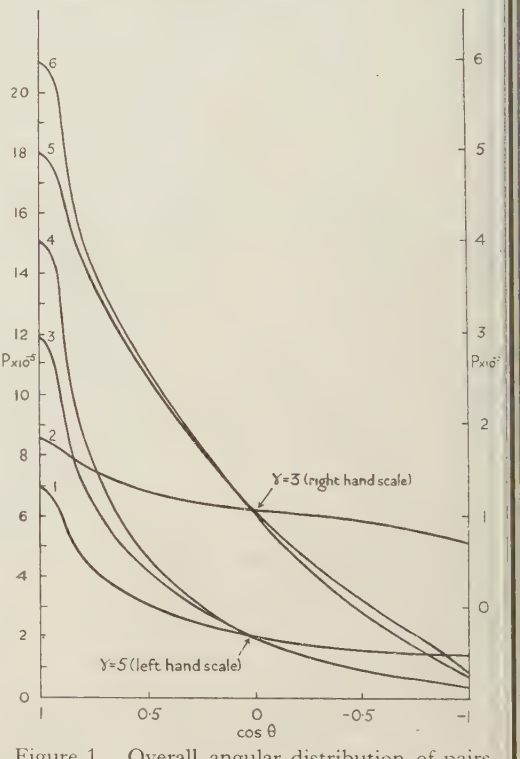

Figure 1. Overall angular distribution of pairs.
1, 2, Electric dipole.
4, 6, Magnetic dipole.
3, 5, Electric quadrupole.
The absolute values are given for the electric dipole case and the other two normalized to coincide with it at $\cos\theta=0$.

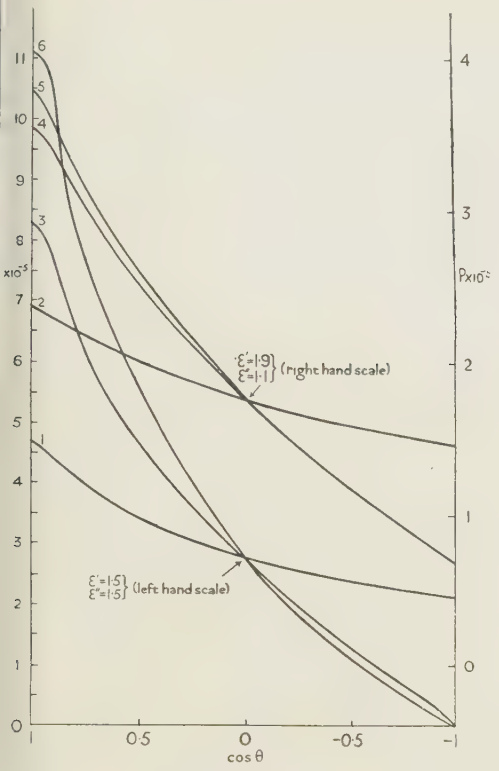

Figure 2. The probability for a given energy distribution with $\gamma=3$.
1, 2, Electric dipole.
5, 6, Magnetic dipole.
3, 4, Electric quadrupole.
The absolute values are given for the electric dipole case and the other two normalized to coincide with it at cos $\theta=0$.

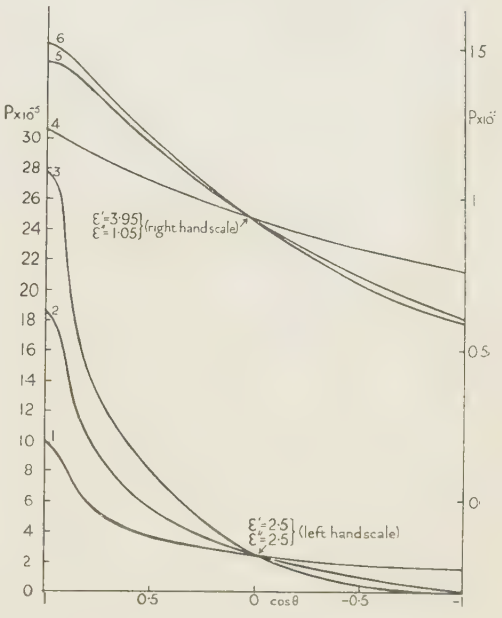

Figure 3. The probability for a given energy distribution with $\gamma=5$.
1, 4, Electric dipole.
3, 5, Magnetic dipole.
2, 6, Electric quadrupole.
The absolute values are given for the electric dipole case and the other two normalized to coincide with it at cos $\theta=0$.

Lastly we show, in figure 4, the average value of $\cos\theta$ plotted against various energy distributions among the components of the pair and for two values of the incident photon energy.

The following conclusions may be drawn. We have obtained results symmetrical in the electron and positron by neglecting the electrostatic field of the nucleus. The magnitude of the effect is of the order $0{\cdot}5-1{\cdot}5.10^{-4}$ pairs per nuclear disintegration. The angular distributions are qualitatively similar. Let us call K_D and K_Q respectively the ratios of the number of pairs per disintegration at $\cos\theta=1$ to those at $\cos\theta=-1$ in

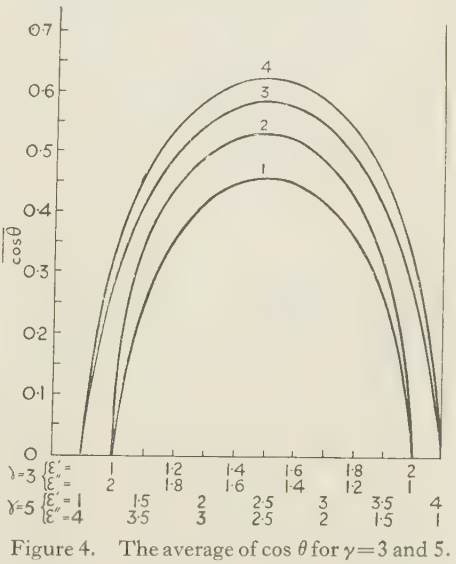

Figure 4. The average of cos θ for $\gamma=3$ and 5.
1, 3, Magnetic dipole or electric quadrupole.
2, 4, Electric dipole.

the case of electric dipole and quadrupole (or magnetic dipole) transitions respectively and let $K = K_Q/K_D$. (We see from the curves that electric quadrupole and magnetic dipole transitions are hardly distinguishable by this method.)

In figure 1, for $\gamma = 5$, $K \simeq 8$ and for $\gamma = 3$, $K \simeq 15$. In figures 2 and 3, for very asymmetric energy distributions between the components of the pair, we find $K \simeq 2$. When the electron and positron share the available energy equally, we find that $K \simeq 5 \cdot 10^3$ for γ equal to both 3 and 5.

In figure 4 we find that the average angle between the pair, for $\gamma = 3$, is the same for both electric quadrupole and magnetic dipole radiation. In both these cases the average angle, for each distribution of energy among the components of the pair, is about 20% larger than in the case of electric dipole transitions. The same applies for $\gamma = 5$ when all the average angles are somewhat smaller.

The method may be used, together with selection rules such as parity and angular momentum, to interpret nuclear spectra by assigning angular momentum quantum numbers to the various levels.

ACKNOWLEDGMENT

The author wishes to thank Professor R. E. Peierls for his guidance of this work and the Department of Scientific and Industrial Research for a maintenance grant.

REFERENCES

Jaeger, J. C., and Hulme, H. R., 1935, *Proc. Roy. Soc.* A, **148**, 708.
Oppenheimer, J. R., and Nedelski, L., 1933, *Phys. Rev.*, **44**, 948 ; corrected in 1934, *Ibid.*, **45**, 283.
Rose, M. E., and Uhlenbeck, G. E., 1933, *Phys. Rev.*, **48**, 211.

The Correction for Self-Weakening in β-Ray Measurements *

By E. Broda [1], W. E. Grummitt [2], J. Guéron [3], L. Kowarski [3] and G. Wilkinson [4]

[1] Now at Department of Natural Philosophy, The University, Edinburgh.
[2] Now at National Research Council, Chalk River, Ontario.
[3] Now at Commissariat à l'Energie Atomique, Paris.
[4] Now at Chemistry Department, University of California.

MS. received 18 *November* 1947

ABSTRACT. Experimental details are given for the determination of self-weakening of β-rays in thick samples. The self-weakening correction factor in the case of twelve radio-elements is found over a considerable region to depend logarithmically on the mass-thickness of the sample. The self-weakening half-thicknesses $\eta_{\frac{1}{2}}$ is as a rule 2·2 times larger than the external weakening half-thickness $\epsilon_{\frac{1}{2}}$. The logarithmic dependence of the self-weakening correction factor on mass-thickness and the value of the ratio $\eta_{\frac{1}{2}}/\epsilon_{\frac{1}{2}}$ are derived in a simplified theoretical treatment.

---

* The work described in this paper was done for the Department of Scientific and Industrial Research, and the National Research Council, Canada, during 1942 and 1943. It was reported at that time, but could not be released for publication due to security regulations.

§ 1. INTRODUCTION

THE measurement of the specific activity, i.e. of the number of disintegrations per unit time and per unit mass, of a given β-ray emitting sample is frequently involved in the exploration of neutron densities with detectors, and in the determination of cross-sections for nuclear reactions leading to the formation of β-emitters. Such measurements are usually carried out by placing the sample close to a β-ray sensitive device (Geiger counter or electroscope), which, however, fails to respond to such β-particles as may be absorbed or scattered away during their passage through the sample itself. This " self-weakening " has to be taken into account as a correction when interpreting the response of the measuring device.

The necessity for this correction can sometimes be circumvented. If the sample is thin enough, self-weakening may be neglected altogether, but the recourse to thicker samples is often necessary in order to get enough intensity. Many kinds of comparative measurements, in arbitrary units, can be carried out by using samples of exactly identical thickness, so that the self-weakening corrections cancel out. The preparation of samples of exactly prescribed thickness is, however, inconvenient, especially if the material is short-lived and needs chemical treatment before counting. Moreover, this device is of no avail if different β-emitters are to be compared.

It might be thought that the "true" specific activity (i.e. that of a sample of vanishing thickness) could be deduced from the observed specific activity (of a thick sample) by applying rules on β-ray absorption, using values of absorption coefficients predetermined in suitably chosen external screens. But absorption and scattering of β-rays are so complex, and the sample-and-counter geometry is so little amenable to mathematical treatment, that a purely empirical approach seems desirable. Broda, Guéron and Kowarski (1942) calibrated the observed specific activity n for various mass-thicknesses of several β-emitters (UX_2, U 239, Mn 56 and I 128) in samples of equal area and in their particular counting geometry. A linear relationship between the mass-thickness and the logarithm of the specific activity was found to hold in a wide range, including in particular the domain of small thicknesses. With the help of such calibration curves the true specific activity, i.e. the specific activity as measured with very thin samples, can be deduced from the value n measured with thick samples. The same authors listed values of the "mass-thickness for self-weakening to one-half" ($\eta_{\frac{1}{2}}$) i.e. the mass thickness at which the β-ray intensity per unit weight of a given sample is reduced to one-half. Grummitt, Guéron and Wilkinson (1943) investigated the same elements in a different counting geometry. They confirmed the general conclusions drawn by Broda, Guéron and Kowarski, but their values of $\eta_{\frac{1}{2}}$ were slightly different, perhaps because of the changes in the geometry. Grummitt, Guéron and Wilkinson also extended the method to Th 233, Ba 139, Ba 140, La 140, and I 131. Results of other authors (Hendricks, Bryner, Thomas and Ivie 1943, Yankwich, Rollefson and Norris 1946, and Cook, private communication) on S 35, C 14 and Ms Th 2 will be shown to be amenable to a similar treatment. While the method, therefore, is widely applicable, the numerical values quoted in this paper are valid only under the given experimental conditions.

§ 2. EXPERIMENTAL PROCEDURES

(i) *Chemical*

(*a*) *Mn* 56 *and I* 128. These activities were obtained by exposure to slow neutrons of manganese oxide (empirical formula $MnO_{1\cdot47}$) and lead iodide. The activity of these compounds was measured without chemical treatment after irradiation.

(*b*) *U* 239. Uranium as sodium uranyl acetate was irradiated with slow neutrons. In order to reduce the natural β-ray activity, and to remove fission products, chemical treatment was necessary. Excess sodium acetate was added with stirring to a cold solution containing 10% uranium by weight and 25% acetic acid by volume. The crystalline precipitate of sodium uranyl acetate was washed on the filter with saturated sodium acetate solution, a small amount of water, and finally with acetone. It was then dissolved in the minimum amount of nitric acid, the concentrations of uranium and acetic acid were adjusted and the uranium reprecipitated. Two sodium uranyl acetate precipitations before irradiation reduced the UX activity almost to zero; after irradiation, a further two precipitations reduced the fission product activity and newly grown UX activity to less than 1% of the initial U 239 count. The samples were ready for counting 10–15 minutes after the end of irradiation.

(*c*) *Th* 233. Thorium also had to be freed from its decay products. The procedure was to add to a solution of thorium nitrate before irradiation barium and lanthanum carriers (for radium and actinium) and to precipitate their carbonates with excess ammonium carbonate. The filtrate, containing the soluble thorium carbonate complex, was acidified with nitric acid, and after addition of more barium salt barium was precipitated again with sulphuric acid and removed by filtration. Now lanthanum, bismuth, lead and barium ions were added as hold-back carriers, and the thorium was precipitated at 60° c. with excess 40% H_2O_2 as thorium peroxynitrate. This was redissolved in the minimum quantity of boiling concentrated HNO_3 with the addition of a little HCl. The peroxynitrate precipitation, again in presence of a hold-back carrier, was repeated, and the precipitate ignited to ThO_2. The residual β-activity of non-irradiated ThO_2 was about 40 counts per minute per gramme (counter efficiency about 25%).

(*d*) *Ba* 140 *and La* 140. These activities were separated from the mixture of fission products formed in the slow neutron irradiation of uranium oxide or uranyl nitrate. The details of the chemical procedure (Grummitt, Guéron, Wilkinson and Yaffe, 1947) follow in general the fuming nitric acid method of Hahn and Strassmann (1942).

(ii) *Preparation of samples and counting*

At first cylindrical aluminium counters of wall thickness 40 mg/cm² were used. The counters were filled to 4 cm. Hg with argon and to 2 cm. Hg with alcohol vapour. The finely powdered activated materials were spread evenly on rectangular aluminium trays of area 2·1 cm². A few drops of an acetone solution of collodion ($\simeq$0·5 mg/cm² collodion) were added as binder, the sources dried by gentle heating and covered with a single layer of "sellotape". The sources were disposed around the central portion of the counter tube. This

method allows efficient utilization of weak sources due to the large area exposed. It is, however, an inconvenient and inaccurate arrangement for work with external absorbers.

In the later measurements (Grummitt, Guéron and Wilkinson 1943) a "bell jar" type of β-ray counter with a mica window of area 7·1 cm² and mass thickness 5 mg/cm² was used. It was filled to 9 cm. Hg with argon, and to 0·5 cm. Hg with alcohol. Circular aluminium trays of area 7·1 cm² were supported 1 cm. below the window by means of a sample holder placed in a slotted frame. Samples were prepared as previously, but were not covered with "sellotape".

In no case were the samples counted without mechanical or chemical mixing after irradiation. This is important as the effect of unequal activation at different depths, due to the absorption of the effective neutrons, particularly resonance neutrons, has to be excluded.

(iii) *Measurements*

The measured activities of the samples were corrected for variations in the counter efficiency with the help of uranium standard. In the cases of U 239 and Th 233 an additional correction of the measured β-ray counts was necessary due to the growth of the natural β-ray activity in the samples after chemical purification. Correction was made with U 239 by counting the UX activity some time after the decay of the 23·5 minutes period with extrapolation back to the time of counting of U 239. With Th 233 a non-irradiated reference sample was used; since the fission products of Th were too weak to interfere, chemical treatment after irradiation was not necessary.

The results were expressed in terms of n, the apparent specific activity of the material, i.e. as the number of counts per minute per gramme of active material at an arbitrary reference time. The logarithm of n was then plotted against the mass thickness M of the sample. In figure 1 typical plots for U 239 are given. As the neutron flux varied between the sets of experiments, the results of each set were normalized at a point in the middle of the mass-thickness range studied. Extrapolation of this composite curve to mass thickness zero gives a value n_0, the true specific activity of the sample. In figure 2 the self-weakening calibration curves, i.e. the plots of $\log(n_0/n)$ against M, are given for the bodies investigated. The self-weakening correction for any thickness is read directly from these curves. For all the radiations measured $\log n_0 n$ depended linearly on M. In table 1 the values of the self-weakening half-thicknesses $\eta_{\frac{1}{2}}$, as read from the calibration curves, are collected. Further, the table gives the weakening half-thicknesses $\epsilon_{\frac{1}{2}}$ as determined by measurement of the β-ray absorption in aluminium foils placed midway between sample and

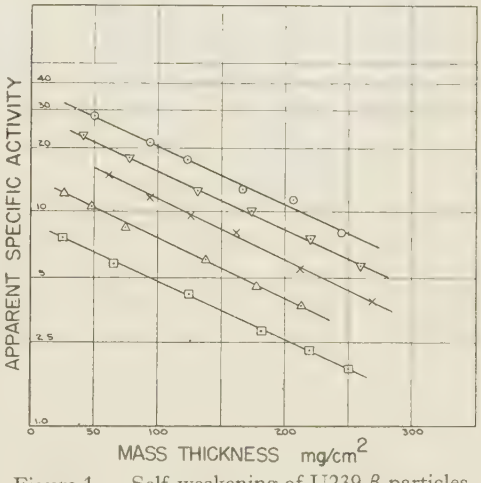

Figure 1. Self-weakening of U239 β-particles in sodium uranyl acetate.

Table 1

Radioactive nucleus	Active material	$\eta_{\frac{1}{2}}$ (mg/cm²)	$\epsilon_{\frac{1}{2}}$ (mg/cm²)	$\eta_{\frac{1}{2}}/\epsilon_{\frac{1}{2}}$
UX_2	Sodium uranyl acetate	243[b] 228[a]	135[b]	1·81
U 239 (23·5 min.)	Sodium uranyl acetate	113[b] 92[a]	54[b]	2·1
Mn 56 (2·54 h.)	$MnO_{1·47}$	458[b] 512[a]	171[b]	2·74
I 128 (25 min.)	PbI_2	266[b] 297[a]	128[b]	2·08
Th 233 (23 min.)	ThO_2	134[b]	56[b]	2·4
La 140 (40 h.)	LaF_3	156[b]	76[b]	2·06
Ba 140 (12·7 d.)	$BaSO_4$	91[b]	41[b]	2·23
S 35 (87·1 d.)	$BaSO_4$	6·9[c]	3·14[c]	2·2
C 14 (4700 y.)	$BaCO_3$	6·0[d]	3[d]	2·0
I 131 (8·0 d.)	CuI	56[b] 60[e]	22[b] 25[e]	2·54 2·4
Ba 139 (86 min.)	$BaSO_4$ $Ba(NO_3)_2$	323[b] 295[e]	147[b]	2·2
MsTh 2 (6·13 h.)	$BaBeF_4$	145[f]		

[a] Broda, Guéron and Kowarski.
[b] Grummitt, Guéron and Wilkinson.
[c] Hendricks, Bryner, Thomas and Ivie 1943.
[d] Yankwich, Rollefson and Norris 1946.
[e] Broda 1943, 1944.
[f] Cook, private communication.

counter. It is to be noted that the external absorption for UX_2, Mn 56 and I 128 in the present geometrical arrangement does not follow an exponential relationship over even a limited portion of the range.

Figure 2 and table 1 also give self-weakening data calculated from experiments by other authors to conform with the $\log n_0/n$ against M presentation as used above. It is noteworthy that even with β-radiations as soft as those of S 35 and C 14 the logarithmic relation holds over a considerable range of mass thicknesses.

In table 1, column 5, the ratio of the self-weakening half-thickness and the weakening half-thickness (with external screens) is listed. With a few exceptions, notably UX_2 and Mn 56, the values of this ratio fall close to the average $\eta_{\frac{1}{2}}/\epsilon_{\frac{1}{2}} = 2.2$.

§ 3. DISCUSSION

The experimental results show that the relationship between the self-weakening correction factor and

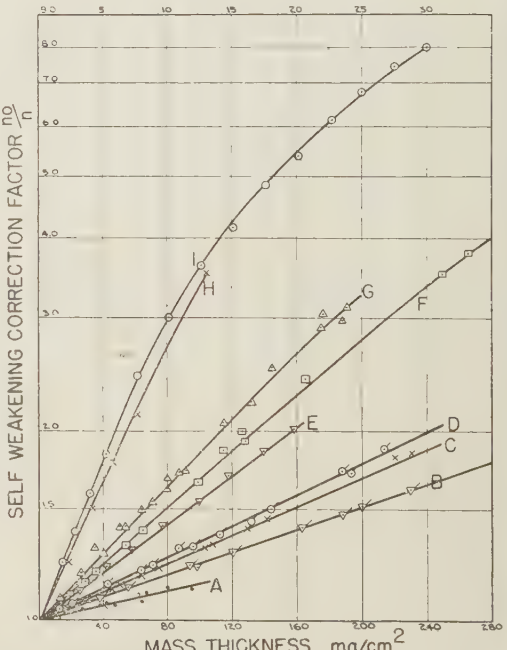

Figure 2. The self-weakening correction factor n_0/n *vs* mass thickness for the following β-radiations:
A. Mn56 in manganese oxide ($MnO_{1·47}$).
B. Ba139 in barium sulphate.
C. I128 in lead iodide.
D. UX_2 in sodium uranyl acetate.
E. La140 in lanthanum fluoride.
F. Th233 in thorium dioxide.
G. U239 in sodium uranyl acetate.
H. S35 in barium sulphate (upper scale).
I. C14 in barium carbonate (upper scale).

the mass-thickness of the active sample can be considered as logarithmic over a considerable mass range.

The relation can be deduced by a simplified theoretical treatment with the following assumptions :

(*a*) The measurements are made in a parallel beam geometry.

(*b*) The weakening of β-rays as measured by external screens obeys an exponential law over the initial portion of the curve, and the weakening is independent of the nature of the screen, i.e. $n = n_0 e^{-\mu x}$ where x is the mass thickness of the absorber, μ the mass absorption coefficient, and n_0 and n the numbers of incident and transmitted particles. The external half-thickness $\epsilon_{\frac{1}{2}}$ is $0{\cdot}693/\mu$.

(*c*) The back-scattering of β-rays by the sample and by the backing material can be considered as identical. This assumption is justifiable if backing material of atomic number similar to that of the active material is used.

Then the contribution to the total β-activity of a layer of mass thickness dm at a depth m in a thick sample of active material of specific activity n_0 is

$$dA = n_0 e^{-\mu m}\, dm.$$

The total activity of the sample of mass thickness M is, therefore,

$$A = \int_0^M n_0 e^{-\mu m}\, dm = (n_0/\mu)(1 - e^{-\mu M}).$$

The apparent specific activity n of the sample is

$$n = A/M = (n_0/\mu M)(1 - e^{-\mu M})$$

and the ratio of the apparent and the true specific activity is

$$\frac{n}{n_0} = \frac{(1 - e^{-\mu M})}{\mu M} = 1 - \frac{\mu M}{2!} + \frac{\mu^2 M^2}{3!} - \frac{\mu^3 M^3}{4!} + \ldots . \qquad \ldots\ldots (1)$$

In figure 3 the expression $\log \mu M/(1 - e^{-\mu M})$ is plotted as a function of M. Thus it appears that on the above assumptions the self-weakening correction curve n_0/n against M is approximately logarithmic over the initial region. The value of μM, which reduces the activity function (1) to $\frac{1}{2}$, is 1·53, i.e. $\mu\eta_{\frac{1}{2}} = 1{\cdot}53$ and $\eta_{\frac{1}{2}} = 2{\cdot}21\,\epsilon_{\frac{1}{2}}$.

Serious divergence from the linear relationship occurs at values of $\mu M > \sim 2$, i.e. at values $M > \sim 3\,\epsilon_{\frac{1}{2}}$. The experimental correction curve for C 14 in barium carbonate shows divergence from linearity at mass thicknesses greater than 8 mg/cm², i.e. approximately 2·7 times the external absorption half-thickness for the β-rays of C 14. However, in the case of S 35 no deviation is evident up to $M = 4{\cdot}5\,\epsilon_{\frac{1}{2}}$.

Feather (1943, 1944) has submitted the whole problem of self-weakening of β-rays to a careful theoretical treatment, and has given

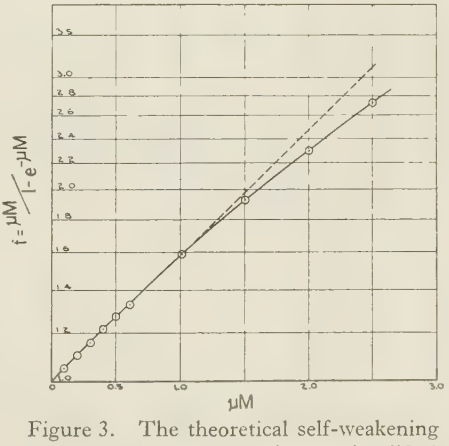

Figure 3. The theoretical self-weakening relation as given by a simplified treatment.

explicitly the conditions under which a logarithmic relation, as found in our work, may be expected to hold.

It is to be expected from the well-known complexities of β-ray scattering and absorption that the numerical values will vary with the geometrical conditions of measurement. However, the relation $\eta_{\frac{1}{2}} = 2{\cdot}2\,\epsilon_{\frac{1}{2}}$ is approximately obeyed in the majority of the experiments listed in table 1. Such discrepancies as exist are not accounted for by the differences between the average atomic number of the active material and the external absorber (Al), nor is there so far any obvious correlation with the energies of the radiation. Data on radiations from more radioelements are necessary before drawing any conclusion.

REFERENCES

Broda, E., 1943, *British Atomic Energy Report*, BR. 365, declassified as BBDA. 45 ; 1944, *Ibid.*, BR. 506, declassified as BBDA. 57.

Broda, E., Guéron, J., and Kowarski, L., 1942, *British Atomic Energy Report*, BR. 44.

Feather, N., 1943, *British Atomic Energy Report*, BR. 315, declassified as BDDA. 114 ; 1944, *Ibid.*, BR. 504

Grummitt, W. E., Guéron, J., and Wilkinson, G. 1944, *Canadian Atomic Energy Report*, MC. 46.

Grummitt, W. E., Guéron, J., Wilkinson, G., and Yaffe, L., 1947, *Canadian J. Res.*, **25 B,** 364 (Canadian Atomic Energy Report, MC. 58).

Hahn, O., and Strassmann, F., 1942, *Naturwissenschaften*, **30,** 325.

Hendricks, R. H., Bryner, L. C., Thomas, M. O., and Ivie, J. O., 1943, *J. Phys. Chem.*, **47,** 469.

Yankwich, P. E., Rollefson, G. K., and Norris, T. H., 1946, *J. Chem. Phys.*, **14,** 131.

The β-Ray Spectrum of ThC″D.

By D. G. E. Martin, H. O. W. Richardson * and Yun-Kuei Hsü

George Holt Physics Laboratory, University of Liverpool

* Now at the Department of Natural Philosophy, University of Edinburgh

MS. received 10 *July* 1947

ABSTRACT. The energies of the β rays of thorium C″D have been measured using a magnetic spectrograph with semi-circular focusing. Corrections have been made for contamination of the source by ThC and ThB deposited by the processes of β-recoil and aggregate recoil. The absolute intensities of the stronger lines have been measured and the shape of the continuous spectrum has been compared with theory using three recently proposed energy level schemes for the product nucleus Pb^{208}.

These level schemes fail to explain the observed shape, partly because they omit the P γ-ray (859 kev) which can now be assigned to ThC″D. Evidence for the β-excitation of energy levels at about 4·5 Mev is discussed.

§ 1. INTRODUCTION

Several level schemes have been proposed for the nucleus ThD. Among the more recent are those of Oppenheimer (1936), Arnoult (1939) and Itoh and Watase (1941). It is of interest to compare the β-ray spectra predicted by these schemes with the β-ray spectrum of ThC″D found by experiment.

The short half life of 3·1 min. of ThC″ indicates that the β-disintegration belongs to the class of allowed transitions. The spectrum is the sum of a number of partial spectra having different end points and intensities and each exciting a different level of the product nucleus ThD (Pb^{208}). All the stronger partial spectra should be allowed transitions and should have the shape predicted by the Fermi theory.

The shape of the experimental spectrum found in the present work deviates from those predicted by the schemes hitherto proposed for the energy levels and γ-ray intensities of the product nucleus Pb^{208}. Much of this deviation may be due to the omission from the schemes of the 859 kev γ ray whose assignment of the ThC″D disintegration has been confirmed by our measurements. A surplus of low energy β rays suggests that one or more levels of Pb^{208} at about 4·5 MeV receive β-excitation.

Caution is required in the interpretation of the observations because of the presence of ThB and C nuclei carried over in the preparation of the ThC″ sources by α-recoil. Corrections for this contamination have been subtracted. The thin mounting used for the source should not have distorted the spectrum above 100 kev.

Alichanian and Zavelskij (1937) found relatively more β rays at both high and low energies than were found in the present work.

§ 2. THE EXPERIMENTAL METHOD

The sources of ThC″ were deposited on the thin aluminium leaf A (figure 1) by α-recoil in vacuo from a source of thorium (B + C + C″). The latter, which may be called the activating source, was withdrawn when counting. The short half life of ThC″ necessitated the use of many recoil sources, whose intensities were correlated by measuring their γ-ray activities with an independent γ-ray counter in a fixed position.

The deposit of ThC″ was found to be contaminated with thorium B and C, which also emit β rays. This contamination was due to the processes of aggregate recoil and β-recoil. In the former, an atom of ThC″ recoiling strongly from the emission of the α ray in the ThC.C″ decay, carries with it a random

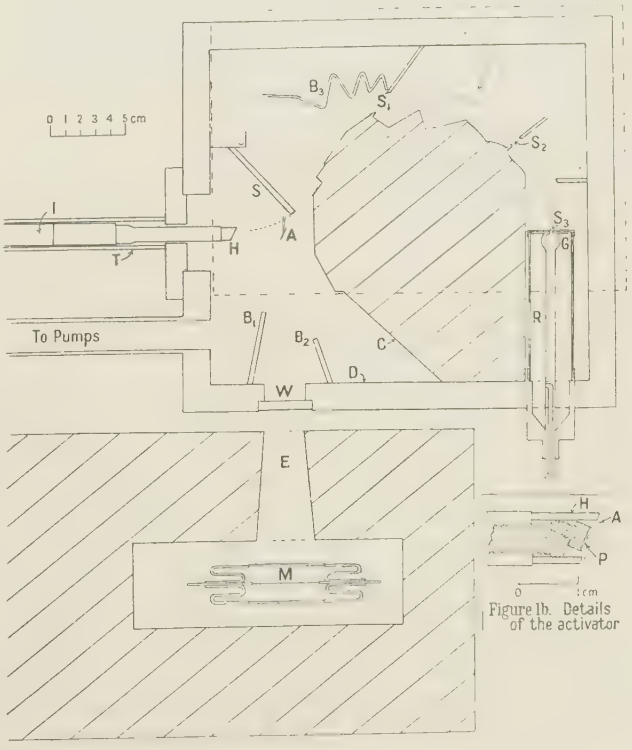

Figure 1. The magnetic spectrograph.

sample of neighbouring atoms from the surface of the activating source. In the second process a small fraction of ThC atoms leaves the surface of the activating source owing to the weak recoil momentum received from the emission of the decay electron and neutrino from ThB.

The aggregate recoil effect was the more serious, and its magnitude was followed in each day's run by repeated measurements of the peak of the very strong F β-ray line (1386 $H\rho$) of thorium B.C. The magnitude of this effect showed wide variations on different days.

§ 3. THE MAGNETIC SPECTROGRAPH

During the preparation of the ThC'' sources recoil particles may be deposited on other surfaces in the spectrograph in addition to the source mounting A. By closing the shutter S (figure 1) during the time when the activating source was near to A, recoil particles were prevented from settling near the main defining slit S_1 or from passing through it. If S was left open during the process of activation the background counting rate of the β-counter showed erratic variations. These were probably due to charged β-recoil atoms of low momentum deviated through the slits by the magnetic field. These atoms of ThC contribute to the count at zero magnetic field when they disintegrate near the counter.

The baffle system shown in figure 1 was designed to exclude from the counter β rays emitted from these deposits on the surfaces of the spectrograph and also scattered β rays. β rays coming from atoms on surfaces other than A and lying on the source side of the main slit S_1 were excluded from the counter slit S_3 by the second defining slit S_2. The surfaces C and D did not, however, lie in the zone of exclusion defined by the slits S_1, S_2, and S_3. β rays from the surface D were excluded by adding baffles B_1 and B_2 of the type used by Neary (1940). β rays from the surface C and from the edges and left sides of B_1 and B_2 were not excluded, but scattering from them was reduced by inclining them so that only their edges were exposed to the source. This should also keep them free from α-recoil particles, which, owing to their great momentum, travel in straight lines in the magnetic field. The baffle B_3 was designed to keep secondary aggregate recoil particles (coming from A when the shutter S was open) away from a region where the thickness of lead screening the β-counter was small.

The aluminium leaf A was 9 mm. wide and 3·5 cm. long and had a weight of 0·13 mg/cm^2. It was inclined at 22° to the central ray of the focused beam of radius 9 cm. The depth and the greatest width of the beam at S_1 were both 1 cm. A high vacuum was maintained by using a 2-stage oil diffusion pump.

The plane pole-faces of the magnet were rectangular in form of sides 19 × 28 in. and were 5·9 cm. apart. Their edges are shown by the broken line in figure 1. The magnet showed the phenomenon of magnetic viscosity and, in order to get a reproducible relation between magnetizing current and field strength, readings were always taken on the ascending branch of the same hysteresis cycle which had a constant maximum field of 1400 oersteds. The field was calibrated by using a flip-coil and ballistic galvanometer. To get an absolute scale of $H\rho$ we assigned to the field settings at the centroids of the β-ray lines the values of $H\rho$ found for the lines by Ellis (1932). This procedure, discussed by Lawson and Tyler (1940), is correct if the curvature of the continuous spectrum is small. (The shape of the F-line of thorium B.C is shown in figure 2 (*a*). The width of the line at half its height is about 1·35% of H. The arithmetic mean or centroid

of the line shape lies about 0·2% of $H\rho$ to the left of the middle of the two points half-way up opposite sides of the line.)

§ 4. THE β- AND γ-RAY COUNTERS

The β and γ Geiger-Müller tubes (G and M in figure 1) were filled with mixtures of argon and alcohol vapour. The cathode of the β-counter was of brass 2 cm. long and 1 cm. diameter. The anode was a tungsten wire 0·1 mm. in diameter. The reservoir R ensured constancy of the gas mixture of 6 cm. of argon with 2 cm. of alcohol. The slit S_3 was 2·4 mm. wide and 1 cm. high and was covered with mica.

The use of the γ rays to correlate the sources requires that the ratio of the efficiencies of the two counters must remain the same over an appreciable time. A source of error is introduced by the finite slopes of the plateaux of the characteristic curves of the two counters. The β-counter had a plateau about 60 volts long and a slope of about 0·15% per volt at 930 volts. The γ-counter had a slope of 0·4% per volt at 1500 volts. The voltages were stabilized by small neon tubes and were kept as constant as possible with respect to the lower end of the plateaux.

On each day the weak ends of the spectrum were counted first, the middle parts being left until the source was weaker. In this way a day's run roughly covered the whole spectrum so that day-to-day changes in relative efficiency should introduce no systematic distortion. This method of sandwiching the measurements should make random the error due to small changes in voltage.

The dependence of the efficiency of the β-counter on the energy of the β rays was found by measuring the spectrum of thorium (B + C + C″) in equilibrium, at different pressures in the counter. The efficiency at high energies (935 kev) did not begin to fall until the pressure of argon was below 6 cm. with 2 cm. of alcohol. It was concluded that at least 98% of the β rays of ThC″D were counted at all energies.

The loss of counts due to the finite resolving time of the counting systems was considered to be negligible. Each counter fed into a Kipp-relay equalizing circuit followed by a pentode scale-of-eight circuit due to O. R. Frisch. The maximum counting rates were about 1200 per minute.

The absorption of slow β rays in the β-counter window was estimated by measuring the spectrum of Th(B + C + C″) and comparing it with the results of Flammersfeld (1939), who used a much thinner window. The surface density of the mica was about 2 mg/cm², β rays begin to penetrate at 600 $H\rho$, while the intensities of the B and Bb lines at 653 and 678 $H\rho$ were respectively 19% and 30% of Flammersfeld's values. At 1000 $H\rho$ the difference between the two spectra was only about 10%, a loss which is much less than that found, for example, by Martin and Townsend (1939). This is probably because the part of the counter slit outside the mica window was narrower than the part inside it, so that rays could suffer appreciable sideways deflection and still be counted. The conditions resembled those in Schonland's experiments (1925) and by fitting his law of absorption for aluminium to the present measurements we estimate the fraction of the incident beam lost in the mica window to be 10%, 2·6%, and 0·6% at $H\rho$ 1085, 1542 and 2186, respectively. These corrections have not been included in figure 4. They would increase the downward convexity of that end of the spectrum.

§ 5. PREPARATION AND CORRELATION OF THE SOURCES

The activating source was obtained by overnight exposure to thoron of a platinum disc P, 4·5 mm. in diameter, which was then screwed into the " activator " shown in figure 1 *b*. A high α-recoil efficiency was obtained by polishing P with chromic oxide and exposing it to the thoron in air at 6 cm. pressure in order to reduce tarnishing.

The hood H was pushed on to the activator to prevent the sideways escape of recoil particles from P, which, if they fell near the glass window W of the spectrograph, would give a disproportionately large γ-count. The gap between H and A was about 0·5 mm.

In order to reduce the effect due to γ-ray sources not on the leaf A, the γ-counter was entirely surrounded by a lead shield 7·3 cm. thick, whose only opening was the collimating channel E, 2·7 cm. wide and 0·8 cm. deep at its outer end.

The usual working cycle was 14 minutes ; of this $6\frac{1}{2}$ minutes were used for counting and the rest for activation. In order to obtain a reliable measure of the source strength it was arranged that the γ-ray count was more than $2\frac{1}{2}$ times the β-ray count, even at the peak of the continuous spectrum.

During counting the activator was withdrawn about 1·3 metres down the curved tube T by means of a sliding magnet acting on an iron rod I. When withdrawn an additional 24 cm. of lead separated the activator from the counters, making the effect of its γ-radiation negligible.

Tests with a fluxmeter showed that the motion of the activator magnet altered the magnetization of the main magnet and that owing to magnetic viscosity the latter took about 1 minute to reach a steady state. It was therefore necessary to go round the standard hysteresis cycle during each activation.

§ 6. THE CORRECTION FOR AGGREGATE RECOIL

Aggregate recoil is the only recoil process which may deposit thorium B on the source mounting A. It may thus be studied separately by measuring the strong F line which contains more than 0·25 electrons per disintegration and stands out about 30 times higher than the maximum of the thorium B continuous spectrum at the resolving power of our apparatus. The growth in each day's run was followed by making about four measurements of β_F, the counting rate at the peak of this line.

The counting rate β_A due to aggregate recoil at a given setting of the magnetic field H can be calculated if β_F and β_A/β_F are known. Using small greek letters for rates and capitals for total counts, we have

$$\begin{aligned} B &= B'' + B_0 + B_B + B_A \\ &= B'' + [\beta_0 + \beta_B + \beta_F(\beta_A/\beta_F)]\Delta t, \end{aligned} \qquad \ldots\ldots(1\,a)$$

where B is the total β-particle count in a counting period of length Δt (usually $6\frac{1}{2}$ minutes) ; B″ is the count due to ThC″D with half-life 3·1 min. ; β_0 is the natural background rate in the β-counter, and β_B is the rate due to β-recoil. β_B decays with the 1-hour period of Th(C + C″) and thus may be considered constant during Δt.

The contribution Γ_A of the aggregate recoil to the γ-count was also proportional to β_F. We have

$$\begin{aligned} \Gamma &= \Gamma'' + \Gamma_0 + \Gamma_B + \Gamma_A \\ &= \Gamma'' + (\gamma_0 + \gamma_B + 0{\cdot}03\beta_F)\Delta t, \end{aligned} \qquad \ldots\ldots(1\,b)$$

where 0·03 is the experimental value found for γ_A/β_F.

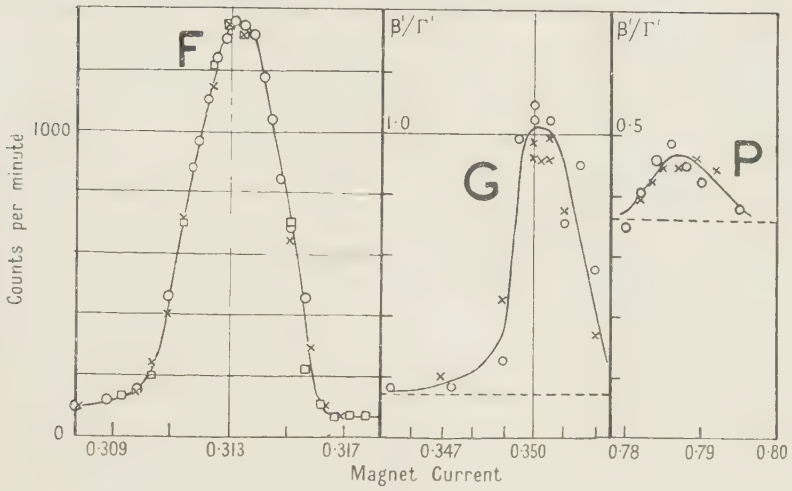

Figure 2. β-ray lines. The F line of ThB . C by aggregate recoil and the G and P lines of ThC″ . D by α-ray recoil. The broken lines indicate the continuous spectrum.

From these equations B''/Γ'', the standardized β-ray intensity of ThC″D, was found for each value of H. The measurement of β_F was made easier by the flatness of the peak of the F line, as seen in figure 2. The flat part had a width of about 0·5% of $H\rho$ and the field was increased through this zone in steps of about 0·2%. β_F was taken as the highest reading lying between two lower ones, all three containing more than 2000 β-counts. This choice of the highest of three readings subject to fluctuation might give rise to a systematic error. Analysis showed that the small overestimation of β_F from this cause was, by a happy chance, nearly cancelled by the mean fall in the highest reading due to its distance from the exact top of the line. This mean fall increases with the spacing of the field settings and the curvature of the peak.

The aggregate recoil efficiency fell during the course of each day, in agreement with the findings of Lawson (1919). It showed big variations from source to source. In order to find B''/Γ'' by equation (1), it is necessary to know β_F during each counting period Δt. β_F was estimated by the method of graphical interpolation shown in curve (1) of figure 3, where B_n and A_{n+1} are values of β_F found from the nth measurement of the F-line. In a group of activations running for example from A_1 to B_1, a little more than half the time was

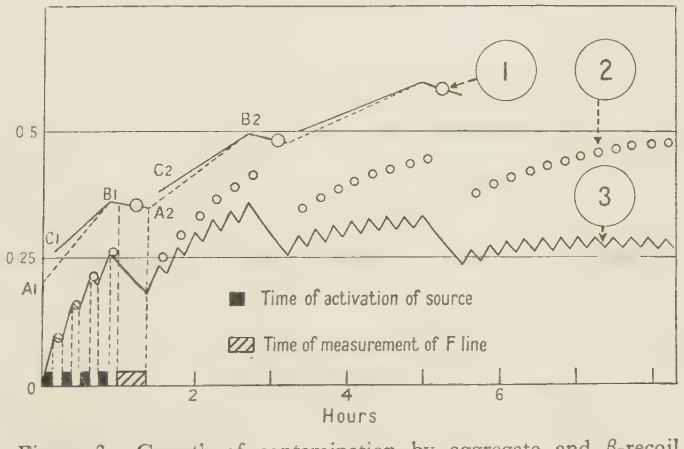

Figure 3. Growth of contamination by aggregate and β-recoil. (1) Counting rate $\times 10^{-3}$ at the peak of the F line of ThB.C. (2) n/n_e, the fraction of the equilibrium strength of the β-recoil contamination. (3) $(n/n_e)\epsilon^{-\lambda_1 t}$, proportional to its absolute strength n.

spent in activation so that the mean rate of growth of β_F during activation was just less than twice the slope of A_1B_1. Since, however, this rate was always falling, a good compromise can be made by taking the rate during the first activation A_1C_1 to be twice the slope of A_1B_1 and then assuming a linear growth from C_1 to B_1. The values of β_F are then read off along C_1B_1, C_2B_2 etc.

The values $(\beta_A\ \beta_F)$ in equation (1) were found in two steps. First, one value of this ratio was found by counting at the maximum of the aggregate recoil spectrum on days when it was strong, applying a correction for β-recoil. The second step was to fit this known value of the ratio at $H\rho = 4541$ to the known spectrum of thorium (B + C + C″) in equilibrium on a thin aluminium leaf, from which other values of β_A/β_F could then be read. The stepwise comparison was necessary because the relative height of the F-line above the continuous spectrum was not necessarily the same in the two spectra, the height and shape of a β-ray line being sensitive to changes in the position and distribution of the source on A. No such changes occurred during the measurement of ThC″D because activation by recoil does not disturb A and seems to give a constant surface distribution.

The errors in the values of ΣB_A given in table 1 arise (i) from the use of only 2000 counts to find β_F, (ii) from the graphical interpolation, (iii) from the value of $(\beta_A\ \beta_F)$ at $H\rho = 4541$ and (iv) from the spectrum of Th(B + C + C″) in which about 30 000 counts per point were used. It is thought that the errors are covered by assigning a standard deviation of 3% to ΣB_A.

Table 1. The continuous spectrum, the corrections for aggregate and β-recoil and values of the Fermi function $F(Z, \eta)$

$H\rho$	ΣB	ΣB_0	ΣB_A	ΣB_B	$\Sigma B''/\Sigma\Gamma''$	$\%\sigma(N)$	$F(Z, \eta)$ for $Z=82$
0	1,542	1017	0	0	0·0078	—	—
1085·5	22,455	2756	6254	306	0·0808	2·1	$3{\cdot}208_3$
1541·6	32,261	2835	8548	547	0·1489	1·7	$4{\cdot}906_{1_6}$
2185·8	21,228	1597	2735	468	0·2390	1·2	$7{\cdot}678_{1_2}$
2770·1	17,906	1115	2049	433	0·3082	1·3	$10{\cdot}667_{8_2}$
3306·7	20,839	1169	2847	635	0·3496	1·3	$13{\cdot}77_1$
3843·5	19,674	1155	2443	595	0·3714	1·3	$17{\cdot}20_1$
4541·2	18,259	1176	2163	603	0·3313	1·3	$22{\cdot}11_8$
5077·9	20,582	1409	2840	813	0·2663	1·3	$26{\cdot}23_3$
5594·7	25,767	2096	4579	1267	0·1787	1·5	$30{\cdot}45_7$
6128·9	23,834	2702	4230	1433	0·1104	1·8	$35{\cdot}08_2$
6662·4	16,497	2847	2992	1151	0·0513	2·5	$39{\cdot}95_4$
6928·6	7,894	1776	1433	519	0·0319	3·7	$42{\cdot}47_8$
7194·4	2,578	1015	462	228	0·0132	16·3	$45{\cdot}05_8$

$\eta = H\rho/1704{\cdot}2$

ΣB = Total number of β-counts.
ΣB_0 = Natural background.
ΣB_A = Counts due to aggregate recoil.
ΣB_B = Counts due to β-ray recoil.
$\Sigma B''/\Sigma\Gamma''$ = Standardized β-ray intensity.
$\%\sigma(N)$ = Percentage standard deviation of N (cf. eqn. (5)).

§ 7. THE CORRECTION FOR β-RECOIL

The counts assigned to this effect are shown as ΣB_B in table 1.

The counting rates are so small that in contrast to aggregate recoil no direct method is available for finding the growth of the contamination at intervals during

the day. For simplicity we assume that the ratio of the α- and β-recoil efficiencies is constant for deposition on A from the activator. The value of β_B in equation (1 *a*) can then be estimated for each counting period Δt.

The first step is to assign to each Δt a measure of the relative strength of the β-recoil source at that time. This measure is given by n/n_e, the ratio of the number n of β-recoil atoms on A to the equilibrium number n_e which would have been reached if the interval had been preceded by a very long period of activation.

Let us assume that a constant fraction β of the ThB atoms decaying on the activator deposits recoil atoms of ThC on A. Then at time t during an activation

$$n = n_i e^{-\lambda_2(t-t_i)} + \beta \frac{\lambda_1 n_0 e^{-\lambda_1 t}}{\lambda_2 - \lambda_1} [1 - e^{(\lambda_1-\lambda_2)(t-t_i)}], \qquad \ldots\ldots (2)$$

where n_i is the initial number of recoil atoms n on A at the start of the activation at $t = t_i$, n_0 is the initial number of ThB atoms on the activator at $t = 0$, and λ_1 and λ_2 are the decay constants of ThB and ThC. Between activations n decays with decay constant λ_2. The equilibrium value n_e is given by

$$n_e = n_0 \beta \lambda_1 e^{-\lambda_1 t}/(\lambda_2 - \lambda_1). \qquad \ldots\ldots (3)$$

Using (2) and (3) average values of n/n_e were estimated for each counting period Δt. An example of the serrated curve of n against t is shown in figure 3 for a typical day's run.

The second step is to find the ratio of the α- and β-recoil efficiencies. Defining the β-recoil efficiency β as in equation (2) and the α-recoil efficiency α as the fraction of ThC . C″ disintegrations which deposits ThC″ on A, let us consider the case of an activation so long that both γ'' and γ_B have reached transient equilibrium and n/n_e is unity. Then every N atoms of ThB decaying on the activator will deposit $N\beta$ atoms of ThC on A by β-recoil and 0·34 $N\alpha$ atoms of ThC″ by α-recoil (because only 34% of ThC atoms decay to ThC″).

If we neglect the weak γ rays of ThC . C′ and ThC . C″ the γ-activity on A will be due to ThC″ . D alone and will be the sum of the counting rates γ'' and γ_B due to the two modes of arrival by recoil. The ratio of the numbers of ThC″ atoms arriving by each mode (neglecting the 10% difference between secular and transient equilibrium) is

$$\frac{0{\cdot}34 N\alpha}{N\beta \times 0{\cdot}34} = \frac{\alpha}{\beta} = \left(\frac{\gamma''}{\gamma_B}\right)_{\text{equilibrium.}} \qquad \ldots\ldots (4)$$

The ratio of γ'' to γ_B at equilibrium was found by measuring the decay of the activity of strong recoil sources made by long activations. The decay of the β-activity at $H\rho = 4541$, and of the γ rays, was followed for several hours and was analysed into three half-periods of 3·1 min., 60·5 min. and 10·6 hours due respectively to α, β and aggregate recoil. Extrapolating back gave γ_B and γ'', but owing to the weakness of the effect large statistical errors in γ_B were present. Seven measurements of $(\gamma''/\gamma_B)_{\text{equil.}}$ on different days gave a mean of 51 with a mean residual of 15%. Five earlier measurements of the decay of the γ-activity, each at the end of a day's run, gave the value 64 with 6% mean residual. As the value of β is known to be sensitive to changes in the emitting surface layer it is possible that the difference is significant and that it arose from a change which was made in the method of making the source. The earlier value was therefore used for measurements taken before the change was made.

The value of γ_B was calculated for each counting period Δt, obtaining γ'' in (4) from the observed γ-count Γ, and using the assigned value of n/n_e. The value of the β-recoil correction β_B in equation (1 *a*) was found by multiplying γ_B by the value ($\beta_B\,\gamma_B$) appropriate to each value of $H\rho$. This ratio was obtained by direct measurements of the β- and γ-counting rates of 1-hour half-life at $H\rho = 4541$. Its value at other fields was estimated from the known shape of the β-spectrum of Th(C + C″) deduced from that of Th(B + C + C″) by subtracting from the four points of lowest energy the contribution due to thorium B. This contribution was estimated from the curves of Flammersfeld (1939), making a small correction for loss of ThC″ by α-recoil from the aluminium.

In view of possible variations of β-recoil efficiency, a standard deviation of 10% is assigned to ΣB_B in table 1 which makes it the major source of error at the four highest values of $H\rho$.

§ 8. THE β-RAY LINES

Flammersfeld (1939) has found intensities of the β-ray lines in the spectrum of Th(B + C + C″) which are higher than those previously accepted. The increase arises in two ways. First, the absolute intensity of the F-line (1386 $H\rho$), used ordinarily as a standard, was found to be 0·284 electrons per disintegration as against the former value of 0·250 (Gurney 1926). Second, the intensity of the lines of ThC″D was increased by about 30% by covering the source with a thin film to prevent the escape of ThC″ atoms by α-recoil. This loss by recoil may be expected to occur from all uncovered sources which are moderately clean.

It is interesting to check these intensities by a method which is independent both of the F-line strength and of loss by α-recoil. A second point of interest is to verify the assignment of some of the many lines of doubtful origin. A ThC″D line will be about three times as strong in our case as it is in the Th(B + C + C″) spectrum, whereas other lines will have reduced intensities set by the amount of the aggregate and β-recoil contamination.

Approximate values for the intensities of the lines are given in table 2. The absolute intensity of each line in electrons per disintegration is equal to the ratio

Table 2. Line intensities in electrons per disintegration

β-ray line	Ec	Fb	G	Jb	Jb3	L	M	N	P	X
$H\rho$ (Ellis)	1251	1469	1594	1929	1980	2603	2887	3164	3924	10 000
Abs. Int. in ThC″D × 10^2	0·12	0·50	2·50	0·35	0·08	1·77	1·49	0·38	0·26	0·18
Int. in Th(B + C + C″) (Flammersfeld)	—	0·356	2·73	0·416 (Jb + Jb1)	—	2·26	1·75	0·356	0·255	0·234
Gamma ray	Ec	Fb	G	G	G	L	L+M	M	P	X

of the area due to the line to that due to the disintegration electrons in the momentum distribution curve. This curve is obtained by plotting N against $H\rho$ where

$$N = \frac{1}{H\rho}\left(\frac{B''}{\Gamma''} - \left[\frac{B''}{\Gamma''}\right]_0\right) \qquad \ldots\ldots(5)$$

$[B''/\Gamma'']_0$ is the standardized β-ray intensity when $H = 0$ and is due to the counts caused by the γ rays of thorium C″ in the β-counter. The area beneath each line is equal to the product of the height by the mean width. The latter was found to be 0·0137 $H\rho$ by measuring the area of the F-line shown in figure 2.

Flammersfeld's values are given for comparison in the table, taking the thorium C branching ratio to be 33·7% (Kovarik and Adams 1938). The intensities in row 2 are subject to error because it was necessary when measuring a ThC″D line to reset the magnetic field after each activation. It was found impossible to reproduce H to better than about 1 in 300 after going round the standard magnetization cycle. It was thus difficult to build up a large number of counts on the flat peak of a line by repeated activations at the same H. A low β-count due to just missing the peak (about $H\rho/200$ wide) is indistinguishable from a statistical fluctuation. This uncertainty did not arise in the measurement of the F-line of thorium B because there was then no magnetic disturbance due to motion of the activator.

In view of this limitation of the method the ratios of the intensities of the G, L, and M lines were found independently from the spectrum of Th(B + C + C″) in transient equilibrium. The lines now stand out less above the continuous spectrum, but it is possible to get about 20 000 counts at each peak.

The relative intensities of the lines are compared with the results of Flammersfeld (1939) and Oppenheimer (1936) in table 3.

Table 3. β-ray line intensity ratios

L : G	M : G	X : G	Source
0·826	0·641	0·0857	Flammersfeld (1939)
0·429	0·353	0·106	Oppenheimer (1936)
0·709	0·597	0·0711	ThC″D data in table 2
0·692	0·619	—	Th(B+C+C″)

Special weight must be attached to the L : G ratio of 0·69 found using Th(B + C + C″) because it is the mean of three independent measurements. It seems likely that the correct ratio lies between the values of Flammersfeld and Oppenheimer.

The uncertainty in setting the field can be seen from the typical plot of the G and P lines in figure 2. Each point is the value of B'/Γ' found from a single activation. B' is the β-ray count not corrected for β-recoil nor for the counts due to the line itself in the aggregate recoil spectrum. This correction, when made, improves the agreement between data taken on different days. The purely statistical standard deviation in B'/Γ' due to the finite numbers counted is about 1·8% for the G line in which about 10 000 β-counts and 12 000 γ-counts were recorded near the peak. In the case of the P line this error is about 10% and it is higher for the weaker lines. It is likely that the error due to just missing the peak was larger than the statistical error for the stronger lines. It would be expected to lead to an underestimate of the intensity because it would effectively flatten out the lines. Thus the fact that our intensities are rather lower than those of Flammersfeld may be due to a systematic error. They confirm his results to the extent that they are appreciably higher than the values of Ellis (1932) and Oppenheimer (1936).

The reduction in apparent height of a β-ray line due to error in setting the field H may be estimated roughly if we represent the line by a gaussian error curve

$$\beta = \beta_1 e^{-h_1^2 x^2} + \beta_0,$$

where β_0 is the counting rate due to the continuous background, β_1 = the peak height of the line at $H = H_1$, and $x = (H_1 - H)/H_1$. Let there now be added an

independent gaussian error in H with a precision index h_2. The broadened line must have the same area so we get

$$\beta' = \beta_1(h/h_1)e^{-h^2x^2} + \beta_0$$

where $h^{-2} = h_1^{-2} + h_2^{-2}$. If we take $h_1 = 1{\cdot}23 \times 10^2$ and $h_2 = 3{\cdot}54 \times 10^2$, equivalent to percentage standard deviations of 0·572 and 0·2 respectively, we get a decrease in the height β_1 of the line of 6%.

Small drifts in the field strength due to magnetic viscosity also lead to an underestimate of the height of the lines.

A search was made for the lines recorded by Meitner and Philipp (1933) as having moderate intensity. Their line with $H\rho = 541$ is below the limit for penetration of the counter window, while that with $H\rho = 1379$, presumably the E_d line, is too close to be separated from the F-line of thorium B in our case. These authors did not survey the region containing the P-line which was attributed to ThC″D by Sze (1933). The P γ-ray must carry an appreciable fraction of the total γ-ray energy.

A weak line was found near $H\rho = 1990$. This was probably the Jb3 line of Ellis (1932) which he attributed to the internal conversion of the Ga γ-ray of thorium CC″ in the L_1 level. However, its energy is also close to that expected for the conversion of the strong G γ-line of ThC″D in the M_1 level. The intensity we find for this line when using ThC″D sources supports its assignment to the G γ-ray, but it may well be a case of a line with a double origin such as the M line. Surugue (1937) found two close lines at $H\rho$ 1978 and 1981 which he attributed to the conversion of the Ga γ-ray in the L_1 level and the G γ-ray in the M_1 level respectively.

§ 9. THE CONTINUOUS SPECTRUM

The momentum distribution for an allowed β-transition (Fermi 1934) may be written

$$\sqrt{(P(\eta)/\mathrm{F}(Z,\eta))} = A^{\frac{1}{2}}(\epsilon_0 - \epsilon), \qquad \ldots\ldots(6)$$

where $P(\eta)d\eta$ is the probability of emission of a β-ray with momentum lying between η and $\eta + d\eta$ and ϵ_0 is the maximum value of ϵ, the energy of the β-ray including its rest-energy, expressed as a multiple of mc^2. We have used $mc^2 = 510{\cdot}89$ kev and $\eta = H\rho/1704{\cdot}2$.

For a given value of the atomic number Z, A is proportional to the square of the matrix element of the heavy particle transition in the nucleus

$$\mathrm{F}(Z,\eta) = \eta^{2S} \cdot e^{\pi\gamma\epsilon/\eta} \cdot |\Gamma(S + i\gamma\epsilon/\eta)|^2 \qquad \ldots\ldots(7)$$

where $\gamma = Z/137$, and $S = \sqrt{(1-\gamma^2)}$.

$\mathrm{F}(Z,\eta)$ has been computed with $Z = 82$ for 13 values of $H\rho$ and is given in table 1. It is believed that the values of F are correct to four significant figures.

$P(\eta)$ is proportional to N, defined in equation (5). The graph of $\sqrt{(N/\mathrm{F})}$ against ϵ is given in figure 4 for values of ϵ chosen to avoid the β-ray lines. The errors to be expected in the values of N are expressed as percentage standard deviations in table 1. These errors were found by assigning zero error to Γ_0 and Γ_B and standard deviations of 1%, 3%, 10% and 5%, to B_0, B_A, B_B and Γ_A respectively. The uncertainty rises rapidly near the end-point at $\epsilon = \epsilon_0$.

The graph deviates from the straight line predicted by (6) for a single β-transition, which suggests that the spectrum is the sum of several partial β-spectra ending on different energy levels of the product nucleus Pb^{208}. All the stronger

partial spectra should be allowed and should have the definite shape predicted by the Fermi theory. At low energies the shape predicted may no longer be definite because it depends on the coefficients in the combination of terms which may be present in the expression for the interaction in β-decay. Evidence on this has been given by Lewis and Bohm (1946) for Cu^{64}, but no clear indication of the effect appears in the present work.

It can be seen from figure 4 that the end-point at $\epsilon = \epsilon_0$ is approached almost linearly. If we adopt the view discussed in the next section that the experimental end-point corresponds to the β-excitation of an energy level 3·20 MEV above the ground state of Pb^{208}, we cannot expect another strongly excited level until a

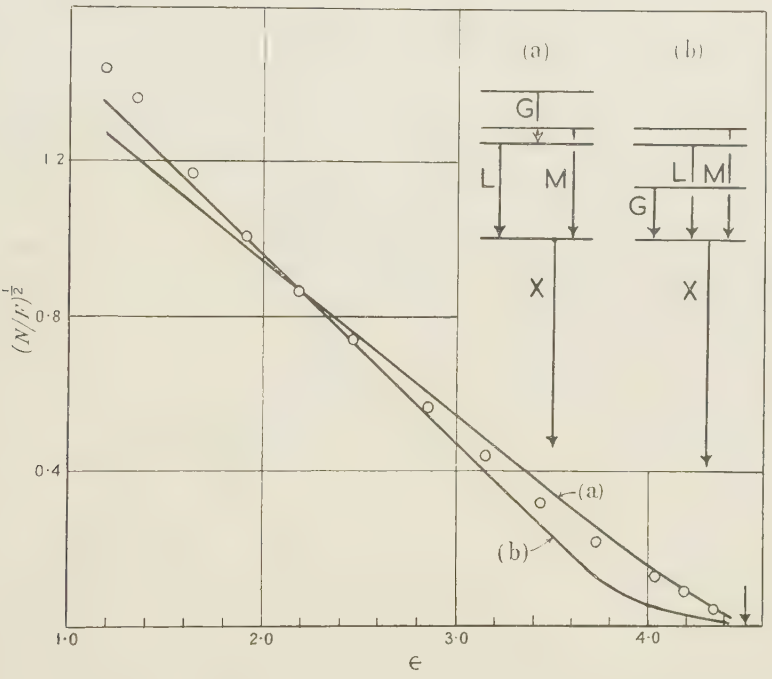

Figure 4. Comparison of the experimental spectrum with the spectra calculated from (*a*) the level scheme of Itoh and Watase and (*b*) from that of Oppenheimer.

space equal to the energy of the G γ-ray of 277 KEV has been bridged. Thus the last 277 KEV of the spectrum should be linear, but below this there should be a small rise in slope. The consequences of such a level scheme are discussed elsewhere, but we may use it provisionally to estimate ϵ_0 by the method of least squares by fitting the four points of highest energy ϵ to a straight line.

The deviations of the four points were weighted in the normal equations inversely as the standard deviations of N given in table 1. The value of $(N/F)^{\frac{1}{2}}$ at the point with $\epsilon = 3{\cdot}73\ mc^2$ was reduced by 4% because it should receive a small contribution from the second partial spectrum. We get for the maximum energy $\epsilon_0 = (4{\cdot}507 \pm 0{\cdot}014)mc^2$, or $(1{\cdot}792 \pm {\cdot}007)$ MEV. This agrees with the value of 1·795 MEV found by Henderson (1934) using a method which avoided the deposition of aggregates on the source, presumably by carrying out the activation in air.

The probable error was calculated by means of the standard formula (Margenau and Murphy, p. 502). It depends only on the deviations of the four points and does not take account of a possible error in our scale of $H\rho$ and may thus be an underestimate.

§ 10. COMPARISON OF ALTERNATIVE ENERGY LEVEL SCHEMES

If the downward convexity of the spectrum in figure 4 is due to its being the sum of a series of m partial β-spectra all having the shape of an allowed transition, it should obey the equation

$$\sqrt{(N/\mathrm{F})} = \sqrt{(\sum_{n=1}^{m} A_n(\epsilon_n - \epsilon)^2)} \qquad \ldots\ldots(8)$$

where $A_n = 0$ for $\epsilon > \epsilon_n$.

A_n is proportional to the square of the heavy particle matrix element for the partial β-transition to the nth energy level of the product nucleus, with end-point at $\epsilon = \epsilon_n$.

A_n can be connected with p_n, the β-transition probability to the nth level, which is usually called the β-excitation.

We have

$$p_n = \int_1^{\epsilon_n} p(\epsilon)d\epsilon \qquad \ldots\ldots(9)$$

where $p(\epsilon)d\epsilon$ is the probability of emission of a β-ray in the nth partial spectrum with energy between ϵ and $\epsilon + d\epsilon$. To evaluate the integral we choose as an approximation for $\mathrm{F}(Z, \eta)$ in (6).

$$\mathrm{F}(Z, \eta) = 3{\cdot}85\eta(1 + 0{\cdot}418\eta). \qquad \ldots\ldots(10)$$

This gives, on integrating (9)

$$p_n = KA_n[\tfrac{1}{12}\epsilon_n^4 - \tfrac{1}{2}\epsilon_n^2 + \tfrac{2}{3}\epsilon_n - \tfrac{1}{4} + 0{\cdot}418(\epsilon_n^2 - 1)^{\frac{1}{2}}(\tfrac{1}{30}\epsilon_n^4 - \tfrac{3}{20}\epsilon_n^2 - \tfrac{2}{15}) + 0{\cdot}418\,.\,\tfrac{1}{4}\epsilon_n \ln(\epsilon_n + (\epsilon_n^2 - 1)^{\frac{1}{2}})]. \qquad \ldots\ldots(11)$$

K is a constant which is adjusted to make $\sum_1^m p_n = 1$ in a given level scheme.

Equation (10) differs from the formula of Fermi (1934) in that 0·418 replaces 0·355. We believe that the value 0·418 covers the energy range which makes the main contribution to p_n in our case.

Among the more recent schemes proposed for the energies and β-excitations p_n of the levels of thorium D are those of Oppenheimer (1936), Arnoult (1939) and Itoh and Watase (1941). The second scheme differs from the first partly in that it includes a number of weak γ-rays some of which are of doubtful origin. It would give much the same shape of spectrum. Using (8) and (11) we have calculated the shapes of composite spectrum predicted by the first and third schemes, taking the largest end-point, ϵ_1, to be 4·50 mc^2. The spectra shown in figure 4 are fitted to the experimental curve at $\epsilon = 2{\cdot}177$ by adjusting K. The values of the constants are given in table 4.

Table 4. The energy level schemes and the resulting complex β-spectra

Author	Oppenheimer			Itoh and Watase		
Energy above ground level (MeV)	2·895	3·13	3·20	3·13	3·20	3·41
γ-ray transitions to ground level	G+X	L+X	M+X	L+X	M+X	G+L+X
β-ray end point ϵ_n	4·50	4·04	3·90	4·50	4·36	3·96
β-excitation p_n	0·08	0·20	0·73	0·45	0·45	0·10
KA_n	0·169	0·722	3·199	0·949	1·16	0·399

The discrepancies between the spectra seem to be beyond the limits of experimental error and are too great to be removed by any changes in the values of p_n which would be compatible with the intensities of the γ-ray transitions. Upper and lower limits to these intensities can be deduced from the theory of internal conversion using the observed intensities of the β-ray lines.

A difficulty in both these schemes is that they do not put the end-point of the β-spectrum on the energy level at 3·20 MeV. It was pointed out by Henderson (1934) that in order that the total energy emission may be equal round both sides of the ThC branching it is necessary to place the β-ray end-point at 1·792 MeV on or near the 3·20 MeV level of ThD. Otherwise one must postulate different rest-masses for the neutrinos emitted in ThC″D and in ThCC′. In order to give a correct balance of the branching energies Arnoult (1939) included in his level scheme a partial spectrum with an excitation p_n of 10% extending to an end-point at 2·10 MeV. No β-ray evidence has been found for such a strong high-energy tail to the spectrum.

On adding the β-ray energy of 1·792 MeV to 3·204 MeV, the sum of the M and X γ-ray energies, we get 4·996 MeV for the difference in energy of the ground states of ThC″ and Pb^{208}. This differs by less than the estimated error from the value deduced from the α-decay energies Briggs (1936, and others), if the β-ray energy of ThC . C′ is taken to be 2·2505 MeV.

Level schemes which include the P γ-ray are discussed by Richardson (1948).

§ 11. THE POSSIBLE β-EXCITATION OF LEVELS OF VERY HIGH ENERGY

The graphs of $\sqrt{(N/F)}$ predicted by the level schemes can be seen to be nearly straight at their low energy ends.

The experimental curve, in contrast, shows a marked downward convexity at energies as low as $\epsilon = 1{\cdot}4$.

The curvature, which is very small between $\epsilon = 3{\cdot}2$ and $\epsilon = 2{\cdot}1$ rises sharply near the latter point. This excess of slow β-rays may be due to one or more partial spectra of low energy. Its magnitude can be estimated by subtracting from the observed values of N the values obtained by approaching $\epsilon = 1$ along a straight line forming a tangent to the graph at about $\epsilon = 2{\cdot}2$. We get surpluses of 16%, 11% and 5% in the values of N at the three points of lowest energy taken in order of increasing ϵ. These figures are compatible with a single partial spectrum with a transition probability p_n of about 3% and an end-point ϵ_n of about 2·1 mc^2 exciting a level of thorium D at about 4·45 MeV above the ground state. So large a value of p_n suggests that there may be several close levels and requires that the excitation is by allowed β-transitions. The selection rules for an allowed transition give the β-excited level values of spin and parity which permit quadripole γ-ray transitions to all lower energy levels also excited by allowed transitions. As there are very probably three such lower levels we expect at least three quadripole γ-rays of about 1 MeV starting from a level at about 4·5 MeV. Owing to the low intensities their internal conversion lines should be difficult to find, but the weak γ-ray of (1350 ± 20) kev found by Alichanow and Dzelepow (1938) may be one of these rays. Its intensity is stated by Latyshev and Kulchitsky (1941) to be 0·036 times that of the X γ-ray.

An alternative explanation of the surplus of slow β-rays is that they are generated in the aluminium leaf A by the processes of inelastic back-scattering and ejection

of secondary (knock-on) electrons in close collisions. The experiments of Flammersfeld (1939), and others, show that these effects do not become appreciable at energies of about 100 kev until the thickness of the mounting material is about 1 mg/cm². In our case with 0·13 mg/cm² they should be negligible.

A third possible explanation is that the surplus is due to an increased efficiency of the β-counter for slow rays due to their greater specific ionization. It seems unlikely that a rise in N of more than 2% for the two lowest points can be accounted for in this way.

§ 12. CONCLUSION

The level schemes considered above all fail both to give agreement with the observed shape of the spectrum and to conform to the requirement of energy balance in the thorium C branching in a way which is compatible with the experimental value of the end-point at 1·792 MeV. It seems probable that no energy levels of thorium D lying below 3·20 MeV can receive more than 1 or 2% β-excitation. In order to account for this low excitation it is evident that the lower levels can only be accessible via forbidden β-transitions and that the transition to the ground level must be highly forbidden.

Owing to the presence of five strong γ-rays and at least three weak ones a great many level schemes are possible. A clue, which may, however, be a chance coincidence, is provided by the P, G, and M γ-rays, which satisfy the combination

$$(h\nu)_{\mathrm{G}} + (h\nu)_{\mathrm{M}} = (h\nu)_{\mathrm{P}}.$$

The evidence is given in table 5.

Table 5

Author	Ellis (1932)	Surugue (1937)
Energy of G γ-ray (kev.)	276·7	276·8
Energy of M γ-ray	582·5	583·4
Sum	859·2	860·2
P β-line	771·6	772·3
Surplus	87·6	87·9

The surplus agrees fairly well with the K-ionization energy of 88·10 kev for $Z = 82$. Each author's values for the energies of the β-lines have been used, but the ionization energies are those of Ingelstam tabulated by Arnoult (1939).

If we assume the spin of the ground state of ThC″ to be four units of $h/2\pi$, the Gamow-Teller β-selection rules for an allowed transition permit the excitation of levels of ThD with spin quantum number $I = 3$, 4 and 5. The distribution of convexity in the graph of $\sqrt{(N/\mathrm{F})}$ shows that levels with these spins are present near the high-energy end-points between 3·1 MeV and 3·75 MeV and that after an interval they appear again at higher energies above 4·4 MeV possibly in the form of a close group of levels. The ground state of ThD has very probably $I = 0$ and the spacing of the levels would be expected to get smaller at high energies of excitation.

ACKNOWLEDGMENTS

We wish to thank Sir James Chadwick for his interest and for preparing the radiothorium, Dr. J. C. P. Miller for his generous help with statistical and computing problems, and Dr. O. R. Frisch for the use of his unpublished scaling circuit.

REFERENCES

ALICHANIAN, A. I., and ZAVELSKIJ, A. S., 1937, *C.R. Acad. Sci., U.R.S.S.*, **17**, 469.
ALICHANOW, A. I., and DZELEPOW, V. P., 1938, *C.R. Acad. Sci., U.R.S.S.*, **20**, 113.
ARNOULT, R., 1939, *Ann. Phys., Paris*, **12**, 241.
BRIGGS, G. H., 1936, *Proc. Roy. Soc.* A, **157**, 183.
ELLIS, C. D., 1932, *Proc. Roy. Soc.* A, **138**, 318.
FERMI, E., 1934, *Z. Phys.*, **88**, 161.
FLAMMERSFELD, A., 1939, *Z. Phys.*, **114**, 227.
GURNEY, R. W., 1926, *Proc. Roy. Soc.* A, **112**, 380.
HENDERSON, W. J., 1934, *Proc. Roy. Soc.* A, **147**, 572.
INGELSTAM, E., 1937, *Nova Acta Reg. Soc. Sci. Uppsala*, **10**, 1.
ITOH, J., and WATASE, Y., 1941, *Proc. Phys. Math. Soc. Japan*, **23**, 142.
KOVARIK, A. F., and ADAMS, N. I., 1938, *Phys. Rev.*, **54**, 413.
LATYSHEV, G. D., and KULCHITSKY, L. A., 1941, *J. Phys. Acad. Sci., U.R.S.S.*, **4**, 515.
LAWSON, R. W., 1919, *Wien. Ber.*, **128**, 795.
LAWSON, J. L., and TYLER, W., 1940, *Rev. Sci. Instrum.*, **11**, 6.
LEWIS, H., and BOHM, D., 1946, *Phys. Rev.*, **69**, 129.
MARGENAU, H., and MURPHY, G. M., 1943, *The Mathematics of Physics and Chemistry* (New York : Van Nostrand Co.).
MARTIN, L. H., and TOWNSEND, A. A., 1939, *Proc. Roy. Soc.* A, **170**, 190.
MEITNER, L., and PHILIPP, K., 1933, *Z. Phys.*, **80**, 277.
NEARY, G. J., 1940, *Proc. Roy. Soc.* A, **175**, 71.
OPPENHEIMER, F., 1936, *Proc. Camb. Phil. Soc.*, **32**, 328.
RICHARDSON, H. O. W., 1948, *Nature, Lond.*, **161** (in press).
SCHONLAND, B. F. J., 1925, *Proc. Roy. Soc.* A, **108**, 187.
SURUGUE, J., 1937, *Ann. Phys., Paris*, **8**, 484.
SZE, S. Y., 1933, *Ann. Phys., Paris*, **19**, 59.

On the Solution of Scattering and Related Problems

BY B. FERRETTI * AND M. KROOK
Department of Mathematical Physics, The University, Birmingham
* Now at University of Milan

Communicated by R. E. Peierls ; MS. received 9 February 1948

ABSTRACT. A method is presented for solving scattering and eigenvalue problems. This is of use mainly in cases where the forces are of short range. The method is based on a Taylor expansion of the radial eigenfunctions about a point where the potential is already rather small. A procedure is given for determining the logarithmic derivative at this point of the solution which is "least singular" at the origin, this is in general the physically admissible solution.

§ 1. INTRODUCTION

IT is well known that for calculating scattering cross-sections one does not require the detailed solution of the relevant wave equation, but only its asymptotic form. Thus for a system with forces of finite range a, the scattering problem is effectively solved when one has determined the logarithmic derivatives of the interior radial solutions at the boundary a; similar considerations apply also to the corresponding eigenvalue problem for the bound states. In more general cases where the forces are of short range one may solve the scattering or eigenvalue problem by subdividing the whole range $(0, \infty)$ into an "interior region" $(0, a)$ and an "exterior region" (a, ∞). In the exterior

region, where the potential is already rather small, the solution may be obtained by a perturbation method together with the condition that this exterior solution fit smoothly on to the interior one. Here again the only information about the interior solution needed in the calculation is the value of its logarithmic derivative at the point of subdivision a.

The object of this paper is to present a method of evaluating the logarithmic derivative of the interior solution at a, without solving the equation explicitly. Usually the origin is a singular point of the radial differential equation. The customary procedure is then to expand the solution in a power series about the origin so as to satisfy a condition of regularity or finiteness there. The present method too is based on a Taylor expansion, not about the origin however, but about the boundary or subdivision point a. The condition of regularity at the origin is then equivalent to a condition on the radius of convergence of the series. It is this latter condition which permits the direct evaluation of the logarithmic derivative of the interior solution at the boundary.

§ 2 METHOD OF CALCULATION

In general the radial differential equation is linear, of second order and with the origin as a regular singular point :

$$\frac{d^2u}{dr^2} + f(r)\frac{du}{dr} + g(r)u = 0. \qquad \ldots\ldots(2.1)$$

The equation may also have singular points other than $r=0$. We are concerned with that solution of (2.1) which is regular at $r=0$; more particularly we wish to determine its logarithmic derivative at the ordinary point $r=a$.

Let $r=0$ be the singular point of (2.1) nearest to a; and let d be the distance from $r=a$ to the next nearest singularity. Since a is an ordinary point of (2.1), any solution can be expanded in a Taylor series about a :

$$u(r) = \sum_{n=0}^{\infty} c_n (r-a)^n$$

where

$$c_n = \frac{1}{n!}u_n = \frac{1}{n!}\left(\frac{d^n u}{dr^n}\right)_{r=a}. \qquad \ldots\ldots(2.2)$$

In general the radius of convergence of this series will be just a, and so by Cauchy's convergence test :

$$\lim_{n\to\infty} |c_n|^{1/n} = 1/a. \qquad \ldots\ldots(2.3)$$

But when, and only when, $u(r)$ is that special solution which is regular at $r=0$, the radius of convergence will exceed a and will in fact be d; i.e.

$$\lim_{n\to\infty} |c_n|^{1/n} = 1/d. \qquad \ldots\ldots(2.4)$$

It is immediately evident that c_n can be represented in the form :

$$c_n = F_n c_0 + G_n c_1, \qquad \ldots\ldots(2.5)$$

where $F_0 = G_1 = 1$, $F_1 = G_0 = 0$ and the coefficients F_n, G_n, $(n=2, 3 \ldots)$ are uniquely determined by the differential equation. Let $b = u'(a)/u(a)$ denote the logarithmic derivative at $r=a$ of the regular solution. We then have

$$b = -\lim_{n\to\infty} F_n/G_n. \qquad \ldots\ldots(2.6)$$

This can be proved as follows : We are free to make either $c_0=0$ or $c_1=0$ in (2.5). Then at least one of the two corresponding functions $u(r)$ must be singular at the origin and thus lead to (2.3). Hence at least one of the relations

$$\lim_{n\to\infty}|F_n|^{1/n}=1/a; \qquad \lim_{n\to\infty}|G_n|^{1/n}=1/a$$

is valid. For definiteness suppose the second equation holds. Then when $c_1/c_0=b$ we have :

$$\begin{aligned}1/d&=\lim_{n\to\infty}|F_nc_0+G_nc_1|^{1/n}\\&=\lim_{n\to\infty}\{|c_0|^{1/n}|G_n|^{1/n}|(F_n/G_n)+b|^{1/n}\}\end{aligned}$$

and so

$$\lim_{n\to\infty}|(F_n/G_n)+b|^{1/n}=a/d \qquad \ldots\ldots(2.7)$$

which establishes (2.6).

Equation (2.7) indicates that the convergence to the limit in (2.6), once it "sets in", is rapid provided a/d is not too close to unity. It also provides a useful control in some applications, enabling us to decide whether or not an empirically determined convergence is real.

In general it is not feasible to attempt to find the exact limiting value b in (2.6). The main use of (2.6), (2.7) in practice is as the basis for an approximation method; and it is just this feature which we wish to emphasize in the present paper. The procedure then consists in regarding $b_n=-F_n/G_n$ for some value of n as representing b, the particular choice of n being guided by the convergence criterion and the order of accuracy required.

To illustrate the procedure we shall now discuss a number of examples : In these we shall write (cf. (2.2), (2.5)).

$$A_nu_n=A_nc_n/n!=P_nu_0+Q_nu_1, \qquad \ldots\ldots(2.8)$$

where A_n is some convenient numerical factor. Then

$$P_n=A_nF_n/n!, \qquad Q_n=A_nG_n/n!$$

and the nth approximation to b is given by

$$b_n=-P_n/Q_n. \qquad \ldots\ldots(2.9)$$

§ 3. EXAMPLE 1

Consider the equation

$$r\frac{d^2u}{dr^2}-u=0, \qquad \ldots\ldots(3.1)$$

which has as solution regular at $r=0$ the function $\sqrt{r}I_1(2\sqrt{r})$, I_1 being the Bessel function of imaginary argument. Differentiating (3.1) $(n-2)$ times and substituting $r=a$ we obtain a recurrence formula for the u_n of (2.2) :

$$au_n=-(n-2)u_{n-1}+u_{n-2}. \qquad \ldots\ldots(3.2)$$

Writing

$$a^ku_k=P_ku_0+Q_ku_1$$

it follows that the P_k and the Q_k separately each satisfy recurrence relations of the same form (3.2) :

$$\left.\begin{aligned}P_n&=-(n-2)P_{n-1}+aP_{n-2},\\Q_n&=-(n-2)Q_{n-1}+aQ_{n-2},\\P_0&=1;\quad Q_0=0=P_1;\quad Q_1=a.\end{aligned}\right\} \qquad \ldots\ldots(3.3)$$

Repeated application of (3.3) then leads to :

$$P_2 = a \qquad Q_2 = 0$$
$$P_3 = -a \qquad Q_3 = a^2$$
$$P_4 = 2a + a^2 \qquad Q_4 = -2a^2$$
$$P_5 = -(6a + 4a^2) \qquad Q_5 = 6a^2 + a^3$$
$$P_6 = 24a + 18a^2 + a^3 \qquad Q_6 = -(24a^2 + 6a^3)$$
$$P_7 = -(120a + 96a^2 + 9a^3) \qquad Q_7 = 120a^2 + 36a^3 + a^4$$
$$P_8 = 720a + 600a^2 + 72a^3 + a^4 \qquad Q_8 = -(720a^2 + 240a^3 + 12a^4)$$
$$P_9 = -(5040a + 4320a^2 + 600a^3 + 16a^4) \qquad Q_9 = 5040a^2 + 1800a^3 + 120a^4 + a^5.$$

The nth approximation, b_n, to $u'(a)/u(a)$ is given by (2.9). To indicate the order of accuracy attainable and the mode of convergence, successive values of b_n for three different values of a are listed in table 1. (The entries for $n = \infty$ were obtained by use of tables of Bessel functions).

Table 1

n	$b_n\,(a=1)$	$b_n\,(a=4)$	$b_n\,(a=9)$
3	1·000000	0·250000	0·111111
4	1·500000	0·750000	0·611111
5	1·428571	0·550000	0·311111
6	1·433333	0·583333	0·380342
7	1·433121	0·578571	0·362540
8	1·433127	0·579060	0·365300
9	1·433127	0·579022	0·365300
∞	1·433127	0·579024	0·365353

Even for comparatively large values of the argument accurate values of b can be obtained rapidly. To obtain comparable accuracy with the use of a Taylor expansion about the origin requires the retention of a large number of terms and more laborious computations.

It is interesting to remark that the procedure may be extended to obtain representation of the function $u(a) = \sqrt{a} I_1(2\sqrt{a})$ over a fairly wide range in terms of elementary functions. Regarding $b_8 = -P_8/Q_8$ as representing $u'(a)/u(a)$ with sufficient accuracy in a range $(0, A)$, an elementary integration leads to the result :

$$u(a) = a e^{a/12} \left(\frac{a^2 + 20a + 60}{60}\right)^{5.3} \left[\frac{(10 - 2\sqrt{10})a + 60}{(10 + 2\sqrt{10})a + 60}\right]^{25.12\sqrt{10}}.$$

Here the constant of integration has been fixed by using the known behaviour of $u(a)$ in the neighbourhood of the origin. The accuracy of the formula (3.4) decreases gradually as a increases. At $a = 9$ it is in error by less than 0·01 %.

§ 4. EXAMPLE 2

Consider the equation

$$r(r+1)\frac{d^2u}{dr^2} - u = 0 \qquad \ldots\ldots (4.1)$$

and suppose that the logarithmic derivative of the regular solution is required for $r = 2$. Here the direct method of series expansion about the origin breaks down on account of the singularity at $r = -1$; the series would have radius of convergence unity. (Of course an expansion about the origin can still be used in conjunction with a bilinear substitution, e.g. one which transforms -1 into ∞). It is here that the method of this paper can be used with particular advantage.

Writing $$(a^2+a)^n u_n = P_n u_0 + Q_n u_1 \qquad \ldots\ldots(4.2)$$
we obtain the recurrence formula :

$$\left.\begin{aligned} P_n &= -(n-2)(2a+1)P_{n-1} - [(n-2)(n-3)-1](a^2+a)P_{n-2} \\ Q_n &= -(n-2)(2a+1)Q_{n-1} - [(n-2)(n-3)-1](a^2+a)Q_{n-2} \end{aligned}\right\} \qquad \ldots\ldots(4.3)$$

with $P_0=1$, $Q_0=P_1=0$, $Q_1=(a^2+a)$.
Proceeding as in § 3, successive approximations to u_1/u_0 (with $a=2$) are given by $b_n=-P_n/Q_n$:

$$\begin{array}{llll} b_3=0{\cdot}8333 & b_4=0{\cdot}7333 & b_5=0{\cdot}7083 & b_6=0{\cdot}6988 \\ b_7=0{\cdot}6945 & b_8=0{\cdot}6923 & b_9=0{\cdot}6911 & b_{10}=0{\cdot}6903. \end{array}$$

Here the differences between successive terms b_k, $(k>4)$, agree quite well with the convergence criterion $|b-b_n| \sim K(2/3)^n$ with K depending only slightly on n. This fact may be used to obtain a more accurate value for b :

$$b'_n = b_n - K(2/3)^n = b_n - 2(b_{n-1}-b_n).$$

The corresponding values of b'_n are $b'_8=0{\cdot}6879$; $b'_9=0{\cdot}6887$; $b'_{10}=0{\cdot}6887$.

§ 5. EXAMPLE 3

The differential equations

$$\frac{d^2u}{dx^2} + \left[k^2 - \frac{l(l+1)}{x^2} + B\frac{e^{-x}}{x}\right]u = 0 \qquad \ldots\ldots(5.1)$$

($l=0, 1, 2, \ldots$) occur in the theory of scattering with a central "meson potential". We consider the case $l=0$ and write

$$u = xV \qquad \ldots\ldots(5.2)$$

$V(x)$ must then be finite at $x=0$. By repeated differentiation of the differential equation for $V(x)$ we obtain for $V_n \equiv V^{(n)}(a)$ the recurrence formula :

$$aV_{n+2} + (n+2)V_{n+1} + k^2[aV_n + nV_{n-1}] = -Be^{-a}\sum_{k=0}^{n}(-1)^k\binom{n}{k}V_{n-k}. \qquad \ldots\ldots(5.3)$$

Writing $a^m V_m = P_m V_0 + Q_m V_1$ with $P_0=1$, $Q_0=P_1=0$, $Q_1=a$, we obtain recurrence formulae for P_m, Q_m separately :

$$P_{n+2} = -(n+2)P_{n+1} - k^2a^2(P_n + nP_{n-1}) - aBe^{-a}\sum_{k=0}^{n}(-1)^k\binom{n}{k}P_{n-k}a^k$$

with an identical formula for the Q_m. Taking the case $k=0{\cdot}8$, $B=1{\cdot}5$ and $l=0$, for which the asymptotic phase has been obtained by numerical integration (Sachs and Goeppert-Mayer 1938), the following values of $b_n=-P_n/Q_n$ are obtained with $a=2$:

$$\begin{array}{llll} b_5=-1{\cdot}161 & b_6=-1{\cdot}284 & b_7=-1{\cdot}348 & b_8=-1{\cdot}375 \\ b_9=-1{\cdot}389 & b_{10}=-1{\cdot}396 & b_{11}=-1{\cdot}399. & \end{array}$$

The differences * between successive b_n, $(n>4)$, behave regularly and provide an improved extrapolated value for $b=V'(2)/V(2)$: $b=-1{\cdot}401$, and so

$$u'(2)/u(2) = -0{\cdot}901.$$

* In most cases it is possible to obtain an improved value in this way by extrapolation using the differences between successive values of b_n.

This provides an accurate value for the phase shift $\bar{\eta}$ of the exact wave function [illegible]

The asymptotic phase η_0 satisfies the exact equation *

$$k \sin(\eta_0 - \bar{\eta}) = B \int_2^\infty \frac{e^{-x}}{x} u(x) \sin(kx + \bar{\eta})\, dx. \qquad \ldots\ldots (5.4)$$

Since the potential is already rather small for $x > 2$, a fairly close approximation [illegible] by evaluating the integral in (5.4) with $\sin(kx + \bar{\eta})$ substituted. A simple-minded numerical evaluation of the integral then leads to $\sin(\eta_0 - \bar{\eta}) = 0{\cdot}0217$ and so $\eta_0 = 0{\cdot}8371$. This is in good agreement with the value $\eta_0 = 0{\cdot}83706$ obtained by Sachs and Goeppert-Mayer (1938).

For higher values of l the procedure converges more rapidly than for $l = 0$; the larger the value of l the more rapid is the convergence. This feature is not [illegible] to the particular potential function in (5.1) but holds in general for [illegible] of the potential. It can easily be understood in terms of the [illegible] of the regular and irregular solutions which increases with l.

An alternative method of performing the calculation is to write the solution [illegible] in the form

$$u(x) = f(x)\psi_l(kx) - g(x)\chi_l(kx)$$

where $\psi_l(x) = \sqrt{\tfrac{1}{2}\pi x} J_{l+\frac{1}{2}}(x)$, $\chi_l(x) = \sqrt{\tfrac{1}{2}\pi x} J_{-l-\frac{1}{2}}(x)$. $J_{l+\frac{1}{2}}$ and $J_{-l-\frac{1}{2}}$ are Bessel [illegible] of the first kind.

Imposing the condition

$$f'(x)\psi_l(kx) + g'(x)\chi_l(kx) = 0$$

we obtain a pair of first order equations for f, g:

$$\left.\begin{aligned} f'(x) &= -\frac{(-1)^l}{k} v(x)\, u(x)\, \chi_l(kx), \\ g'(x) &= +\frac{(-1)^l}{k} v(x)\, u(x)\, \psi_l(kx). \end{aligned}\right\} \qquad \ldots\ldots (5.5)$$

The condition $f'(a) = 0$ then leads to an approximation for $g(a)\, f(a)$ and so to an approximation for the phase shift at $x = a$. The repeated differentiations [illegible] are more complicated than in the above direct method, but f, g are more slowly varying functions than u and the procedure would thus converge more rapidly.

§ 6. APPLICATION TO TENSOR FORCES

In the discussion of neutron–proton scattering with tensor forces one encounters the pair of simultaneous equations (cf. Rarita and Schwinger 1941),

$$\frac{d^2 u}{dx^2} + \left[k^2 - \frac{l(l+1)}{x^2} - v_1(x)\right] u = v_3(x) w; \quad \frac{d^2 w}{dx^2} + \left[k^2 - \frac{6}{x^2} - v_2(x)\right] w = v_3(x) u \quad \ldots\ldots (6.1)$$

associated with the triplet state of unit angular momentum and even parity; v_1, v_2, v_3 are specified potential functions. The physical solutions are required to satisfy, amongst other conditions, that of vanishing at least like x at the origin. For simplicity we shall consider the case of a rectangular potential; v_1, v_2, v_3 are then constant in $(0, 1)$ and vanish for $x > 1$.

* This is easily obtained e.g. by a slight modification of the argument leading to equation (6.6) in Bethe and Bacher (1936).

An examination of (6.1) in the neighbourhood of the origin shows that the physically admissible solutions are of the form :

$$\left.\begin{aligned} u(x) &= \sum_{n=0}^{\infty} A_n x^{n+1} + \ln x \sum_{n=0}^{\infty} C_n x^{n+5}, \\ w(x) &= \sum_{n=0}^{\infty} B_n x^{n+3} + \ln x \sum_{n=0}^{\infty} D_n x^{n+3}. \end{aligned}\right\} \quad \ldots\ldots (6.2)$$

The constants A_0, B_0 can be assigned arbitrary values independently. There are thus exactly two independent solutions which vanish as required at $x=0$. On account of the linearity of (6.1) any linear combination of solutions is again a solution. A fundamental system of solutions

$$\left.\begin{aligned} u &= \alpha(x) \\ w &= \beta(x) \end{aligned}\right\} \qquad \left.\begin{aligned} u &= \phi(x) \\ w &= \psi(x) \end{aligned}\right\} \quad \ldots\ldots (6.3)$$

can then be chosen so as to satisfy two arbitrary independent pairs of conditions at $x=1$. In particular, there exists one such system with the property

$$\left.\begin{aligned} \alpha(1) &= 1 \\ \beta(1) &= 0 \end{aligned}\right\} \qquad \left.\begin{aligned} \phi(1) &= 0 \\ \psi(1) &= 1 \end{aligned}\right\}. \quad \ldots\ldots (6.4)$$

Once the derivatives $\alpha'(1)$, $\beta'(1)$, $\phi'(1)$ and $\psi'(1)$ are known for the system (6.3) satisfying (6.4) (or any other set of conditions), the scattering problem is, in effect, solved. It only remains to calculate the asymptotic phases by fitting appropriate exterior solutions (expressible in terms of Bessel functions) on to the interior solutions at $x=1$. A knowledge of the above first derivatives of the interior solution is sufficient for this purpose.

The discussion in the preceding sections has been based on the translation of a regularity condition at the origin into a condition on the radius of convergence of a power series. This point of view is, however, unnecessarily restricted. The selection of the regular solution is a special case of a more general property of the procedure. It is in fact applicable to problems in which the required solution is not regular at the origin. In this case the method selects the "least singular" solution consistent with the specified data *. A proof of this, in a form sufficiently general for our purposes, is given in the Appendix.

Now, the physical solutions of type (6.2), although not regular at the origin, have the property of being "least singular" in the sense of the Appendix. The remaining solutions become infinite at $x=0$. Our method can thus be extended to apply to this problem.

We introduce new dependent variables U, W :

$$u = xU, \qquad w = x^2 W. \quad \ldots\ldots (6.5)$$

Then repeated differentiation of the differential equations for U, W, leads to recurrence relations for $U_m = U^{(m)}(1)$ and $W_m = W^{(m)}(1)$. Writing

$$\left.\begin{aligned} X_n &= U_n + nU_{n-1}, \\ Y_n &= W_n + 2nW_{n-1} + n(n-1)W_{n-2}, \\ Z_n &= (k^2+v_1)X_n - v_3 Y_n, \\ T_n &= (k^2+v_2)Y_n - v_3 X_n, \end{aligned}\right\} \quad \ldots\ldots (6.6)$$

* We are indebted to Professor Peierls for this suggestion.

we have
$$\left.\begin{aligned} U_{n+2} &= -(n+2)U_{n+1} - Z_n, \\ W_{n+2} &= -(2n+4)W_{n+1} - (n-1)(n+4)W_n - T_n. \end{aligned}\right\} \quad \ldots\ldots(6.7)$$

(The relations $X_{n+2} = -Z_n$; $Y_{n+2} = 6W_n - T_n$ are useful in application of (6.6), (6.7)).

We now write
$$\left.\begin{aligned} U_m &= P_m U_0 + Q_m U_1 + R_m W_0 + S_m W_1, \\ W_m &= K_m U_0 + L_m U_1 + M_m W_0 + N_m W_1. \end{aligned}\right\} \quad \ldots\ldots(6.8)$$

Then
$$\left\{\begin{aligned} &P_0 = Q_1 = M_0 = N_1 = 1. \\ &\text{All other } P_m, \ldots, N_m \text{ with } m = 0, 1 \text{ zero.} \end{aligned}\right\} \quad \ldots\ldots(6.9)$$

It is evident that the pair of coefficients (P_m, K_m), $(m = 0, 1, 2 \ldots)$ by themselves satisfy the recurrence relations (6.6), (6.7) with P_m replacing U_m and K_m replacing W_m; the same is true for the remaining pairs (Q_m, L_m), (R_m, M_m), (S_m, N_m). This simplifies the calculation of successive U_m, W_m.

The procedure is now to set both $U_m = 0$ and $W_m = 0$ in (6.8). Putting $U_0 = 1$, $W_0 = 0$ then leads to the equations :
$$Q_m U_1 + S_m W_1 = -P_m\,; \quad L_m U_1 + N_m W_1 = -K_m. \quad \ldots\ldots(6.10)$$

The values of U_1, W_1 thus obtained provide the required first derivatives
$$\alpha'(1) = 1 + U_1, \quad \beta'(1) = W_1$$
of one solution of the fundamental system (6.3, 6.4). $\phi'(1)$, $\psi'(1)$ are obtained in the same way by solution of :
$$Q_m U_1 + S_m W_1 = -R_m\,; \quad L_m U_1 + N_m W_1 = -M_m$$
together with
$$\phi'(1) = U_1\,; \quad \psi'(1) = W_1 + 2.$$

To illustrate the mode of convergence of the procedure, successive approximations to $(\alpha'(1), \beta'(1); \phi'(1), \psi'(1))$ are listed in table 2. As our object in the present paper is exposition of method rather than actual calculation of cross-sections the calculations for table 2 were performed with the simple values
$$k^2 + v_1 = 3, \quad k^2 + v_2 = -1, \quad v_3 = -6.$$

Table 2

n	$\alpha'(1)$	$\beta'(1)$	$\phi'(1)$	$\psi'(1)$
3	−7·4615	−3·2308	+0·4615	+3·2308
4	+0·5000	−1·3500	−2·8750	+2·5625
5	−0·3421	−1·3953	−1·1245	+3·1031
6	−0·8654	−1·5320	−1·7084	+2·8668
7	−1·0189	−1·5711	−1·5093	+2·9178
8	−0·8721	−1·5316	−1·5381	+2·9109
9	−0·8634	−1·5287	−1·5260	+2·9141
10	−0·8694	−1·5300	−1·5305	+2·9131
11	−0·8690	−1·5297	−1·5292	+2·9134
12	−0·8687	−1·5293	−1·5291	+2·9135

APPENDIX

Let $f(z)$ and $g(z)$ be analytic functions having no singular point other than $z = 0$ in some circle $|z - a| = b$, $(b > |a|)$. Without loss of generality, a may be assumed real and positive. If either f or g or both are many-valued with the

origin as a branch point, a cut is made along the negative real axis from 0 to ∞; we then restrict our considerations to a single branch of f and g.

Suppose, further, that in the cut plane : (a) there exists a real number σ, $(0<\sigma<1)$, such that

$$z^{1-\sigma}f(z)\to 0 \text{ as } z\to 0, \qquad \ldots\ldots(7.1)$$

(b) $g(z)$ can be expressed as :

$$g(z)=\phi(z)+\psi(z), \qquad \ldots\ldots(7.2)$$

where $\phi(z)$ satisfies the same conditions as $f(z)$; the "more singular" part $\psi(z)$ will be assumed to have either of the forms :

$$\psi(z)=\sum_{k=1}^{\nu}\frac{A_k}{z^{\lambda k}}, \qquad \ldots\ldots(\mathrm{I})$$

$$\psi(z)=\ln z\sum_{k=1}^{\nu}\frac{B_k}{z^{\lambda k}}, \qquad \ldots\ldots(\mathrm{II})$$

where $\lambda_1>\lambda_2>\ldots\ldots>\lambda_\nu\geqslant 1$.

We consider the Taylor series

$$\begin{cases} f(x)=\sum_{n=0}^{\infty} f_n(x-a)^n, \\ g(x)=\sum_{n=0}^{\infty} g_n(x-a)^n=\sum_{n=0}^{\infty}(\phi_n+\psi_n)(x-a)^n \end{cases}$$

and shall prove that $\lim_{n\to\infty} f_n/g_n=0$.

Let $h<b-a$ and let $\mathscr{C}_\delta$ denote the contour $\Gamma+\mathscr{L}_\delta+\gamma_\delta+\mathscr{L}'_\delta$ in the cut plane. Γ is the circle with centre a and radius $a+h$, γ_δ the circle $|z|=\delta$; $\mathscr{L}_\delta$ and $\mathscr{L}'_\delta$ are straight-line paths between $-h$ and $-\delta$ along the upper and lower lips of the cut respectively (see figure). Then

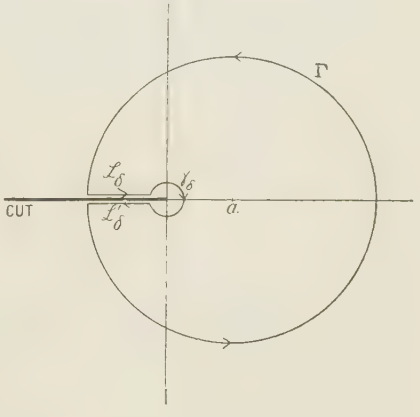

$$f_n=\frac{1}{2\pi i}\int_{\mathscr{C}_\delta}\frac{f(z)}{(z-a)^{n+1}}dz$$

$$=\frac{1}{2\pi i}\left\{\int_\Gamma+\int_{\mathscr{L}_\delta}+\int_{\gamma_\delta}+\int_{\mathscr{L}'_\delta}\right\}\frac{f(z)\,.\,dz}{(z-a)^{n+1}}.$$

Let $M_1(h)=$ maximum of $|f(z)|$ on Γ,

$m(h)=$ maximum of $|z^{1-\sigma}f(z)|$ on the two lines $-h\leqslant z<0$,

$M_2(\delta)=$ maximum of $|f(z)|$ on γ_δ.

Then

$$\left|\frac{1}{2\pi i}\int_{\mathscr{L}_\delta}\frac{f(z)dz}{(z-a)^{n+1}}\right|=\frac{1}{2\pi}\left|\int_{\mathscr{L}_\delta}\frac{z^{1-\sigma}f(z)dz}{z^{1-\sigma}(z-a)^{n+1}}\right|$$

$$\leqslant\frac{1}{2\pi}\frac{m(h)}{(a+\delta)^{n+1}}\int_{\mathscr{L}_\delta}\left|\frac{dz}{z^{1-\sigma}}\right|$$

$$<\frac{h^\sigma m(h)}{2\pi\sigma(a+\delta)^{n+1}}.$$

Similarly for the integral along $\mathscr{L}'_\delta$. Hence

$$|f_n| < \frac{M_1(h)}{(a+h)^n} + \frac{2h^\sigma m(h)}{2\pi\sigma(a+\delta)^{n+1}} + \frac{\delta M_2(\delta)}{(a-\delta)^{n+1}}.$$

By (7.1), $\delta M_2(\delta) \to 0$ as $\delta \to 0$. Thus, proceeding to the limit $\delta \to 0$:

$$|f_n| \leqslant \frac{1}{a^n}\left\{M_1(h)\left(1+\frac{h}{a}\right)^{-n} + \frac{h^\sigma . m(h)}{\sigma\pi a}\right\}.$$

Now, given $\epsilon > 0$, however small, we can choose h so that

$$\frac{h^\sigma m(h)}{\pi\sigma a} < \frac{\epsilon}{2}.$$

Then we can find a number N_0 such that for all $n > N_0$

$$M_1(h)(1+h/a)^{-n} < \epsilon/2.$$

Hence, for all $n > N_0$,

$$|f_n| < \epsilon/a^n. \qquad \ldots\ldots(7.3)$$

On the other hand, by direct differentiation of $\psi(z)$ in the forms (I), (II) we have

$$\psi_n \equiv \frac{\psi^{(n)}(a)}{n!} = \begin{cases} (-1)^n \dfrac{A_1}{a^{\lambda_1+n}}\dbinom{n+\lambda_1-1}{n} + \ldots\ldots & \ldots\ldots(\mathrm{I}) \\ (-1)^n \dfrac{B_1}{a^{\lambda_1+n}}\left\{\dbinom{n+\lambda_1-1}{n}\ln a - \sum_{k=1}^{n}\dfrac{1}{k}\dbinom{n+\lambda_1-k}{n-k}\right\} & \\ \qquad + \ldots\ldots & \ldots\ldots(\mathrm{II}) \end{cases}$$

where the dots denote terms which are of lower order as $n \to \infty$. In both cases the coefficient of $a^{-(\lambda_1+n)}$ is at least non-zero : in general it becomes infinite as $n \to \infty$ (except for $\lambda_1 = 1$ in case (I)). Thus, for both (I) and (II), there exists a number N_1 such that, for all $n > N_1$

$$|\psi_n| > M_3 |a^{\lambda_1+n}, \qquad \ldots\ldots(7.4)$$

where M_3 is a constant independent of n.

Thus, combining (7.3), (7.4), it follows that for all $n > \mathrm{Max}(N_0, N_1)$, $|f_n/\psi_n| < a^{\lambda_1}\epsilon/M_3$, and so $\lim_{n\to\infty} f_n/\psi_n = 0$.

Since $\phi_n/\psi_n \to 0$ as $n \to \infty$ (ϕ_n behaves "at worst" like f), we have $\lim_{n\to\infty} f_n/g_n = 0$.

If now $f(x)$, $g(x)$ form a fundamental system of solutions for a given second order differential equation, the general solution is of the form

$$u = \sum_{n=0}^{\infty} u_n(x-a)^n = Af(x) + Bg(x). \quad \text{Then } u_n = Af_n + Bg_n.$$

Our procedure is to set $u_n = 0$. This gives $B/A = -f_n/g_n$ which $\to 0$ as $n \to \infty$. In this way the "least singular" solution $f(x)$ is selected.

The proof can easily be extended to the case of a differential equation of order k, with $(k-1)$ conditions specified at $x = a$; the method will again select the "least singular" solution consistent with the specified data.

ACKNOWLEDGMENTS

We would like to record our thanks to Professor Peierls for his interest in this work and for a number of stimulating discussions, and to Mr. T. H. R. Skyrme for useful suggestions and criticism in connection with the mathematical theorem of the Appendix.

REFERENCES

Bethe, H. A., and Bacher, R. F., 1936, *Rev. Mod. Phys.*, **8**, 82.
Rarita, W., and Schwinger, J., 1941, *Phys. Rev.*, **59**, 434.
Sachs, R. G., and Goeppert-Mayer, M., 1938, *Phys. Rev.*, **53**, 991.

Characteristics of Radio Echoes from Meteor Trails: I. The Intensity of the Radio Reflections and Electron Density in the Trails

By A. C. B. LOVELL and J. A. CLEGG
Physical Laboratories, University of Manchester

Communicated by P. M. S. Blackett ; MS. received 26 January 1948

ABSTRACT. Recent observations of radio echoes reflected from meteor trails have given a large amount of information about the electron densities in the trails and the physical processes occurring in the atmosphere after the passage of the meteor. In this paper, which is Part I of three papers dealing with the work, formulae are derived for the intensity of the radio wave scattered from a meteor trail on the assumption that the electrons are created in a long narrow column, of diameter small compared with the wavelength of the radio wave. Experimental work is described which shows that the predicted variation of received power with wavelength is correct for the wavelength range 4·2 m. to 8·3 m., and according to preliminary results down to 1·4 m. The formulae can then be used to measure the electron density in the trails of meteors. Of particular interest are the measurements for meteors which are also observed visually. The results show that the density in the trail of a 5th magnitude meteor (on the limit of naked eye visibility) is approximately 2×10^{10} electrons per cm. path. Brighter meteors ($\sim$ magnitude $+1$) produce 10^{12} electrons per cm. path. These results are in very good agreement with contemporary theoretical calculations. The theory is compared with earlier calculations made by Eckersley and Pierce.

§ 1. INTRODUCTION

When a meteor enters the earth's atmosphere it creates a trail of electrons at a height of about 100 km. above the earth's surface. The trail is dense enough to reflect energy from an incident radio wave and under suitable conditions a short-lived response can be obtained on the receiver. These transient radio responses have been studied since 1929 (see Lovell (1948) for a review of this work) and recently the technique has been developed for the study of the activity of meteor showers and the delineation of meteor radiants. (Appleton and Naismith 1947, Hey and Stewart 1946, 1947, Prentice, Lovell and Banwell 1947, Lovell, Banwell and Clegg 1947). The present papers are concerned with the mechanism of reflection of the radio waves and the physical processes occurring in the atmosphere after the creation of the meteor trail. In Part I formulae are derived for the intensity of a radio echo received from a column of electrons in the atmosphere; from these can be calculated the density of electrons in meteor trails. Part II will deal with the distribution of electron densities in the trails of the shower meteors and with the distribution of meteoric mass. In Part III the factors which determine the duration of the transient echoes and the behaviour of the trails after formation will be discussed.

§ 2. CALCULATION OF THE INTENSITY OF THE RADIO REFLECTION FROM AN ELECTRON CLUSTER

Blackett and Lovell (1941) have calculated the intensity of a radio wave scattered from a long narrow column of ionization in the atmosphere, assuming that the electrons scatter coherently. These calculations will now be extended to include the parameters of the radio apparatus and will be applied to the particular case of meteor trails.

Consider a cluster of N electrons at a distance R cm. from a radio transmitter and receiver working on a wavelength of λ cm. If the size of the cluster is small compared with λ and if the electrons reach their full velocity under the influence of the impressed E.M.F. and are not impeded by collisions, then the cross section for scattering by the N electrons will be $(8\pi/3)(\boldsymbol{e}^2/\boldsymbol{mc}^2)^2N^2\,\mathrm{cm}^2$, where $\boldsymbol{e}$ is the charge, $\boldsymbol{m}$ the mass of the electron and $\boldsymbol{c}$ the velocity of light.

If the peak power in the pulse of the radio transmitter is P watts, and if the aerial system of the transmitter has a power gain G' over a source radiating uniformly through 4π, then the power density at a distance R cm. will be $PG'/4\pi R^2$ watts/cm^2. Hence the amount of energy scattered by the electron cluster will be $\frac{8}{3}\pi\left(\frac{\boldsymbol{e}^2}{\boldsymbol{mc}^2}\right)^2 N^2\frac{PG'}{4\pi R^2}$ watts.

If the receiver is situated in the same place as the transmitter, the power density of this scattered radiation when it returns to the receiving aerial will be $\frac{8}{3}\pi\left(\frac{\boldsymbol{e}^2}{\boldsymbol{mc}^2}\right)^2 N^2\frac{PG'}{4\pi R^2}\,\frac{1{\cdot}5}{4\pi R^2}$ watts/cm^2. (The factor 1·5 is introduced to allow for the fact that the electrons scatter as Hertzian dipoles and not uniformly through 4π).

The effective collecting area of the receiving aerial will be $G_0'\lambda^2/4\pi\,\mathrm{cm}^2$ where G_0' is its power gain over a spherical source. Hence the power which it delivers to a matched load when situated in a field of mean power density σ will be $G_0'\lambda^2\sigma/8\pi$. Thus in the case under consideration the amount of energy delivered to the receiver input after scattering from the cluster of N electrons will be

$$\epsilon=\frac{8}{3}\pi\left(\frac{\boldsymbol{e}^2}{\boldsymbol{mc}^2}\right)^2 N^2\frac{1{\cdot}5PG'}{16\pi^2R^4}\,\frac{G_0'\lambda^2}{8\pi}\,\text{watts.} \qquad \ldots\ldots(1)$$

For comparison with experiment it is convenient to take the gain of the transmitting and receiving aerials as the same, and to express the gain in terms of that of a half-wave dipole so that $G'=G_0'=1{\cdot}64G$, where G is the power gain of the aerial system over a half-wave dipole. Then (1) becomes

$$\epsilon=\frac{8}{3}\pi\left(\frac{\boldsymbol{e}^2}{\boldsymbol{mc}^2}\right)^2 N^2\,\frac{PG^2\lambda^2}{32\pi^3R^4}\,\text{watts.} \qquad \ldots\ldots(2)$$

In terms of the voltage amplitude V at the receiver input

$$V^2=2r\epsilon, \qquad \ldots\ldots(3)$$

where r is the input resistance of the receiver. Or for constant P

$$V=k\,\lambda N/R^2, \qquad \ldots\ldots(4)$$

where the constant k is given by $k^2=\frac{8}{3}\pi\left(\frac{\boldsymbol{e}^2}{\boldsymbol{mc}^2}\right)^2\frac{PG^2}{32\pi^3}2r$.

§ 3. APPLICATION TO THE CASE OF A METEOR TRAIL

If it is assumed that the meteor trail consists of a long narrow column of ionization whose diameter is small compared with λ, the appropriate number of electrons N to be included in (2) can be calculated by using ordinary optical diffraction theory. The voltage amplitude returned to the receiver from a small element of track at an angle θ to the perpendicular from the receiver to the trail is given by $dV=k\lambda\alpha d\theta/R$, where α is the number of electrons/cm. path in the trail and k is the constant occurring in equation (4) above.

The voltage amplitude from the portion of the trail $\theta=0$ to $\theta=\theta_1$ is then given by Fresnel's integral in the form

$$V_{\theta_1}=\frac{k\alpha}{2}\left(\frac{\lambda}{R}\right)^{3/2}\int_0^{\nabla}\cos\frac{\pi}{2}\nabla^2 d\nabla+\frac{ik\alpha}{2}\left(\frac{\lambda}{R}\right)^{3/2}\int_0^{\nabla}\sin\frac{\pi}{2}\nabla^2 d\nabla,$$

where $\nabla=2\theta\sqrt{(R/\lambda)}$.

The voltage amplitude at the receiver due to the whole track is then $V=(1/\sqrt{2})k\alpha(\lambda/R)^{3/2}$. Hence by comparison with (4) the appropriate number of electrons N is given by

$$N=\alpha\sqrt{(\lambda R/2)}. \qquad \ldots\ldots(5)$$

In this calculation the phase correction is applied twice because of the curvature of the incident and reflected wave surfaces. The wavelength is then effectively reduced to $\lambda/2$, giving equation (5) instead of the more familiar form $N=\alpha\sqrt{(\lambda R)}$ used by Blackett and Lovell (1941).

Hence from (2) the amount of energy at the receiver input due to scattering from a meteor trail with an electron density of α electrons/cm., will be

$$\epsilon=\frac{8}{3}\pi\left(\frac{\boldsymbol{e}^2}{\boldsymbol{mc}^2}\right)^2\left(\alpha^2\frac{\lambda R}{2}\right)\left(\frac{PG^2\lambda^2}{32\pi^3R^4}\right)=\alpha^2\frac{PG^2\lambda^3}{24\pi^2R^3}\left(\frac{\boldsymbol{e}^2}{\boldsymbol{mc}^2}\right)^2 \text{ watts.} \qquad \ldots\ldots(6)$$

Alternatively

$$\alpha=\sqrt{24\pi}\left(\frac{\boldsymbol{mc}^2}{\boldsymbol{e}^2}\right)\frac{1}{G}\sqrt{\left(\frac{\epsilon R^3}{P\lambda^3}\right)}. \qquad \ldots\ldots(7)$$

§ 4. THE EFFECT OF ELECTRON COLLISIONS

The above calculations assume a cross section for scattering of

$$(8\pi/3)(\boldsymbol{e}^2/\boldsymbol{mc}^2)^2N^2.$$

This is correct only if the electrons are free, and it is necessary to examine the assumption, since an electron may collide with a neutral atom or molecule before it has attained its full velocity under the influence of the impressed E.M.F. This effect was neglected in the calculations of Blackett and Lovell (1941) and it will be considered here for the particular case of meteor trails.

Let ν_c be the collisional frequency of electrons with neutral atoms and ν_0 the radio wave frequency. Then the cross section for scattering is effectively reduced to

$$(8\pi/3)(\boldsymbol{e}^2/\boldsymbol{mc}^2)^2N^2(1+(\nu_c/\pi\nu_0)^2)^{-1}. \qquad \ldots\ldots(8)$$

Except at high altitudes this term has a considerable influence in any practicable experiment. For example at 20 km. altitude in the atmosphere an electron will make approximately 10^{11} collisions sec. with atmospheric molecules. Now, even with a wavelength as low as 10 cm. ($\nu_0=3\times10^9$/sec.), $(\nu_c/\pi\nu_0)^2\simeq100$; and for wavelengths in the region of 4 m. it rises to about $2{\cdot}5\times10^4$.

In the particular case of meteors the radio echoes are observed to originate at a height of approximately 100 km. At this altitude $\nu_c\simeq3\times10^5$ sec. and except for long wavelengths (e.g. $\lambda>100$ m.) the effect of damping can be neglected. The assumption made in deducing equation (6), that the electrons are free, is therefore justified.

§ 5. EXPERIMENTAL TEST OF THE THEORY

An attempt to verify equation (6) experimentally as regards the predicted variation of ϵ with λ has been made by observing the same meteor trail simultaneously on different wavelengths. The essential features of the apparatus

have been described elsewhere (Prentice, Lovell and Banwell 1947; Lovell, Banwell and Clegg 1947). The wavelengths used were 8·3 m., 6·5 m., 4·2 m., and 1·4 m., and the main characteristics of the apparatus are summarized in table 1. A preliminary account of the measurements on 8·3 m., 6·5 m. and 4·2 m. has been given by Lovell (1947).

Table 1

λ (m.)	(*a*)	(*b*)	(*c*)	(*d*)
8·3	150	15	50	4·2
6·5	50	15	50	4·6
4·2	50	8	50	2·2
1·4	50	2	180	2·2

(*a*) peak transmitter power P (kw.); (*b*) pulse width (μ sec.); (*c*) pulse recurrence frequency; (*d*) receiver sensitivity : voltage input for twice signal/noise (μv.).

For each equipment the aerial systems consisted of half-wave dipoles mounted at equivalent heights above the ground such that in equation (6) G can be treated as constant. Observations of the transient echoes were made visually on a cathode-ray tube display. The quantity measured is the amplitude of the echo in terms of the normal receiver noise level. This is converted into equivalent voltage input at the aerial by appropriate calibration of the receiver. Thus if simultaneous echoes are observed from the same meteor trail on wavelengths λ_1, λ_2 of amplitude V_1, V_2 equation (6) predicts that $V_1/V_2=(\epsilon_1/\epsilon_2)^{\frac{1}{2}}=(\lambda_1/\lambda_2)^{1\cdot5}$ since R, α are constants for the same trail, G is assumed to be the same and the equivalent voltage inputs are corrected for any variations in P by assuming $V_1\ V_2=(P_1/P_2)^{\frac{1}{2}}$.

In the actual reduction of observations the exponent n in the expression

$$V_1/V_2=(\lambda_1/\lambda_2)^n \qquad \ldots\ldots(9)$$

has been calculated for each pair of simultaneous observations for comparison with the theoretical value of $n=1\cdot5$.

(i) *Simultaneous Observations on 72 Mc/s. (4·2 m.) and 36 Mc/s. (8·3 m.)**

Simultaneous observations of the radio echoes from the same meteor trail on wavelengths of 4·2 m. and 8·3 m. using apparatus with the characteristics specified in table 1 have been made in 1947 as follows : 12–27 August, 104 observations on the Perseid radiant (21 observations rejected); 23–24 September, 158 observations on an unknown radiant (17 rejected); 9–10 October, 59 observations on an unknown radiant (2 rejected).

For each of the 321 pairs of observations the exponent n has been calculated from equation (9) as described above. The distribution curve for these measurements is plotted in figure 1 and gives a mean value of 1·4 for n with a standard deviation of 0·5.

* *Note added in proof.* Equation (6) applies to the case of scattering from a meteor trail which crosses through the aerial beam in such a way that the foot of the perpendicular from the station to the trail lies within the beam. This is the only condition under which the main radio echo can be observed on wavelengths shorter than 6·5 m. On longer wavelengths some experimental evidence exists that the trails lose this critical aspect sensitivity (Millman, McKinley and Burland, *Nature, Lond.*, 1948, **161**, 278, Lovell 1948). The measurements on 8·3 m. in this paper apply to the case of perpendicular reflection, since the only echoes selected are those appearing simultaneously on the shorter wavelength, which implies that the aspect condition is satisfied.

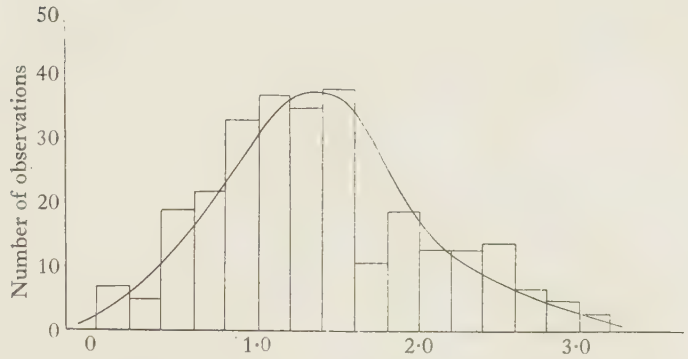

Figure 1. Distribution curve for simultaneous observations on λ=4·2 and 8·3 m. Mean value n=1·4; standard deviation=0·5.

(ii) *Simultaneous Observations on* 72 *Mc/s.* (4·2 *m.*) *and* 46 *Mc/s.* (6·5 *m.*)

A similar series of simultaneous observations on wavelengths of 4·2 m. and 6·5 m. have been made as follows : 12–27 August 1947, 57 observations on the Perseid radiant (11 rejected); 14 December 1947, 79 on the Geminid radiant (17 rejected); 3–4 January 1948, 30 on the Quadrantid radiant (2 rejected).

The distribution in values of the exponent n calculated for each pair from equation (9) is plotted in figure 2 and gives a mean value of 1·7 for n with a standard deviation of 0·6.

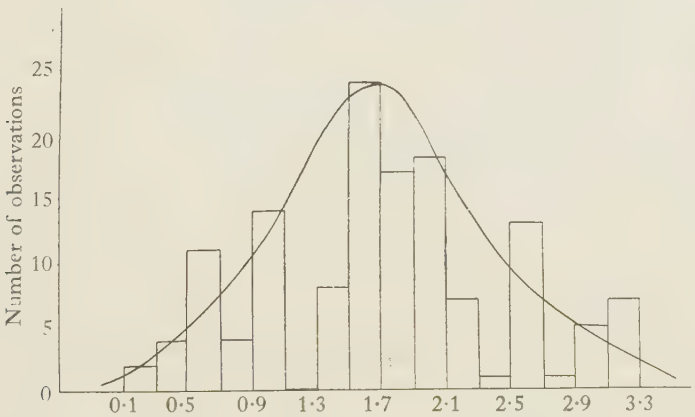

Figure 2. Distribution curve for simultaneous observations on λ=4·2 and 6·5 m. Mean value n=1·7; standard deviation=0·6.

(iii) *Triple Simultaneous Observations on* 208 *Mc/s.* (1·4 *m.*) 72 *Mc/s.* (4·2 *m.*) *and* 46 *Mc/s.* (6·5 *m.*).

Preliminary attempts have been made to observe the same meteor trail simultaneously on wavelengths of 1·4, 4·2 and 6·5 m. Equations (6) and (7) indicate that the voltage amplitude at the receiver can be expected to decrease as $\lambda^{3/2}$ and hence only the trails with very dense ionization can be expected to give echoes on the 1·4 m. equipment specified in table 1. This expectation has been realized and only four triply observed radio echoes have so far been measured. These yield 12 values for the exponent n, calculated from equation (9) with

mean values as follows : λ 4·2 m. and 6·5 m., mean $n = 1{\cdot}7$; λ 6·5 m. and 1·4 m., mean $n = 1{\cdot}5$; λ 4·2 m. and 1·4 m., mean $n = 1{\cdot}4$.

§ 6. DISCUSSION OF RESULTS

There are two principal uncertainties in these observations. (i) Although geometrically similar aerial systems were used in the comparison equipments, slight differences of terrain and surroundings inevitably introduce variation in the polar diagrams of the aerials. It can therefore be anticipated that a certain number of meteor trails will form in regions where the polar diagrams of the comparison equipments are not exactly similar. (ii) The measurements of signal/noise ratio were made by visual observation of the cathode-ray tube display. Two observers may not agree exactly over the amplitude of a single echo, and for a given observer there will be a certain inconstancy in his estimates of amplitude. Any systematic bias due to the first effect has been counterbalanced by alternating the observers between the equipments but the second effect could not be eliminated in this work.

Both (i) and (ii) will give rise to a considerable scatter of the results about the mean value. In the results described in § 5 (*a*) 40 of the 321 pairs deviated from the mean by more than three times the standard deviation and were rejected. Similarly under § 5 (*b*) 30 of the 166 pairs were rejected.

The final mean values for n are in very reasonable agreement with the predicted value of 1·5 given by equations (6) and (7) over the wavelength range $\lambda = 4{\cdot}2$ to 8·3 m. and the preliminary results on $\lambda = 1{\cdot}4$ m. indicate that the law also holds down to this wavelength.

§ 7. ELECTRON DENSITY IN THE TRAILS

By using equation (7) it is possible to calculate the electron density in the meteor trails, since G, P, λ are constants of the apparatus, and ϵ and R are measured for individual echoes. The measured densities lie in the range 10^9 to 10^{12} electrons/cm. path. The distribution of these densities in the major showers will be dealt with in Part II.

Of particular interest are those cases where visual observations have been made concurrently with the radio echo observations, since it is then possible to measure the electron density of the trails of meteors which are of visual magnitude. Coincidence measurements of this type between a visual meteor and the radio echo on a single wavelength were made during the 1946 Perseid shower (Prentice, Lovell and Banwell 1947), during the 1946 Giacobinid shower (Lovell, Banwell and Clegg 1947) and between a visual meteor and the radio echo on two wavelengths during the 1947 Perseid shower. Detailed associations of visual magnitude with electron density have not yet been made but the results agree in giving electron densities of 10^{10} to 10^{12} electrons/cm. path for the visually observed meteors. The measurements on the 1946 Perseid and 1947 Perseid showers indicate that a 5th magnitude meteor which is on the limit of naked eye visibility produces approximately 2×10^{10} electrons cm. path and that a very bright meteor ($\sim$magnitude + 1) produces approximately 10^{12} electrons/cm. path. These results are in very good agreement with the theoretical calculations of Herlofson (1948).

§ 8. COMPARISON WITH OTHER THEORIES

Previous calculations of the densities of electron concentrations which give rise to the transient radio echoes have been made by Eckersley (1940) and Pierce (1938).

Eckersley considered that the echoes were due to clouds of electrons and treated the scattering of radio waves as analogous to the scattering of α-particles by heavy atoms. On this theory the voltage amplitude returned to the receiver should be proportional to λ^2. Eckersley's measurements in the wavelength range $\lambda = 15$ m. to 35 m. showed agreement with this λ^2 law. The measurements described in this paper do not cover this wavelength range but it is evident that the λ^2 law does not apply over the wavelength range $\lambda = 1{\cdot}4$ to $8{\cdot}3$ m. discussed here. Eckersley's theory does not explain the critical orientation effect of the meteor trails with respect to the aerial beam (Pierce 1938, Hey and Stewart 1946, 1947, Lovell, Banwell and Clegg 1947) and it also yields values for the electron density in visibly observed trails which are in disagreement with Herlofson's calculations (1948). As discussed by Lovell (1948) the transient echo phenomena show a sudden change as the wavelength increases beyond 8 m. Below this wavelength the radio echoes are due to the trails of meteors which are associated with the visible showers originating from definite radiants. In the higher wavelength range the echoes due to these shower meteors are generally submerged in a very high background rate showing a diurnal and seasonal variation (Eckersley 1940, Appleton and Naismith 1947, Eastwood and Mercer 1948). These diurnal and seasonal variations can be explained if the earth is passing through a general distribution of meteoric dust, too minute to produce visible meteors. Eckersley's measurements refer to these latter type of transient echoes, and although the reasons are not yet understood it is possible that the change from the λ^2 to $\lambda^{3/2}$ law may be associated with the change in origin of the transient echoes.

Pierce (1938) calculated the scattered energy from a meteor trail compared with that scattered from an ionized layer, by assuming that the electrons in the trail formed a long column with a diameter *large* compared with the wavelength and with such a high electron density that the radio wave did not penetrate to the inner parts of the trail. These calculations predict the same variation of scattered energy with λ and R as equation (6) and from this point of view the experimental results described here are not in disagreement with Pierce's theory. There are, however, two facts which indicate that Pierce's fundamental assumptions are in error.

(i) Pierce assumes that the meteor trail has already diffused so that its diameter is large compared with λ before the radio echo is observed. Other aspects of the work described in this paper (Part III, see also Ellyett and Davies 1948) show that this assumption is incorrect, at least for observations in the wavelength range $\lambda = 1{\cdot}4$ to $8{\cdot}3$ m. The echo is obtained from the trail in process of formation as it crosses the beam of the aerial. The subsequent expansion of the electron column by diffusion, to the dimensions assumed by Pierce to be the initial state, can then be shown to be a necessary consequence of the change of duration of the transient echoes with the azimuth of the aerial beam described by Lovell (1948; see also Part III) and explained by Herlofson (1948).

(ii) Pierce's calculations lead to estimates of the electron density in visible meteor trails which differ by orders of magnitude from the densities calculated from equation (6) and are thus in disagreement with contemporary theory

(Herlofson 1948). Also in order to explain the intensity of a meteor echo compared with the intensity of the echo from the F region, Pierce, following Maris (1929) has to assume that the entire kinetic energy of the meteor is spent in ionization, whereas Herlofson (1948) shows that only 10^{-6} of the kinetic energy of the meteor is spent in this manner.

ACKNOWLEDGMENTS

The work described in this paper has been carried out at the Jodrell Bank Experimental Station of the University of Manchester. The authors wish to thank Professor P. M. S. Blackett for his interest and encouragement during the development of the work. The authors are indebted to their colleagues who shared the task of making these measurements, particularly to A. Aspinal, J. G. Davies, C. D. Ellyett, I. A. Gatenby, V. A. Hughes and F. Moran.

REFERENCES

Appleton, E. V., and Naismith, R., 1947, *Proc. Phys. Soc.*, **59,** 461.
Blackett, P. M. S., and Lovell, A. C. B., 1941, *Proc. Roy. Soc.* A, **177,** 183.
Eastwood, E., and Mercer, K. A., 1948, *Proc. Phys. Soc.* (in publication).
Eckersley, T. L., 1940, *J. Instn. Elect. Engrs.*, **86,** 548.
Ellyett, C. D., and Davies, J. G., 1948, *Nature, Lond.* (in publication).
Herlofson, N., 1948, *Rep. Progr. in Phys.*, **11.**
Hey, J. S., and Stewart, G. S., 1946, *Nature, Lond.*, **158,** 481 ; 1947, *Proc. Phys. Soc.* **59,** 858.
Lovell, A. C.B., 1947, *Nature, Lond.*, **160,** 670 ; 1948, *Rep. Progr. in Phys.*, **11.**
Lovell, A. C. B., Banwell, C. J., and Clegg, J. A., 1947, *Mon. Not. R. Astr. Soc.*, **107,** 164.
Maris, H. B., 1929, *Terr. Magn. Atmos. Elect.*, **34,** 309.
Pierce, J. A., 1938, *Proc. Inst. Radio Engrs.*, **26,** 892.
Prentice, J. P. M., Lovell, A. C. B., and Banwell, C. J., 1947, *Mon. Not. R. Astr. Soc.*, **107,** 155.

LETTERS TO THE EDITOR

Polarization of Second Order Raman Effect in Alkali Halides

We have succeeded in obtaining Raman spectra of sodium chloride, potassium bromide and potassium chloride which show polarization effects. The spectra obtained for NaCl correspond to the unpolarized spectrum obtained by Rasetti (1931) and by Krishnan (1946). With a Hilger medium quartz spectrograph using 2537 A. as the exciting line, with a mercury vapour filter to absorb the resonance line after scattering, and a Wollaston prism in the scattered beam, useful spectra were obtained in two days with NaCl and KBr, and in four days with KCl. Single crystals were grown for these experiments.

In order to achieve this, a wide-angled cone of incident radiation was necessary. In practice, no limitation was put on the beam other than that naturally afforded by the critical angle. For high values of depolarization little error results from this, while for low values, for example for KBr, a depolarization of zero would be measured as 0·2. Thus it is clearly possible to distinguish between " polarized " and " depolarized " scattered radiation.

The general appearance of the spectra is that of peaks on a continuous background : this simply means that under the given conditions one could not distinguish between peaks of intensity in a continuum or lines imperfectly resolved. There is a considerable difference between the spectra of NaCl and KBr on the one hand and KCl on the other. The two former were similar in that there were a number of peaks which were partially polarized,

and one outstanding peak depolarized with a depolarization in excess of unity. This peak was at 232 cm^{-1} in NaCl and at 127 cm^{-1} in KBr.

KCl gave a much weaker spectrum, and there was no outstanding depolarized peak ; all those strong enough to be observed were well polarized.

It is thought that an explanation can be sought in the approximate equality of mass of the two atoms in KCl and the disparity of mass of the constituent atoms in the other two crystals. On the cyclic lattice theory of Born, it is sufficient to consider the one-dimensional lattice of two atoms to see that peaks of intensity of the continuum present when the ratio of the atom masses differs considerably from unity will fade as the ratio approaches unity. This at once accounts for the relative absence of peaks of intensity in KCl present in NaCl and KBr.

An attempt is now being made to grow a single crystal of RbBr which has a mass-ratio of 1·07 which, if the above explanation is correct, should give polarized spectra similar to those of KCl, which has a mass-ratio of 1·1.

The type of spectrum obtained is seen in the figure, which shows microphotometer curves of the vertically and horizontally polarized spectra for rocksalt. In each case 232 cm^{-1} is

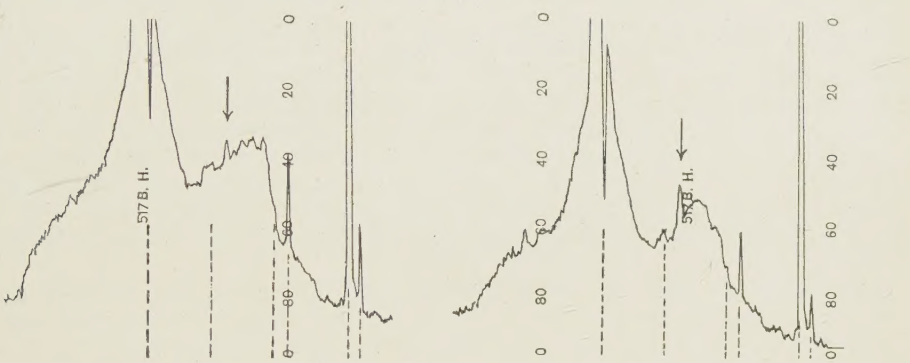

Vertical component. Horizontal component.

Raman spectrum of rocksalt.

Note: The numbers 517 B.H. in the diagram are merely the recording paper code and are to be ignored.

marked with an arrow. The dip in the high peak is the position of the exciting (resonance) line . The vertical component is privileged in the arrangement used, and this should be remembered in comparing the two curves. The position of mercury lines is indicated by vertical dashed lines.

Adam Hilger Ltd., London N.W. 1. A. C. Menzies.
30 January 1948. J. Skinner.

Krishnan, R. S., 1946, *Proc. Roy. Soc.* A, **187,** 188.
Rasetti, F., 1931, *Leipziger Vorträge, Molekülstruktur*, p. 59.

REVIEWS OF BOOKS

Theory and Applications of Electricity and Magnetism, by Charles A. Culver. First Edition. Pp. 594, 407 figs. (London and New York : McGraw Hill Book Co. Inc., 1947.) 25*s*. net.

This attractive text book was written to provide an introduction to electromagnetism for students at American Universities and " is intended to serve as a basis for advanced study in physics and chemistry and also to lay the foundation for courses in electrical

engineering ", but it should also meet the needs of second and third year students of physics and electrical engineering at British Universities.

In its thirty chapters the book surveys the elements of electricity and magnetism, applied electricity, particle physics and electronics. The theoretical approach to electrostatics, magnetostatics and the magnetic effects of currents conforms to the conventional pattern to be found in most text books, but the treatment is clear and comprehensive, with no mathematical demands on the reader beyond a knowledge of elementary algebra and calculus. The electrostatic, electromagnetic and practical systems of units are employed in the text but a welcome passing reference is made to the metre-kilogram-second system of units.

The distinctive feature of the book which calls for special comment is the very large number of practical applications that are described both for their intrinsic importance and to supplement theoretical discussions. To illustrate how the author has justified the word " applications " in the title of the book, it suffices to state that there are excellent chapters on each of the following topics : D.C. measurements (bridges and potentiometers) ; applications of the thermal effects of currents (electric furnaces, welding, arcs and lighting) ; electrolysis and primary and secondary cells ; thermoelectricity and its uses ; the magnetic effect of currents (ammeters and voltmeters).

The book contains one chapter on A.C. theory which expounds the vector method and another short chapter explaining the j-notation with applications. Alternating current instruments claim a chapter and electrical units another.

The last third of the book is a rapid survey of electronics and atomic physics with a stress on practical applications rather than on theoretical details. All this, within the author's terms of reference, is very well done, although the chapter on electricity in gases would seem to indicate that the author has not read sufficiently widely in this subject.

The final two chapters deal respectively with thermionic tubes and their uses and with electromagnetic waves and their applications.

The student's interest is stimulated by frequent reference to the history of ideas and applications but in this the author proves himself by no means infallible. For instance, it comes as a surprise (p. 468) to learn that Moseley worked at the Cavendish Laboratory. On p. 428 we learn, with reference to the nature of cathode rays, that "the German school of thought held, more or less, to the view that the rays consisted of some sort of wave disturbance ; while English physicists felt that they were dealing with some type of electrified particles ". This statement is inconsistent with the fact that in 1897 both Wiechert and Kaufmann published values of e/m, and that the former was the first to draw the correct conclusion concerning the mass of the cathode corpuscles. On p. 57 it is stated that sunspots and terrestrial magnetism have been studied in relation to each other for over 1000 years. This is presumably a misprint for 100 years.

These, however, are trivialities. More serious is a diagram (figure 338) of a cyclotron showing the pole pieces spanning scarcely one-third of the diameter of the dees, and a diagram illustrating the principle of radar (figure 399) in which six pulses are shown in flight simultaneously between the ground equipment and the airborne target. It is also time that writers of text books abandoned the practice of attributing the external magnetic field of the earth to an enormous internal bar magnet (figure 24) ; a doublet source near the centre is a much closer representation. In this context the author remarks : " The terrestrial poles are below the earth's surface ". Whether they can be reached by a suitable mining operation is not stated.

Useful sets of test problems accompany most chapters and the book is well bound and excellently printed.

The author ends his book on an optimistic note : " The science of electricity and magnetism has brought countless blessings to mankind. In the years to come it will make the earth a still better place in which to live and have our being ". Be this as it may, the author has given practical effect to his belief in writing a book which can give to an imaginative student a vision of what is possible. The book can be confidently recommended.

L. G. H. HUXLEY.

SCIENTIFIC BOOKS

Messrs. H. K. LEWIS can supply from stock or to order any book on the Physical and Chemical Sciences.

CONTINENTAL AND AMERICAN works unobtainable in this country can be secured under Board of Trade licence in the shortest possible time.

SECOND-HAND SCIENTIFIC BOOKS. 140 GOWER STREET.
An extensive stock of books in all branches of Pure and Applied Science may be seen in this department. Large and small collections bought. Back volumes of Scientific Journals.

SCIENTIFIC LENDING LIBRARY

Annual subscription from One Guinea. *Details of terms and prospectus free on request.*

THE LIBRARY CATALOGUE revised to December 1943, containing a classified index of authors and subjects: to subscribers 12*s.* 6*d.* net, to non-subscribers 25*s.* net, postage 9*d.* **Supplement** from 1944 to December 1946. To subscribers 2*s.* 6*d.* net; to non-subscribers 5*s.* net; postage 4*d.* **Bi-monthly List of Additions, free on application**

Telephone: EUSton 4282

Telegrams: "Publicavit, Westcent, London"

H. K. LEWIS & Co. Ltd.

136 GOWER STREET, LONDON, W.C.1

Established 1844

PIPE COUPLINGS

ELECTRICALLY HEATED PRESSURE HEADS

FILM ASSESSORS AND SCANNING MICROSCOPES

CONTINUOUS FILM RECORDING CAMERAS AND EQUIPMENT FOR CATHODE RAY OSCILLOGRAPHY, ETC.

AVIMO

We undertake the Design, Development and Manufacture of any type of Optical —Mechanical—Electrical Instrument. Including Cameras for special purposes.

Avimo Limited, Taunton, England · Telephone Taunton 3634

11790

ELECTRICAL MEASURING INSTRUMENTS OF THE HIGHER GRADES

ERNEST TURNER ELECTRICAL INSTRUMENTS LIMITED

CHILTERN WORKS
HIGH WYCOMBE
BUCKS

Telephone :
High Wycombe 1301/2

Telegrams
Gorgeous, High Wycombe